Summer 2015

Investigation of robust optimization and evidence theory with stochastic expansions for aerospace applications under mixed uncertainty

Harsheel R. Shah

Department: Mechanical and Aerospace Engineering

INVESTIGATION OF ROBUST OPTIMIZATION AND EVIDENCE THEORY WITH STOCHASTIC EXPANSIONS FOR AEROSPACE APPLICATIONS UNDER MIXED UNCERTAINTY

by

HARSHEEL R. SHAH

A DISSERTATION

Presented to the Graduate Faculty of the

MISSOURI UNIVERSITY OF SCIENCE AND TECHNOLOGY

In Partial Fulfillment of the Requirements for the Degree

DOCTOR OF PHILOSOPHY

in

AEROSPACE ENGINEERING

2015

Approved by

Dr. Serhat Hosder, Advisor
Dr. Xiaoping Du
Dr. K.M. Isaac
Dr. David Riggins
Dr. Leifur Leifsson

PUBLICATION DISSERTATION OPTION

This dissertation has been prepared in the style utilized by the Missouri University of Science & Technology in the form of three journal papers. From here on, the papers will be referred to by their Roman numerals. The papers are printed as per the university format however the content is according to their originally published state. The list of journal publications appended to this dissertation is given below:

(I) Shah, H., Hosder, S., and Winter, T., "A Mixed Uncertainty Quantification Approach Using Evidence Theory and Stochastic Expansions", *International Journal for Uncertainty Quantification*, Vol. 5, No. 1, 2015, pp. 21-48.

(II) Shah, H., Hosder, S., and Winter, T., "Quantification of Margins and Mixed Uncertainties Using Evidence Theory and Stochastic Expansions", *Reliability Engineering and System Safety*, Vol. 138, 2015, pp. 59-72.

(III) Shah, H., Hosder, S., Koziel, S., Tefahunegn, Y. A., and Leifsson, L., "Multi-fidelity Robust Aerodynamic Design Optimization Under Mixed Uncertainty", *Aerospace Science & Technology*, Vol. 45, 2015, pp. 17-29.

ABSTRACT

One of the primary objectives of this research is to develop a method to model and propagate mixed (aleatory and epistemic) uncertainty in aerospace simulations using DSTE. In order to avoid excessive computational cost associated with large scale applications and the evaluation of Dempster Shafer structures, stochastic expansions are implemented for efficient UQ. The mixed UQ with DSTE approach was demonstrated on an analytical example and high fidelity computational fluid dynamics (CFD) study of transonic flow over a RAE 2822 airfoil.

Another objective is to devise a DSTE based performance assessment framework through the use of quantification of margins and uncertainties. Efficient uncertainty propagation in system design performance metrics and performance boundaries is achieved through the use of stochastic expansions. The technique is demonstrated on: (1) a model problem with non-linear analytical functions representing the outputs and performance boundaries of two coupled systems and (2) a multi-disciplinary analysis of a supersonic civil transport.

Finally, the stochastic expansions are applied to aerodynamic shape optimization under uncertainty. A robust optimization algorithm is presented for computationally efficient airfoil design under mixed uncertainty using a multi-fidelity approach. This algorithm exploits stochastic expansions to create surrogate models utilized in the optimization process. To reduce the computational cost, output space mapping technique is implemented to replace the high-fidelity CFD model by a suitably corrected low-fidelity one. The proposed algorithm is demonstrated on the robust optimization of NACA 4-digit airfoils under mixed uncertainties in transonic flow.

ACKNOWLEDGMENTS

The journey of completing my PhD has been a marathon event in my life and a very satisfying one too. This would not have been possible without the aid and support of countless people over the past four years. Foremost, I would like to express my sincere gratitude towards my advisor, Dr. Serhat Hosder. His leadership, hard work, expertise and enthusiasm have set an excellent example I hope to match some day. I am extremely thankful for the time and effort Dr. Hosder has dedicated to me as my advisor towards my development as a better researcher.

I would also like to thank the rest of my PhD committee: Dr. Xiaoping Du (who was also my advisor for my Masters degree and laid a good foundation for my post-graduate studies), Dr. K.M. Isaac, Dr. David Riggins and Dr. Leifur Leifsson for their constant encouragement, insightful comments and time commitment towards my research. I would like to thank Mr. Tyler Winter from M4 Engineering Inc., Dr. Yonatan A. Tesfahunegn, Iceland and Dr. Slawomir Koziel Poland for their invaluable collaboration to this research. I thank my fellow graduate students Thomas West and Joe Ray Gramanzini for the deep technical discussions. I would like to thank the Department of Mechanical & Aerospace Engineering at the Missouri University of Science & Technology for providing the facilities and funding to help me shape my future with an academic base.

I would like to dedicate this dissertation to my friends, relatives, my family and my wife Dimple, for their love, patience and understanding. This surely has been a challenging journey and Dimple has always been fruitful in instilling the required confidence and the drive in me to pursue my PhD. This is a huge moment in my life and will cherish the same throughout !

TABLE OF CONTENTS

Page

LIST OF ILLUSTRATIONS

LIST OF TABLES

SECTION

1. INTRODUCTION

A famous quote states "Uncertainty quantification attempts to express the known unknowns[1]." In the context of aerospace systems, modern research and engineering increasingly rely on computer simulations (e.g., computational fluid dynamics). As the simulations are based on numerical modeling of the physics, uncertainties are introduced to the analysis and design through various assumptions and approximations made in the models. The inherent variations in design parameters and lack of knowledge of the underlying physical processes add to the sources of possible uncertainty in the system. All these uncertainties can affect the solution dramatically, which in turn, becomes uncertain. If the uncertainties in aerospace simulations are rigorously quantified, the results can be used in risk analysis, robust optimization and decision making processes during aerospace vehicle analysis and design.

1.1. MOTIVATION

The challenges that motivate the studies in this dissertation are: (1) computational cost of uncertainty quantification (UQ) [1, 2, 3] for high-fidelity aerospace simulations, (2) existence of both inherent and epistemic (mixed) uncertainties in aerospace simulations, and (3) efficient design of aerospace vehicles under mixed uncertainty with high fidelity models. The following sections outline how these challenges can be addressed.

[1] Dr. William Oberkampf, Virginia Tech

1.1.1. Uncertainty Quantification Using Stochastic Expansions. UQ becomes challenging for large-scale aerospace engineering systems due to various factors such as high dimensionality of non-deterministic design parameters, complexity of underlying physical processes and high-fidelity simulations. The most common methods addressed in literature for the propagation of uncertainty and reliability assessment are those based on local expansion such as first order second moment (FOSM) [4], first order reliability method (FORM), second order reliability method (SORM) [5] etc. mainly due to low computational cost and ease of implementation. However, these methods are restricted to relatively small ranges of variation and low degrees of non-linearity. As a result, Monte Carlo methods [6] (sampling according to a joint probability distribution function) gained attention as they were independent of the number of uncertain parameters. However, for these methods, the rate of convergence of the statistics is known to be of the order $N^{-1/2}$, (where N is the number of samples) indicating the large sample size requirement for accuracy.

A more recent class of uncertainty propagation methods are those based on stochastic expansions [7, 8, 9], which include both, intrusive and non-intrusive approaches. The intrusive method involves reformulation of the original governing equations and hence new solvers must be developed. Non-intrusive methods treat the existing solvers as black boxes and directly acts over the output quantities of interest. In the current study, non-intrusive stochastic expansion methods based on polynomial chaos theory have been implemented due to their capability to formulate and propagate uncertainty in highly non-linear stochastic problems at a significantly reduced cost compared to Monte Carlo methods.

1.1.2. Dempster Shafer Theory of Evidence for Mixed UQ. During the analysis and design of complex aerospace systems, available resources, such as knowledge of the physical behavior of the system, experimental budget, literature to rely on may be very limited. Some of the uncertainties in these systems which occur with the nature of randomness

can be modeled with well known probabilistic functions depending on the available data. However, the information available for other parameters might not be sufficient to assign a probability distribution. Therefore, uncertainties have been segregated mainly as aleatory uncertainty (irreducible due to the inherent nature of uncertainty) and epistemic uncertainty (reducible uncertainty due to lack of knowledge or ignorance).

Traditionally, probability theory [10] has been implemented to characterize both types of uncertainty. However, a probabilistic analysis requires information on the probability of all events, which is not always possible for epistemic uncertainty unless a uniform distribution is assumed. Consequently, the result of uncertainty analysis using the probabilistic framework might be the mere reflection of the reinforced assumption. To address these limitations and to incorporate multiple sources of epistemic uncertainty derived from expert opinion, Dempster Shafer theory of evidence [11] has been implemented for uncertainty propagation in this work. Although evidence theory has been extensively used for propagating epistemic uncertainty, very little attention has been given to mixed (aleatory and epistemic) uncertainty quantification using evidence theory. This research focuses on developing a new approach to handle mixed uncertainty with evidence theory.

1.1.3. Multi-fidelity Robust Design Optimization Under Mixed Uncertainty. Various design and optimization approaches have been implemented within the aerospace industry to increase performance and reduce cost. Deterministic optimization simplifies the design process as the uncertain parameters are assumed to be constant at their nominal values. However, the final design may have degraded performance metrics if the parameters are varied from their nominal values.

Figure 1.1 (design parameter versus performance plot) shows a good example to differentiate between a robust and deterministic design. The point D is obtained with deterministic optimization. It is clear that any variation in the design variables or operating

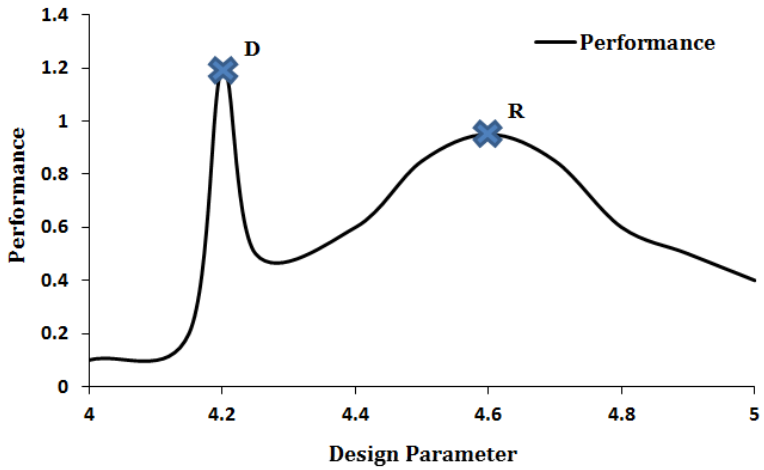

Figure 1.1. Robust versus deterministic optimum.

conditions, will significantly reduce the performance of this design. The point R that denotes the robust optimum is a preferable design, since a small variation in design parameters affects the optimum performance marginally. Design methods that are least sensitive to inherent and epistemic uncertainties are of prime importance in aerospace engineering. To address this requirement, a robust optimization algorithm is proposed for aerodynamic design under mixed (epistemic and aleatory) uncertainty. However, performing robust optimization can be expensive due to the computational cost of high-fidelity CFD simulations, which are required for accurate analysis and design. Thus, a combined stochastic expansion approach has been utilized to create a surrogate response model which is used during the optimization process. To further improve the computational efficiency, a multi-fidelity approach has been implemented to replace the high-fidelity model with a corrected low-fidelity one using output space mapping technique [12, 13].

1.2. OBJECTIVES OF THE CURRENT STUDY

There are three objectives of this study, which are addressed by each of the journal papers included in this dissertation. A detailed literature review has been presented in each paper for the better understanding of the readers.

1. to develop a new methodology to incorporate mixed (aleatory and epistemic with multiple sources) uncertainty within the Dempster Shafer Theory of Evidence framework and apply them to aerospace problems (Paper I).

2. to define procedures for reliability assessment of complex aerospace systems or a sub-system through the use of quantification of margins and uncertainties (QMU) framework based on Dempster Shafer structures (Paper II).

3. to present a robust optimization algorithm for computationally efficient aerodynamic design under mixed (inherent and epistemic) uncertainty using a multi-fidelity approach (Paper III).

1.3. CONTRIBUTIONS OF THE CURRENT STUDY

Specifically, the research accomplishments are:

1. A new method is proposed to represent the aleatory uncertainty in terms of well-characterized epistemic uncertainty. Traditionally, the DSTE approach is used to model and propagate epistemic uncertainty only. This method enables the user to directly treat the aleatory uncertainty within the DSTE framework for uncertainty propagation (Paper I).

2. A unified QMU framework based on DSTE is defined. The framework addresses the certification and risk analysis of systems or a sub-system subject to multiple types

of uncertainty in operating conditions and physical models used in the calculation of design and performance boundaries. The focus in this part of the research is to leverage accurate estimation of the reliability of a system, when there exist multiple sources of epistemic uncertainty along with aleatory uncertainty (Paper II).

3. A robust aerodynamic design algorithm using a multi-fidelity approach under mixed uncertainty is developed. The proposed algorithm exploits stochastic expansions derived from the non-intrusive polynomial chaos (NIPC) technique to create surrogate models utilized in the optimization process. The goal behind using a multi-fidelity approach is to replace the high-fidelity CFD model with a low-fidelity one, in order to further reduce the computational cost (Paper III).

4. The proposed approaches are applied to several numerical examples and aerospace design problems: a high fidelity CFD study of transonic flow over RAE 2822 airfoil (see Paper I), a multi-disciplinary analysis of a High Speed Civil Transport (HSCT) (see Paper II) and the robust design of NACA 4-digit airfoils in transonic flow under mixed uncertainties (see Paper III).

1.4. ORGANIZATION OF THE DISSERTATION

This dissertation is organized in the form of three journal publications. A mixed uncertainty quantification approach using evidence theory and stochastic expansions (pages 8-61) has been published in the International Journal for Uncertainty Quantification, March 2015. Quantification of margins and mixed uncertainties using evidence theory and stochastic expansions (pages 62-109) has been published in Reliability Engineering & System Safety journal, January 2015. Multi-fidelity robust aerodynamic design optimization under mixed uncertainty (pages 110 - 151) has been published in the Aerospace Science &

Technology journal, March 2015. A detailed literature review has been done for each of the publications and the reader is advised to refer the respective paper in the dissertation. Lastly, Section 2 discusses general conclusions from this research and outlines possible future work areas.

PAPER

I. A MIXED UNCERTAINTY QUANTIFICATION APPROACH USING EVIDENCE THEORY AND STOCHASTIC EXPANSIONS

Harsheel Shah[1], Serhat Hosder[1] and Tyler Winter[2]

[1]Missouri University of Science & Technology, Rolla, MO, 65409, USA
[2]M4 Engineering Inc., Long Beach, CA, 90807, USA

ABSTRACT

Uncertainty Quantification (UQ) is the process of quantitative characterization and propagation of input uncertainties to the response measure of interest in experimental and computational models. The input uncertainties in computational models can be either aleatory i.e. irreducible inherent variations or epistemic i.e. reducible variability which arises from lack of knowledge. Previously, it has been shown that Dempster Shafer Theory of Evidence (DSTE) can be applied to model epistemic uncertainty in case of uncertainty information coming from multiple sources. The objective of this paper is to model and propagate mixed uncertainty (aleatory and epistemic) using DSTE. In specific, the aleatory variables are modeled as Dempster Shafer structures by discretizing them into sets of intervals according to their respective probability distributions. In order to avoid excessive computational cost associated with large scale applications, a stochastic response surface based on Point-Collocation non-intrusive polynomial chaos has been implemented as the surrogate model for the response. A convergence study for accurate representation of aleatory uncertainty in terms of minimum number of subintervals required is presented. The mixed UQ approach is demonstrated on a numerical example and high fidelity computational fluid dynamics study of transonic flow over RAE 2822 airfoil.

NOMENCLATURE

n	number of random variables
R	support region of random input variable
n_p	oversampling ratio
p	order of polynomial chaos
$\vec{\xi}$	standard input random variable vector
$p(\vec{\xi})$	probability density function of $\vec{\xi}$
ψ	random basis function
α	coefficient in polynomial chaos expansion
α^*	stochastic function
μ	mean
σ	standard deviation
$\mathbb{U}$	Universal set
$\mathscr{U}$	set of focal elements of $\mathbb{U}$
Bel	Belief
Pl	Plausibility
BPA	basic probability assignment
$m(\varepsilon)$	BPA corresponding to subset ε of $\mathscr{U}$
PCE	polynomial chaos expansion
N_t	number of terms in a total-order PCE
c_l	coefficient of lift
c_d	total coefficient of drag
C_p	coefficient of pressure
M	Mach number

$\tilde{\alpha}$ angle of attack in degrees

Re Reynolds number

1. INTRODUCTION

Uncertainty Quantification (UQ) is the process of quantitative characterization and propagation of input uncertainties to the response measure of interest in experimental and computational models. Depending upon the amount of available information, researchers have been constantly trying to differentiate and characterize various forms of uncertainty. For decades, uncertainties have been segregated mainly as aleatory uncertainty (if sufficient amount of data is available such that it can be characterized with a probability distribution) and epistemic (probabilistic distributions are assumed or non-probabilistic methods are used e.g., interval analysis). Oberkampf et al. [1] have described various methods for estimating total uncertainty by identifying all possible sources of variability, uncertainty and error in computational simulations. As the data is sparse for an epistemic variable, there is a possibility of multiple sources of uncertainty (different information through expert opinion). This led to the formulation of mathematical structures for appropriate representation of uncertainty like the evidence theory [2], also known as the Dempster Shafer Theory of Evidence (DSTE). The introduction of this theory was accompanied by a discussion of merits, demerits and different mathematical operations possible with Dempster Shafer structures [3, 4, 5].

In previous years, a number of studies have implemented and explored the concept of evidence theory. Helton et al. [6] have compared the use of several uncertainty representations like the probability theory, evidence theory, possibility theory and interval analysis

on a range of test problems proposed as a part of a workshop [7]. In the past decade, extensive research has been dedicated to improvement of the practical application of the Dempster Shafer theory due to implicit nature of simulations and excessive computational costs. Bae et al. [8] introduced an approximation approach for uncertainty quantification using evidence theory. Their proposed algorithm includes identifying the failure region in a defined UQ space by employing an optimization routine. Specifically, failure region in this case is considered as the region in which the limit state function for the system under consideration exceeds a particular limit state value. For example, in an analysis of a composite cantilever beam with a point load, the failure region is determined by the assessment of the likelihood that the tip displacement (limit state function) of the beam exceeds the maximum possible displacement (limit state value). Further, a surrogate model constructed using Two-point Adaptive Non-linear Approximation (TANA2) and Multi Point Approximation approach (MPA) is used for repetitive simulations in UQ analysis. Later, they demonstrated the newly proposed algorithm on a large scale structure problem like the structural model of an intermediate complexity wing (ICW) [9]. Agarwal et al. [10] investigated uncertainty quantification in multidisciplinary systems analysis subject to epistemic uncertainty through the application of evidence theory. The methodology has been demonstrated using a higher dimensional multidisciplinary aircraft concept sizing.

In view of aforementioned developments in evidence theory for propagating epistemic uncertainty, very little attention has been given to mixed (aleatory and epistemic) uncertainty quantification using evidence theory. This is mainly due to two reasons: (1) incorporation of aleatory uncertainty in Dempster Shafer structures and (2) computational costs due to implicit nature of simulations required for deriving evidence theory uncertainty measures. The objective of this paper is to explore the incorporation of aleatory uncertainty in Dempster Shafer structures and to implement Non-Intrusive Polynomial Chaos (NIPC),

a computationally efficient stochastic response approach, for mixed uncertainty quantification using evidence theory.

Eldred and Swiler [11] have reported efficient algorithms for mixed UQ which consist of optimization based interval estimation and stochastic expansion methods. Recently, Eldred et al. [12] have demonstrated mixed UQ using DSTE by calculating evidence theory uncertainty measures for outer loop of epistemic variables characterized by Dempster Shafer structures over the inner loop aleatory statistics. They have compared the DSTE results obtained through global optimization and sampling approach for a short column test problem. Our work focuses on representing aleatory uncertainty in terms of Dempster Shafer structures by discretizing the probability distributions into sets of intervals and treating them as epistemic variables. In order to reduce the computational costs from simulation point of view, NIPC [13, 14, 15, 16, 17] technique is employed using Point Collocation approach to construct a stochastic surrogate model which can replace the deterministic model in interval optimization routines for DSTE analysis.

In Section 3, different types of uncertainties that exist in a model are discussed. In Sections 4 and 4, the necessary mathematical framework for Point-Collocation NIPC and Dempster Shafer Theory of Evidence is presented, respectively. Further, an approach for mixed uncertainty quantification using DSTE is presented in Section 5. A numerical analysis is performed in Section 6 in order to quantify the minimum number of subintervals required to accurately represent aleatory uncertainty within the proposed framework. The approach is demonstrated on a numerical example and a high fidelity Computational Fluid Dynamics (CFD) study of a transonic supercritical airfoil RAE 2822 in Section 7. We conclude the paper with important interpretations of the results obtained from mixed UQ analysis using DSTE in Section 9.

2. TYPES OF UNCERTAINTY

In computational simulations, uncertainties are assigned to the specification of input physical parameters that are required for computational models. Two types of uncertainties exist in numerical modeling of physical systems: aleatory uncertainty and epistemic uncertainty.

2.1. Aleatory Uncertainty. Aleatory uncertainty, also known as probabilistic uncertainty, arises due to inherent physical variability present in the system. A specific probability distribution can be attributed to an aleatory random variable based on the data available. Aleatory uncertainty is irreducible as it is naturally present in the system under consideration. For example, the Mach number can be considered as an aleatory uncertain variable in a CFD study of airfoils or wings.

2.2. Epistemic Uncertainty. The epistemic uncertainty, also known as model-form uncertainty, arises due to lack of knowledge and is reducible by performing more experiments. The stimulant to epistemic uncertainties are the assumptions introduced in the derivation of mathematical models. This type of uncertainty cannot be defined in a probabilistic framework unless a specific distribution is assumed, which may lead to inaccurate results as shown by Oberkampf et al. [18]. Thus, epistemic variables are usually modeled using intervals derived from experimental data or expert judgment with lower and the upper bound. For example, the uncertainty in the closure coefficients for a particular turbulence model used in CFD simulations can be treated as epistemic in nature.

3. POINT-COLLOCATION NON-INTRUSIVE POLYNOMIAL CHAOS

The Point-Collocation non-intrusive polynomial chaos is derived from the polynomial chaos theory, which is based on spectral representation of uncertainty. In previous

years, many researchers have utilized polynomial chaos theory in stochastic computations. Importance of spectral representation of uncertainty lies in the fact that a stochastic response function can be decomposed into deterministic and stochastic components. Thus, for any stochastic response function α^*,

$$\alpha^*(\vec{x},\vec{\xi}) \approx \sum_{j=0}^{P} \alpha_j(\vec{x})\psi_j(\vec{\xi}), \tag{1.1}$$

where $\alpha_j(\vec{x})$ is the deterministic component and ψ_j is the random basis function corresponding to j^{th} mode. Generally, α^* can be a function of deterministic independent variable vector $\vec{x}$ and the n-dimensional standard random variable vector $\vec{\xi} = (\xi_1, \ldots, \xi_n)$. Theoretically, Eq. (1.1) should include infinite number of terms for absolute accuracy. However, for practicality purposes, a discrete sum is taken over a number of output modes. For a total order expansion, the number of output modes is given by:

$$N_t = P + 1 = \frac{(n+p)!}{n!p!}, \tag{1.2}$$

where p denotes the order of polynomial chaos and n is the number of random variables. The basis functions used in Eq. (1.1) are polynomials that are orthogonal with respect to a weight function $(p(\vec{\xi}))$ over the support region (R) of the input random variable vector. In terms of convergence of statistics, the Hermite polynomial is optimal for normal distribution whereas the Laguerre and Legendre polynomials are used for exponential and uniform input uncertainty distributions, respectively. Mathematical basis for the formulation of the polynomial basis functions is well explained by Hosder et al. [14].

The main objective of NIPC method is to obtain the polynomial coefficients without making any modification to the deterministic code i.e. treating it as a "black box". The coefficients are solely based on deterministic code evaluations. The coefficients and

orthogonality of the basis functions can be used to evaluate the statistics of the distribution for a stochastic function. For example, the zeroth mode of the expansion corresponds to the expected value of $\alpha^*(\vec{x},\vec{\xi})$, which is given by:

$$\mu_{\alpha^*} = \bar{\alpha}(\vec{x}) = \int_R \alpha^*(\vec{x},\vec{\xi}) p(\vec{\xi})\, d\xi = \alpha_0(\vec{x}). \tag{1.3}$$

Similarly, by inferring $\psi_0 = 1$ from Eq. (1.3), the variance of the distribution can be obtained as:

$$\sigma^2_{a^*} = Var[\alpha^*(\vec{x},\vec{\xi})] = \int_R (\alpha^*(\vec{x},\vec{\xi}) - \alpha_0(\vec{x}))^2 p(\vec{\xi})\, d\xi = \sum_{j=1}^{P} [\alpha_j^2(\vec{x}) \langle \psi_j^2(\vec{\xi})\rangle]. \tag{1.4}$$

We use the fact that $\langle \psi_j(\vec{\xi})\rangle = 0$ for $j > 0$ and $\langle \psi_i(\vec{\xi})\psi_j(\vec{\xi})\rangle = \langle \psi_j^2(\vec{\xi})\rangle \delta_{ij}$. Also, the inner product of $\psi_i(\vec{\xi})$ and $\psi_j(\vec{\xi})$ in the support region R is given by:

$$\langle \psi_i(\vec{\xi})\psi_j(\vec{\xi})\rangle = \int_R \psi_i(\vec{\xi})\psi_j(\vec{\xi}) p(\vec{\xi})\, d\xi. \tag{1.5}$$

Further, the strategy for point selection in random space for deterministic code evaluations depend upon the non-intrusive technique used. Three techniques often used are; Sampling based, Quadrature based and Point-Collocation based NIPC. In this paper, the focus is on using Point-Collocation method to obtain the surrogate model.

The collocation based NIPC starts with replacing uncertain variables of interest with their polynomial expansions derived from Eq. (1.1). Next, $P+1$ (N_t) vectors $(\vec{\xi}_i = \{\xi_1, \xi_2, \ldots, \xi_n\}_i, i = 0, 1, 2, \ldots, P)$ are chosen in design space with a Latin Hypercube (LH) structure for a given polynomial chaos expansion with number of modes evaluated using Eq. (1.2) and the deterministic code is evaluated at these points. LH design improves

the coverage of the design space when a small sample set is used. A linear system of equations can be obtained using the left-hand side of Eq. (1.1) evaluated from the solution of deterministic code at chosen random points:

$$\begin{pmatrix} \psi_0(\vec{\xi}_0) & \psi_1(\vec{\xi}_0) & \dots & \psi_P(\vec{\xi}_0) \\ \psi_0(\vec{\xi}_1) & \psi_1(\vec{\xi}_1) & \dots & \psi_P(\vec{\xi}_1) \\ \vdots & \vdots & \ddots & \vdots \\ \psi_0(\vec{\xi}_P) & \psi_1(\vec{\xi}_P) & \dots & \psi_P(\vec{\xi}_P) \end{pmatrix} \begin{pmatrix} \alpha_0 \\ \alpha_1 \\ \vdots \\ \alpha_P \end{pmatrix} = \begin{pmatrix} \alpha^*(\vec{x}, \vec{\xi}_0) \\ \alpha^*(\vec{x}, \vec{\xi}_1) \\ \vdots \\ \alpha^*(\vec{x}, \vec{\xi}_P) \end{pmatrix}. \tag{1.6}$$

Eq. (1.6) represents a linear system of equations which needs to be solved in order to determine the spectral modes α_k for the stochastic function α^*. Eq. (1.2) is considered as the minimum number of deterministic samples required to solve the linear system of equations. However, if more deterministic samples are available, the over determined system is solved using a least squares approach. The term Over-Sampling Ratio (OSR) denoted by n_p is related to Eq. (1.2) in the following manner:

$$N_t = n_p \times \frac{(n+p)!}{n!p!}. \tag{1.7}$$

Thus, an OSR of 1 corresponds to the minimum number of deterministic samples required. Hosder et al. [13] demonstrated through different stochastic model problems that an OSR of 2 is the optimum value. Once the spectral modes are evaluated, various statistics like the mean and the variance of the solution can be obtained as shown in Eqs. (1.3) and (1.4), respectively.

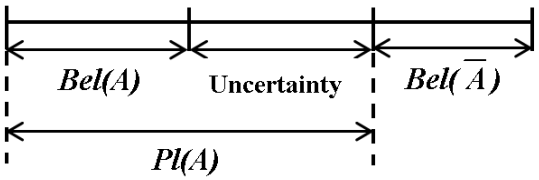

Figure 1.1. Schematic of belief and plausibility

4. DEMPSTER SHAFER THEORY OF EVIDENCE

This section summarizes the evidence theory which is traditionally used for pure epistemic analysis. The next section will extend this idea to perform mixed UQ analysis with NIPC based stochastic expansions and converting the aleatory uncertain variables into Dempster Shafer structures.

4.1. Fundamentals of Evidence Theory. In comparison to probability theory, evidence theory introduces two new measures of uncertainty, Belief (Bel) i.e. lower limit of probability and Plausibility (Pl) i.e. upper limit of probability. Evidence theory application involves the specification of $(\mathbb{U},\mathscr{U},m)$ where $\mathbb{U}$ denotes the universal set, $\mathscr{U}$ denotes the collection of subsets or set of focal elements of $\mathbb{U}$ and m is the Basic Probability Assignment (BPA), which can be viewed as the belief of the user of how likely it is that the uncertain input falls within the specified interval. BPA, a value between 0 and 1, can be assigned for any possible subset of the universal set based on experimentation or expert opinion. The advantage of this theory is that it does not assume any particular value within the interval and nor does it assign a specific distribution to the interval. Figure 1.1 illustrates that the axiom of additivity is not imposed, as the evidential measure for the occurrence and negation of an event does not have to sum to unity $(Bel(A)+Bel(\bar{A})\leq 1, Pl(A)+Pl(\bar{A})\geq 1, Bel(A)+Pl(\bar{A})=1)$ where $\bar{A}$ represents the negation of event A.

According to the definition, $m(\varepsilon)$ denotes the BPA corresponding to subset ε of $\mathscr{U}$. Any additional evidence supporting the claim that the uncertain variable lies within a subset of ε, say $B \subset \varepsilon$, must be assigned another non-zero BPA $m(B)$. Further, $m(\varepsilon)$ should satisfy following axioms of evidence theory:

- $m(\varepsilon) > 0$ for any $\varepsilon \in \mathscr{U}$,
- $m(\varepsilon) = 0$ if $\varepsilon \subset \mathbb{U}$ and $\varepsilon \ni \mathscr{U}$,
- $m() = 0$ where denotes an empty set,
- $\sum m(\varepsilon) = 1$ for all $\varepsilon \in \mathscr{U}$.

Once the uncertainty associated with the domain is characterized by an evidence space in the form of BPA's, an input sample space is constructed. For example, if $y = f(\vec{x})$ where $\vec{x} = [x_1, x_2, \ldots, x_n]$ with the evidence space defined as $(\mathbb{X}_i, \mathscr{X}_i, m_i)$, the input sample space is given by:

$$\mathbb{X} = \{x : x = [x_1, x_2, \ldots, x_n] \in \mathbb{X}_1 \times \mathbb{X}_2 \times \ldots \times \mathbb{X}_n\}. \tag{1.8}$$

Further for $\vec{x}$, the evidence space can be defined by $(\mathbb{X}, \mathscr{X}, m_X)$ where $\mathscr{X}$ is developed from the sets contained in Eq. (1.9):

$$\mathscr{C} = \{\varepsilon : \varepsilon = [\varepsilon_1, \varepsilon_2, \ldots, \varepsilon_n] \in \mathscr{X}_1 \times \mathscr{X}_2 \times \ldots \times \mathscr{X}_n\}. \tag{1.9}$$

Assumption that the x_i are independent, m_X is defined for subsets ε of $\mathbb{X}$:

$$m_X(\varepsilon) = \begin{cases} \prod_{i=1}^{n} m_i(\varepsilon_i) & \text{if} \quad \varepsilon = \varepsilon_1 \times \varepsilon_2 \times \ldots \times \varepsilon_n \in \mathscr{X} \\ 0 & \text{otherwise} \end{cases}, \tag{1.10}$$

Once the BPA's for input sample space in Eq. (1.8) are defined by Eq. (1.10), belief and plausibility for the output y with evidence space $(\mathbb{Y}, \mathscr{Y}, m_Y)$ can be evaluated as:

$$Bel_Y(\varepsilon) = \sum_{\mathscr{S}|\mathscr{S}\subseteq f^{-1}(\varepsilon)} m_X(\mathscr{S}), \tag{1.11}$$

$$Pl_Y(\varepsilon) = \sum_{\mathscr{S}|\mathscr{S}\cap f^{-1}(\varepsilon)\neq} m_X(\mathscr{S}), \tag{1.12}$$

where $m(\mathscr{S})$ is the likelihood associated with $\mathscr{S}$ that cannot be further assigned to specific subsets of $\mathscr{S}$.

As no assumptions were made to calculate these measures, *Bel* and *Pl* provide a more realistic uncertainty structure consistent with the given evidences. It is clear from Eqs. (1.11) and (1.12), belief is the minimum likelihood associated with an event i.e. the sum of BPA's of the propositions that totally agree with the event and plausibility is the maximum likelihood associated with an event i.e. the sum of BPA's of the propositions that agree partially and totally with the event. The evidence theory statistics can be summarized in terms of Cumulative Belief Function & Cumulative Plausibility Function (CBF & CPF) and Complementary Cumulative Belief Function & Complementary Cumulative Plausibility Function (CCBF and CCPF). Figure 1.2 below shows an example of these uncertainty measures obtained through the application of DSTE.

Let the uncertainty in y be characterized by the evidence space $(\mathbb{Y}, \mathscr{Y}, m_Y)$, consequently the evidence theory statistics can be defined as follows:

$$\text{CBF} = [\rho, Bel_Y(f^{-1}(\mathbb{Y}_\rho^c))], \rho \in \mathbb{Y}, \tag{1.13}$$

$$\text{CCBF} = [\rho, Bel_Y(f^{-1}(\mathbb{Y}_\rho))], \rho \in \mathbb{Y}, \tag{1.14}$$

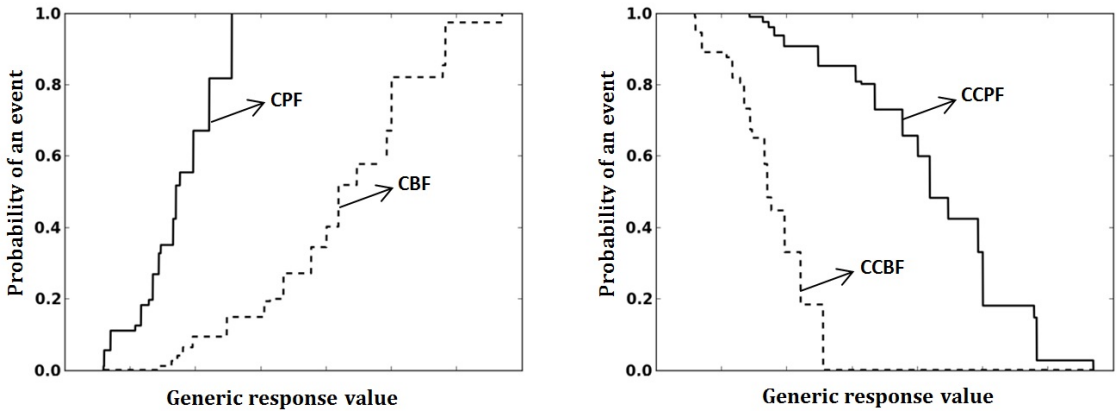

Figure 1.2. Example of cumulative and complementary cumulative belief and plausibility functions

$$\text{CPF} = [\rho, Pl_Y(f^{-1}(\mathbb{Y}_\rho^c))], \rho \in \mathbb{Y}, \tag{1.15}$$

$$\text{CCPF} = [\rho, Pl_Y(f^{-1}(\mathbb{Y}_\rho))], \rho \in \mathbb{Y}, \tag{1.16}$$

where $\mathbb{Y}_\rho = \{y : y \in \mathbb{Y} \quad \text{and} \quad y > \rho\}$ and $\mathbb{Y}_\rho^c = \{y : y \in \mathbb{Y} \quad \text{and} \quad y \leq \rho\}$. Detailed explanation of the evidence theory with numerical examples has been provided by Oberkampf et al. [18] and Nikolaidis et al. [19].

4.2. Rule for Combination of Evidences. Dempster Shafer theory is capable of handling data from a single source or multiple sources for an uncertain variable with the only assumption that the different sources and the random variables are independent of each other. Information from different sources is aggregated using the *rules of combination* to further evaluate the evidence theory uncertainty measures. The detailed explanation for the rules of combination is beyond the scope of this paper and can be referred from the research work of different authors [20, 5, 3]. In this study, the mixing or averaging rule of combination is implemented which generalizes the averaging operation used for probability distributions. The formula for the mixing combination rule is given by:

$$m_{1\ldots n}(A) = \frac{1}{n}\sum_{j=1}^{n} w_j m_j(A), \tag{1.17}$$

where $m'_j s$ are the BPA's for belief structures being aggregated and $w'_j s$ are the weights assigned according to the reliability of the sources. For demonstration purposes, the weights are assumed to be 1 for the examples presented in Section 6. However, Eq. (1.17) can be effectively used to incorporate the reliability or the confidence that can be associated with any of the sources.

5. APPROACH FOR MIXED UQ USING DSTE AND STOCHASTIC EXPANSIONS

In this section, the implementation of the stochastic response surfaces based on NIPC (Section 4) is described in DSTE for mixed UQ. The stochastic response surface will be used as a surrogate for the deterministic code with the overall objective of reducing original function evaluations, which can be expensive. The flow chart in Figure 1.3 describes the integration procedure of NIPC into DSTE and steps to compute belief and plausibility structures.

5.1. Aleatory Uncertainty Representation in Terms of Dempster Shafer Structures. Although Dempster Shafer theory is primarily used for epistemic uncertainty quantification, there may be instances when aleatory uncertainties are present in the model along with the epistemic. One may choose to segregate the aleatory uncertainties and treat them within an inner loop. This may result in multiple belief and plausibility structures as shown by Eldred et al. [12] or one may choose to discretize the aleatory variables into sets of intervals according to their respective probability distributions. In this paper, the focus is on the latter option of discretizing the aleatory variables into sets of intervals and assign BPA's to each interval based on the probability distribution. Figure 1.4 shows an example

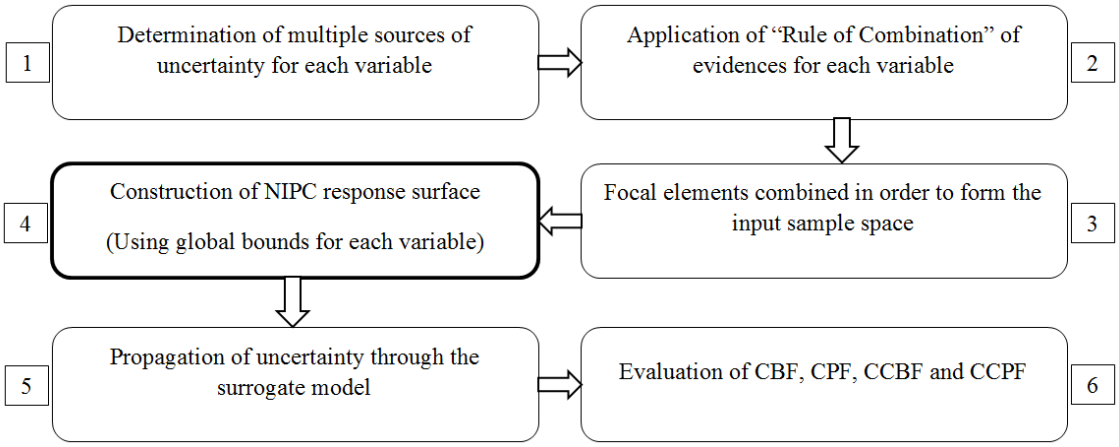

Figure 1.3. Flowchart for utilization of NIPC methodology for evidence theory

of the discretization process for the normal (left plot) and uniform (right plot) distributions. The same kind of analysis (as presented in this paper) can be carried out for any general dsistribution to formulate the optimum number of intervals equation.

The discretization process depends upon the amount of information needed by the Dempster Shafer structure to accurately cover the uncertainty domain. For example, a random variable with uniform distribution between 0.3 and 0.7 as lower and upper bounds, respectively can be divided into *n* number of intervals with an equal BPA of 1/n assigned to each sub-interval. In order to discretize a random variable with normal distribution, one needs to characterize the same with a lower bound and an upper bound. The left plot in Figure 1.4 shows a standard normal distribution i.e. with 0 mean $(\mu = 0)$ and 1 standard deviation $(\sigma = 1)$. As per the theory, for a normally distributed random variable with mean μ and σ as the standard deviation, 99.7% of the area under the curve is within $\mu \pm 3\sigma$. Hence, this can be treated as a benchmark for bounding all the normal variables in any analysis. However, the BPA should be assigned to each sub-interval according to the Gaussian distribution by solving the definite integral in Eq. (1.18).

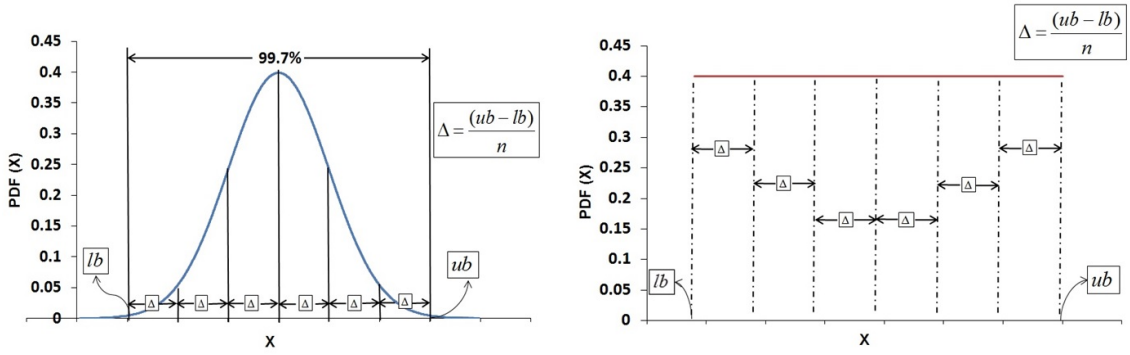

Figure 1.4. Discretization of normal and uniform variable distributions; standard normal distribution with $\mu = 0$ and $\sigma = 1$ (left plot), uniformly distributed variable with lower and upper bounds [0.3, 0.7] (right plot)

$$P(a < X < b) = \int_a^b f(X)dx \quad \text{where} \quad f(X) = \frac{1}{\sigma\sqrt{2\pi}} \exp \frac{-(X-\mu)^2}{2\sigma^2}, \tag{1.18}$$

where a and b denote the upper and lower bounds of the sub-interval and $P(a < X < b)$ denotes the probability of X between a and b.

Theoretically, infinite number of intervals for the aleatory variables with appropriate BPA's will accurately represent the uncertainty domain. However, we focus on determining the optimum number of subintervals needed to accurately represent the aleatory domain. Within a different perspective, suppose that the epistemic interval is modeled with a single interval with 100% BPA. As the number of subintervals for the aleatory variable in the analysis are increased, the results (belief & plausibility) will tend to approach the Second Order Probability (SOP) measures (upper and lower bounds for Cumulative Distribution Function (CDF)). The SOP [17] method uses a double loop for mixed uncertainty propagation: inner aleatory loop and outer epistemic loop. In the outer loop, a specific value for the

epistemic variable is prescribed and passed on to the inner loop. Any traditional aleatory uncertainty method may then be used to perform aleatory uncertainty analysis in the inner loop. SOP provides the interval bounds for the output variable of interest at different probability levels. The SOP method is widely used for mixed uncertainty quantification with a single interval for the epistemic variable. In this paper, DSTE is utilized since it can handle multiple sources with different BPA's for the characterization of epistemic variables.

5.2. Evidence Theory Analysis. Once the aleatory variables are represented as Dempster Shafer structures, the procedure described in the flow chart (Fig. 1.3) is followed, where the first step is to interpret data for each variable from different sources and to define a matrix for identifying intervals with non-zero evidences. These intervals are referred to as 'focal elements' of each variable in DSTE terminology. The next step is to combine the evidences for each uncertain variable using Eq. (1.17). This will lead to step 3 wherein the input sample space is constructed in the form of different combinations of the focal elements from each uncertain variable using Eq. (1.8). Consequently, the composite BPA for each combination in the input sample space is evaluated using Eq. (1.10), which is the product of the BPA's of individual focal elements. The 4^{th} step is to construct the stochastic surface based on Point-Collocation NIPC to be used as a surrogate for the response as mentioned in Section 4. The response surface is created within the global bounds (global minimum and global maximum) for each uncertain variable. Step 5 is to propagate the uncertainty through the surrogate model which involves finding the minimum and maximum response values for each input sample space. This can be accomplished using two different approaches: sampling or optimization.

5.2.1. Sampling approach. Akram et al. [21] compared Monte Carlo simulation and evidence theory approach for technology portfolio planning. Their work presented the impact of sample size, uncertainty quantification method selection and combination rule

selection. Helton [22] used a sampling approach for the representation of epistemic uncertainty in his work. First, hundreds of thousands of samples were chosen in the domain (e.g., for each input sample space) and the samples with minimum and maximum response values were treated as the bounds of that particular sample space. However, accuracy of the sampling approach is highly dependent on the number of samples chosen for the analysis. This method would eventually become computationally expensive with the increase in the number of variables and the uncertainty information per variable. To overcome the computational costs, the optimization procedure is implemented to find the minimum and maximum response.

5.2.2. Interval optimization approach (implemented in the proposed methodology). As the epistemic uncertainties are characterized by lower and upper bounds, bound-constrained optimization is performed within each input sample space. Limited memory Broyden-Fletcher-Goldfarb-Shanno Bound constrained optimization (L-BFGS-B [23]); a local gradient-based solver is used for interval minimization and maximization which uses the BFGS update to approximate the inverse Hessian matrix. Thus, we perform two different optimizations: one for the minimum response and the other for the maximum response. This procedure is computationally efficient as compared to the sampling approach and also the accuracy is improved. An important point to note is that the optimization is performed using the surrogate model which further reduces the computational cost.The uncertain variables are transformed into their respective standard random variable bounds within each input sample space before the optimization procedure. Mathematically, the bound constrained problem can be expressed as follows:

$$\begin{array}{ll} \text{minimize/maximize} & f(\vec{\xi}) \\ \text{subject to} & \vec{\xi}_L \leq \vec{\xi} \leq \vec{\xi}_U \end{array}^{,}$$

where $f(\vec{\xi})$ is the required response value, $\vec{\xi}_L$ and $\vec{\xi}_U$ correspond to lower and upper bounds of the standard random variable. The final step is to calculate the belief and plausibility structures using the minimum and maximum response values according to Eqs. (1.11) and (1.12).

The advantage of using NIPC as the surrogate of the response can be understood especially for high fidelity simulations if the output statistics are approximated accurately with a second degree polynomial. In such cases, we can directly use Newton's optimization method which would require 1 iteration to optimize the NIPC response surface due to its Taylor series approximation. In this manner, one can even reduce the NIPC function evaluations along with the original function evaluations.

6. ANALYSIS FOR OPTIMUM DISCRETIZATION OF ALEATORY VARIABLES

In order to provide a baseline for discretization of an aleatory uncertain variable and quantify the number of subintervals required to accurately represent the aleatory uncertainty, a numerical analysis based on mixed UQ using evidence theory is presented. Numerous combination of uncertain variables (normal or uniform) have been adopted for the analysis in two multi-dimensional test functions; 1. exponential function and 2. Runge function. These problems have been widely used as challenge problems due to the inherent nature of variation which is feasible for any optimization algorithm testing. A stochastic response surface based on Point-Collocation NIPC as explained in Section 4 is implemented as the surrogate model for each of the test functions. At first, NIPC order convergence is achieved in order to demonstrate the efficiency of DSTE with NIPC.

Mathematically, the two test functions are given by:

- Exponential function

$$Y1 = f1(\vec{x}) = \exp\left\{ -\sum_{i=0}^{n-1} \frac{1}{i+1} x_i \right\}, \tag{1.19}$$

- Runge function

$$Y2 = f2(\vec{x}) = \frac{1}{1 + \sum_{i=1}^{n} x_i^2}, \tag{1.20}$$

where n represents the number of random variables.

6.1. NIPC Order Convergence. We study the NIPC order convergence with the exponential function in Eq. (1.19) including 8 input variables (x_i with $i = 0, 1, \ldots, 7$) and the Runge function in Eq. (1.20) consisting of 4 input variables (x_i with $i = 1, 2, \ldots, 4$), characterized by purely epistemic multiple source uncertainty. $Y1$ and $Y2$ denote the system responses, respectively. The input uncertainty information for both test functions is given in Tables 1.1 and 1.2.

The evidence theory analysis is carried out for both test functions as explained in Section 5-5.2. There are 7680 and 96 combinations in the input sample space structure for the exponential and the Runge function, respectively. The NIPC response surface was constructed based on the global bounds for each uncertain variable. For example, x_0 in Table 1.1 has 2 sources of uncertainty with 1 interval from the first source and 3 intervals from the second. Using these intervals, we choose the global minimum i.e. 0.1 as the lower bound and the global maximum i.e. 0.9 as the upper bound for x_0. Similarly, choosing the global bounds for the other variables, NIPC order convergence analysis is conducted. An over sampling ratio of 2 is utilized and the linear system of equations in Eq. (1.6) is solved using least squares approach. The DSTE analysis results for both test problems are presented in Figure 1.5.

Table 1.1. Input uncertainty information for the exponential function *(The format for uncertainty information is: '[lower bound, upper bound]' BPA (%)'*

Variable	**Source 1**	**Source 2**	**Source 3**
x_0	[0.6, 0.9] 100%	[0.1, 0.3] 33%	-
		[0.4, 0.6] 34%	-
		[0.5, 0.9] 33%	-
x_1	[0.2, 0.3] 50%	[0.0, 0.6] 70%	[0.1, 0.4] 100%
	[0.4, 0.5] 50%	[0.5, 0.9] 30%	-
x_2	[0.1, 0.5] 40%	[0.3, 0.8] 100%	[0.4, 0.5] 100%
	[0.6, 0.9] 60%		-
x_3	[0.1, 0.4] 100%	[0.3, 0.7] 100%	-
x_4	[0.2, 0.4] 100%	[0.5, 0.8] 20%	-
		[0.7, 0.9] 80%	-
x_5	[0.1, 0.3] 100%	[0.2, 0.5] 100%	[0.3, 0.6] 30%
			[0.7, 1.0] 70%
x_6	-	[0.1, 0.5] 100%	[0.3, 0.6] 100%
x_7	[0.2, 0.8] 100%	-	[0.7, 0.9] 100%

Table 1.2. Input uncertainty information for the Runge function

Variable	**Source 1**
x_1	[0.6, 0.9] 30%, [0.2, 0.4] 20%, [0.1, 0.5] 40%, [0.9, 1.0] 10%
x_2	[2.1, 3.5] 30%, [1.5, 3.0] 40%, [1.0, 2.0] 30%
x_3	[0.12, 0.25] 20%, [0.3, 0.6] 25%, [0.1, 0.4] 15%, [0.5, 0.9] 40%
x_4	[0.4, 0.6] 40%, [0.3, 0.8] 60%

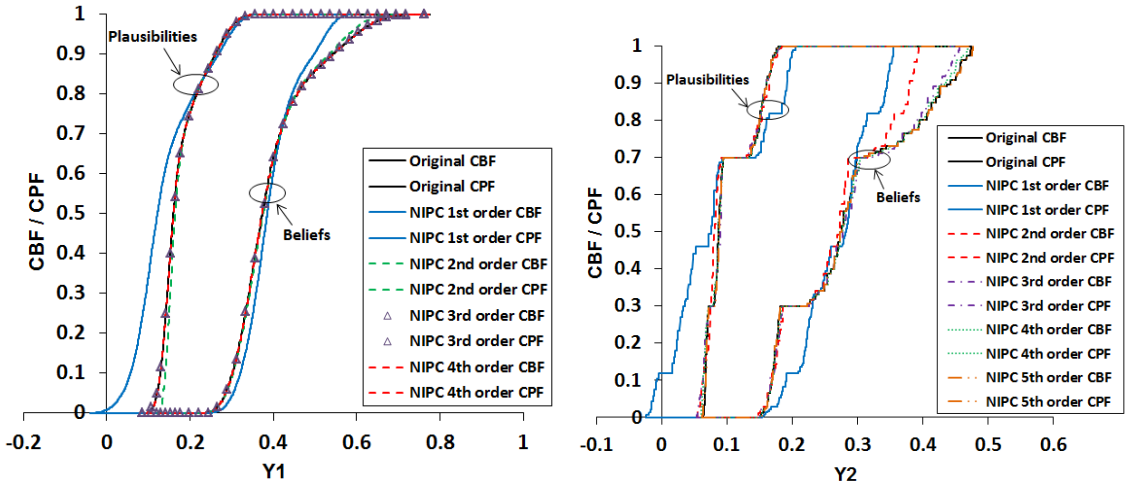

(a) Exponential function (b) Runge function

Figure 1.5. Results for DSTE with NIPC

It is evident that as the polynomial degree increases, the accuracy of the approximation increases. In order to quantify accuracy, the error in area is defined as integral of absolute difference between the original function value $Y_{org}(z)$ and NIPC response value $Y_{nipc}(z)$ at z^{th} belief / plausibility level. Mathematically it can be represented as given in Eq. (1.21) and the integral is evaluated numerically. Further, the error is scaled with respect to the error in 1^{st} order NIPC approximation. Error convergence plots are shown in Figure 1.6.

$$Error = \int_0^1 |Y_{org}(z) - Y_{nipc}(z)|dz. \tag{1.21}$$

The 95% Confidence Interval (CI) is evaluated in terms of belief and plausibility measures. The lower bound of CI is represented by the response value at 2.5% plausibility level and the upper bound is indicated by 97.5% belief level. Tables 1.3 and 1.4 show the convergence summary for different NIPC orders as compared to the original function

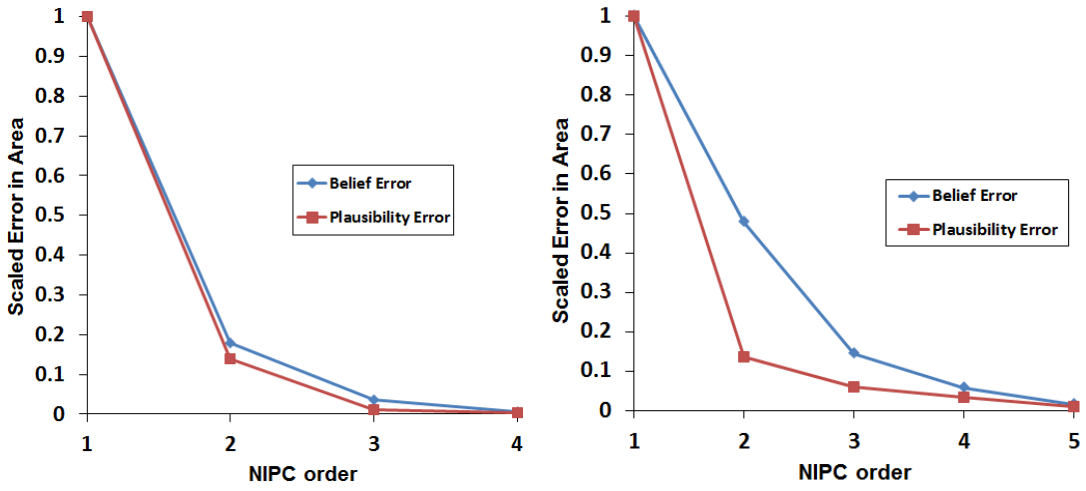

(a) Exponential function (b) Runge function

Figure 1.6. Error convergence results using Eq. (1.21)

statistics. This gives a good comparison basis to show the computational efficiency achieved through the use of stochastic expansions.

Based on the results of the polynomial order convergence study, a 3^{rd} order expansion is used for the exponential function and a 4^{th} order expansion for the Runge function in further analysis for computational efficiency as the results are within acceptable limits of accuracy for demonstration purposes ($< 4\%$ difference). It is certain that the final results for the minimum number of discretized intervals required for an aleatory variable will not be affected. 330 original function evaluations are needed to construct an inexpensive 3^{rd} order NIPC response surface for the exponential function over the uncertainty domain as opposed to 82496 crude deterministic evaluations. Similarly, 140 original function evaluations will be needed in order to represent the Runge function accurately. Thus, Point-Collocation NIPC is an effective and computationally efficient uncertainty propagation tool even in case of multiple sources of uncertainties.

Table 1.3. Exponential function: convergence of 95% CI with increasing NIPC order

	Exponential function		
Case (Response used in optimization)	# of original function evaluations	95% CI results	% Difference
Original function	82496	[0.1151, 0.6348]	-
order 1	18	[0.0209, 0.5421]	[138.53, 15.75]
order 2	90	[0.1325, 0.6170]	[14.05, 2.84]
order 3	330	[0.1125, 0.6310]	[2.28, 0.60]
order 4	990	[0.1154, 0.6344]	[0.26, 0.06]

Table 1.4. Runge function: convergence of 95% CI with increasing NIPC order

	Runge function		
Case (Response used in optimization)	# of original function evaluations	95% CI results	% Difference
Original function	1046	[0.0645, 0.4729]	-
order 1	10	[-0.0160, 0.3548]	[162.46, 28.54]
order 2	30	[0.0548, 0.3927]	[11.42, 18.53]
order 3	70	[0.0558, 0.4541]	[10.18, 4.06]
order 4	140	[0.0613, 0.4669]	[3.63, 1.28]
order 5	252	[0.0632, 0.4754]	[1.46, 0.53]

Table 1.5. Combination of uncertain variables studied for optimum interval discretization

Case	Description
1	1 Epistemic (single source with 100% BPA) and 1 aleatory variable
2	1 Epistemic (single source with 100% BPA) and multiple aleatory variables ($2, 4, 6$ and 8)
3	1 Epistemic (multiple sources) and 1 aleatory variable
4	2 Epistemic (single source with 100% BPA each) and 1 aleatory variable
5	2 Epistemic (single source with 100% BPA each) and 2 aleatory variables
6	2 Epistemic (multiple sources) and 2 aleatory variables

6.2. Optimum Number of Intervals for Representing Aleatory Domain. This study will provide an overview of different parameters affecting the number of subintervals needed to accurately represent aleatory variables in terms of Dempster Shafer structures. The parameters (listed below) and different cases considered for the numerical analysis are summarized in Table 1.5.

1. Number of aleatory variables
2. Number of epistemic variables
3. Number of sources for epistemic variables
4. Distribution of the aleatory variables (normal and uniform distributions studied)

Note that cases $1, 2, 4$ and 5 are with single source epistemic uncertainty with 100% BPA. These cases are specifically chosen so as to be compared with the SOP results and present the error convergence based on Eq. (1.21). For cases 3 and 6, which exhibit multiple source epistemic uncertainty, the analysis is based on the asymptotic convergence of relative error between successive iterations as the number of subintervals for the aleatory

Table 1.6. Uncertainty information for the cases described in Table 1.5 ($k = 0$ for Exponential function and $k = 1$ for Runge function)

Case	**Aleatory uncertainty** [No. of subintervals per variable per iteration]	**Epistemic uncertainty**
1	x_k: $N(2.5, 0.15)$ or $U(3.5, 5.5)$ $[5, 15, 50, 75, 100, 125]$	x_{k+1} : $[0.1, 1.0]100\%$
2	x_k to $x_i (i = 2, 4, 6, 8)$: $N(2.5, 0.15)$ or $U(0.5, 1.5)$ For $i = 2$: $[5, 15, 50, 75, 100, 125]$ For $i = 4$: $[5, 10, 15, 25, 30, 35]$ For $i = 6$: $[2, 4, 6, 8, 10]$ For $i = 8$: $[2, 3, 4, 5]$	x_p : $[0.1, 1.0]100\%$ p: total number of variables
3	x_k: $N(2.5, 0.15)$ or $U(3.5, 5.5)$ $[5, 15, 50, 75, 100, 125]$	x_{k+1} : $[0.1, 0.4]30\%$, $[0.3, 0.7]40\%, [0.8, 0.9]30\%$
4	x_k: $N(2.5, 0.15)$ or $U(3.5, 5.5)$ $[5, 15, 50, 75, 100, 125]$	x_{k+1} : $[0.1, 1.0]100\%$ x_{k+2} : $[2.0, 3.5]100\%$
5	x_k and x_{k+2} $N(2.5, 0.15)$ or $U(3.5, 5.5)$ $[5, 15, 50, 75, 100, 125]$	x_{k+1} : $[0.1, 1.0]100\%$ x_{k+3} : $[2.0, 3.5]100\%$
6	x_k: $N(2.5, 0.15)$ or $U(0.5, 1.5)$ x_{k+2}: $N(2.5, 0.15)$ or $U(0.5, 1.5)$ $[5, 15, 50, 75, 100, 125]$	x_{k+1} : $[0.1, 0.4]20\%$, $[0.35, 0.6]40\%, [0.7, 1.2]40\%$ x_{k+3} : $[0.2, 0.5]30\%$, $[0.9, 1.5]40\%, [0.6, 1.0]30\%$

variable are increased. Table 1.6 provides the uncertainty information for both test problems (Exponential and the Runge function).

Evidence theory analysis using NIPC response surface is carried out for each case, starting with particular number of subintervals for aleatory variables. For iterative convergence, 5 subintervals are chosen for each aleatory variable in case of $1, 2$ and 4 aleatory variables per analysis and increase it by 5 at every iteration. Similarly, in case of 6 and 8 aleatory variables, 2 subintervals are chosen. The difference in choosing initial number of subintervals is due to the fact that the combined BPA of more number of variables is

expected to be smaller due to the multiplicative effect for the product space expressed in Eq. (1.10). As two aleatory distributions are studied in this paper, the mathematical functions are tested for each case with 1 aleatory distribution at a time which will enable us to compare the interval discretization for both distributions.

6.3. An Exponential Decay Model for Predicting Error Convergence. As the number of aleatory variables increase, the analysis for error convergence becomes more and more expensive in terms of number of combinations in the input sample space. This subsection will describe an exponential decay model which can predict the convergence based on initial 3 to 4 error evaluations. This is especially useful in problems with higher dimensions which is computationally expensive otherwise. For example, in the present analysis, the decay model is used to predict the error convergence for the cases with 4, 6 and 8 aleatory variables. The decay model is given by:

$$Err_p = E_0 \times \frac{1}{1 - \exp(\frac{-N}{k})}, \tag{1.22}$$

where Err_p is the predicted error, E_0 and k are constants based on initial error evaluations, and N is the number of subintervals.

The constants are evaluated by minimizing the sum of squares of differences between the initial error evaluations and predicted error values for the same number of subintervals. A Generalized Reduced Gradient (GRG) solver was used to minimize the sum of squares in this analysis. Once they are evaluated, the error prediction model can be used for different number of intervals N, being the only variable in Eq. (1.22).

Figures 1.7 and 1.8 show the error convergence for both test functions in terms of increasing subintervals. The most important parameter affecting the choice of number of subintervals is the number of aleatory variables in the design problem. The other three parameters i.e. distribution of aleatory variables, number of sources for the epistemic

Table 1.7. Optimum number of intervals for each case

Description	N_{opt}
1 Epistemic (single source with 100% BPA) and 1 aleatory variable	75
1 Epistemic (single source with 100% BPA) and multiple aleatory variables (2, 4, 6 and 8)	(50, 40, 20,and 12) respectively)
1 Epistemic (multiple sources) and 1 aleatory variable	75
2 Epistemic (single source with 100% BPA each) and 1 aleatory variable	75
2 Epistemic (single source with 100% BPA each) and 2 aleatory variables	50
2 Epistemic (multiple sources) and 2 aleatory variables	50

variables and number of epistemic variables seemed to have minimal effect with decreasing order of sensitivity. As a result, the analysis focus was shifted towards the number of aleatory variables and optimum number of intervals were formulated. It can also be inferred that the increase in number of subintervals and thereby the accuracy of the approximation, will be accompanied with increased computational time and effort. Thus, a trade off needs to be made between the required accuracy and the computational efficiency.

In case of 1 and 2 aleatory variables, deciding the number of subintervals required is straightforward as the number of intervals at which the convergence achieved is evident. For higher dimensions i.e. 4, 6 and 8 variable cases, the minimum number of subintervals are chosen at a point where there is approximately 90% reduction in error as compared to the first iteration. Increasing the number of intervals beyond this point will be considered infeasible in terms of reduction in error with significant increase in number of combinations for DSTE analysis. Table 1.7 lists the optimum number of subintervals for each case which is the minimum recommended to cover the aleatory uncertainty domain.

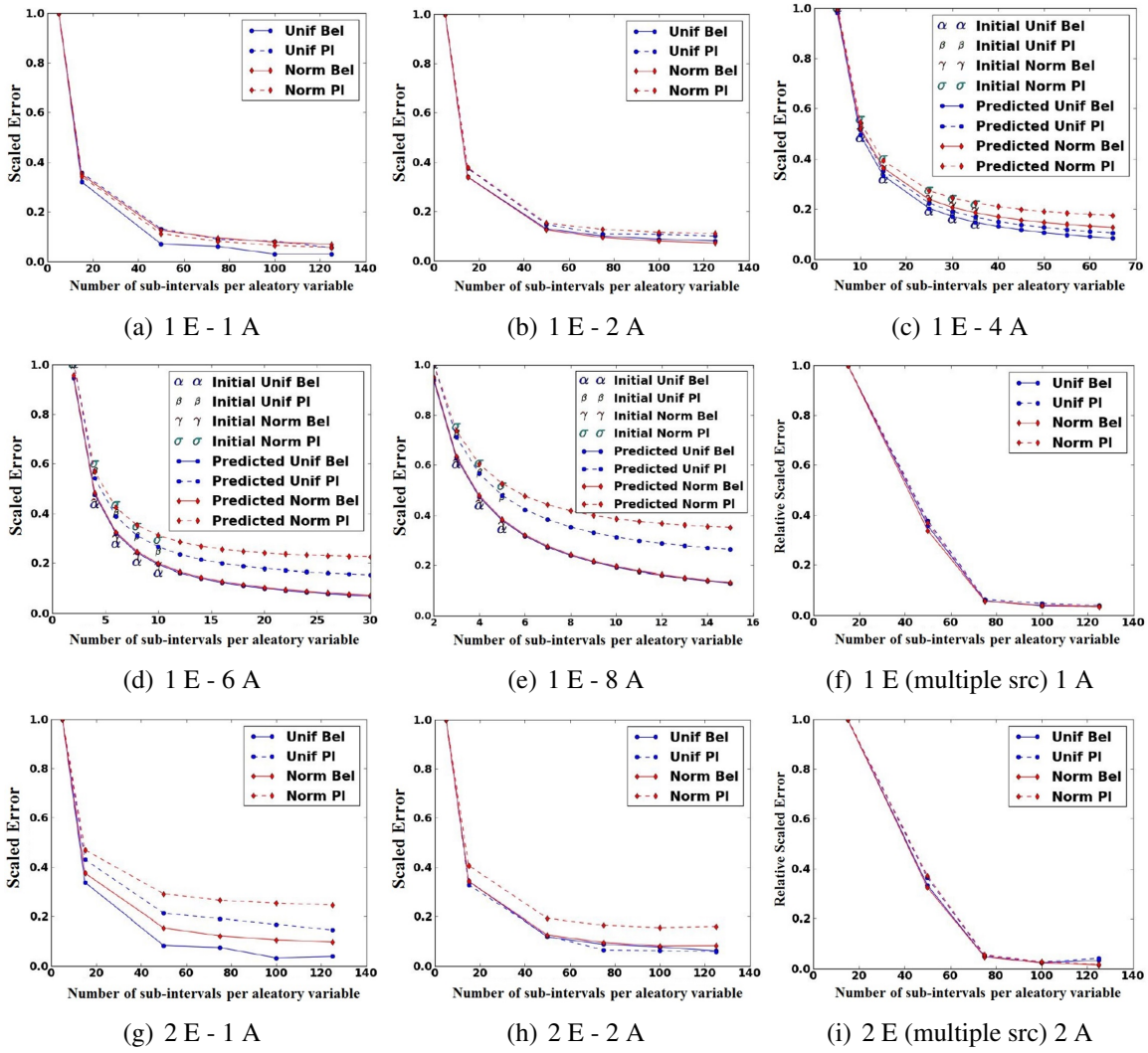

(a) 1 E - 1 A (b) 1 E - 2 A (c) 1 E - 4 A

(d) 1 E - 6 A (e) 1 E - 8 A (f) 1 E (multiple src) 1 A

(g) 2 E - 1 A (h) 2 E - 2 A (i) 2 E (multiple src) 2 A

Figure 1.7. Exponential function error convergence (a)-(i) with normal and uniform distributions for aleatory variables (E:epistemic variable, A: aleatory variable)

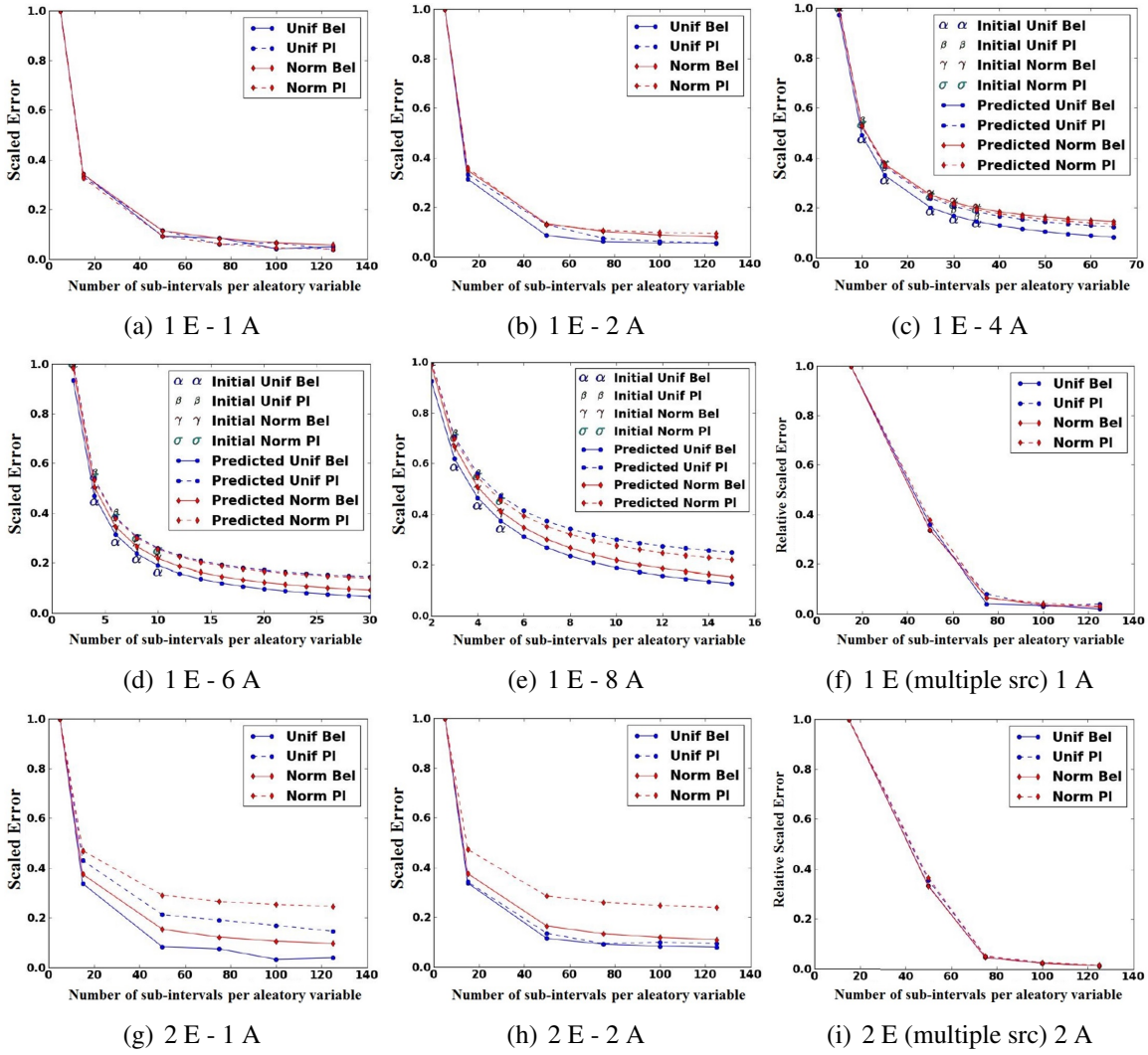

(a) 1 E - 1 A (b) 1 E - 2 A (c) 1 E - 4 A

(d) 1 E - 6 A (e) 1 E - 8 A (f) 1 E (multiple src) 1 A

(g) 2 E - 1 A (h) 2 E - 2 A (i) 2 E (multiple src) 2 A

Figure 1.8. Runge function error convergence (a)-(i) with normal and uniform distributions for aleatory variables (E:epistemic variable, A: aleatory variable)

In case of odd number of uncertain aleatory variables, the optimum number of subintervals can be evaluated using interpolation. The optimum number of subintervals should be interpreted as a good enough approximation to accurately represent an uncertain aleatory variable. The accuracy can always be improved by taking more number of subintervals per variable and /or by increasing the ± 3 standard deviation limit to ± 6 for a normal random variable if the computational architecture permits. In case of huge number of uncertain variables, advanced dimension reduction techniques based on sensitivity analysis may be adopted.

6.4. The Effect of the Distribution Type on Aleatory Interval Discretization. As the distributions of aleatory variables vary, the contribution of each discretized interval also varies. Error convergence plots in Figures 1.7 and 1.8 imply two mathematical conclusions: (1) the error while discretizing the uniform variable is less as compared to that of the normal variable due to the truncation effect at the tail region and (2) after a certain number of subintervals, the rate of decrease in error is not as prominent for a normal variable as compared to an uniform variable. This is mainly due to the fact that as the number of subintervals increase, the resulting BPA's for most of the intervals is derived from the tail regions which has a minimal probability value.

In case there are random variables with different distributions in the design problem, which is the most practical case, a relation can be proposed to identify the number of subintervals for each distribution:

$$\tilde{N}_{opt} = \frac{N_{opt}}{\text{number of distributions}}, \tag{1.23}$$

where $\tilde{N}_{opt}$ represents the number of subintervals for each distribution, N_{opt} corresponds to the case of total number of aleatory variables in the problem under consideration and 'number of distributions' in this paper is adopted as 2. This proposition is based on the

numerical experiments performed in the previous section where two types of distributions were studied (normal and uniform). Each of these distributions represented the complete aleatory domain in the problem. In case of multiple distributions in a specific problem, the aleatory domain is shared by those distributions and hence the optimum number of intervals required to represent the domain can be divided between the participating distributions.

Now the question is that which distribution should be given more preference in terms of number of intervals in case of multiple distributions? Using the fact that the normal variable contributes less as compared to a uniform variable with same number of subintervals and based on the numerical analysis performed, the required number of subintervals can be reduced for the normal variable by approximately 20% of $\tilde{N}_{opt}$. For example, evaluating Eq. (1.23) for a specific problem yields an $\tilde{N}_{opt}$ of say 25, the required number of subintervals for the normal variable can be reduced by $25 \times 0.2 = 5$ intervals i.e. the variable divided into 20 subintervals. However, in order to cover the aleatory domain after the correction for the normal variable, the number of subintervals for the uniform are increased by the same amount (i.e. $\tilde{N}_{opt}$ for uniform variable will be 30). This point will be clear in the next subsection and Section 7 where the implementation of Eq. (1.23) is demonstrated and verified.

6.5. Demonstration of Difference Between DSTE and Pure Interval Analysis. One approach in epistemic uncertainty quantification is to approximate the range of output uncertainty by adopting the interval defined by the global minimum and maximum of the input uncertainty. Ignoring the multiple sources of information for the input uncertainty may provide a conservative estimation of the output uncertainty. This subsection provides a comparison between pure interval analysis and the Evidence theory with the proposed methodology. The Runge test function is reconsidered with the uncertainty information as presented in Table 1.8.

Table 1.8. Input uncertainty information for the Runge function for comparison with pure interval approximation

Variable	Distribution	Uncertainty information
x_1	Uniform	(0.5, 1.5)
x_2	Epistemic	Source 1: [1.5, 2.0] 30%, [1.7, 2.5] 40%, [2.1, 3.0] 30%
x_3	Epistemic	Source 1: [0.2, 0.6] 70%, [0.55, 0.85] 30%
x_4	Normal	(2.5, 0.15)

Two different analyses are carried out for the above problem: (1) SOP analysis by choosing global bounds for both the epistemic variables (i.e. $[1.5, 3.0]$ for x_2 and $[0.2, 0.85]$ for x_3) and (2) Evidence theory analysis for mixed uncertainty incorporating the information from the sources. Note that for both methods; SOP and DSTE, a fourth-order chaos expansion was chosen in order to propagate the uncertainty. The number of original function evaluations required were 140, evaluated using Eq. (1.7) with an OSR of 2. Ideally, using Eq. (1.23), $\tilde{N}_{opt}$ is evaluated as 25 which corresponds to the number of subintervals needed for each distribution. After the correction is implemented for the normal variable, the number of subintervals are obtained as 20 and 30 for normal and uniform, respectively. For the purpose of convergence demonstration, five different cases for number of subintervals is summarized in Table. 1.9 with results plotted in Figure 1.9.

It shows that the interval analysis provides us with a conservative or over-prediction of the uncertainty range. However, an important point to note is that the global bounds of the uncertainty range does match with the pure interval analysis results which is due to the fact that the uncertainty domain (i.e. the minimum and maximum bound) is unchanged. The response values using DSTE analysis and pure interval analysis are compared at different levels in Table 1.10.

Case	Normal	Uniform
1	2	5
2	5	10
3	10	15
4	**20**	**30**
5	25	40

Table 1.9. Number of intervals for aleatory variables

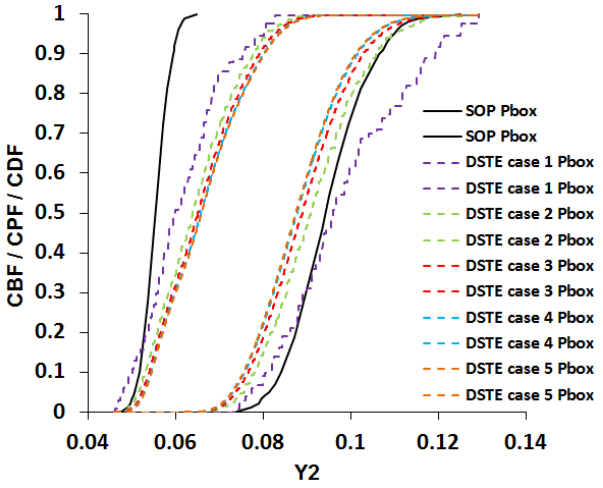

Figure 1.9. SOP and DSTE results for Runge function

Table 1.10. UQ results for the Runge function

Probability / Belief / Plausibility level	**Pure interval analysis** [Lower bound, Upper bound]	**DSTE analysis** [Plausibility, Belief]
0	[0.04765, 0.07377]	[0.04611, 0.06754]
2.5%	[0.04987, 0.07926]	[0.05167, 0.07101]
25%	[0.05337, 0.08847]	[0.05835, 0.08092]
50%	[0.05543, 0.09429]	[0.06577, 0.08768]
75%	[0.05746, 0.10031]	[0.07316, 0.09489]
97.5%	[0.06108, 0.11235]	[0.08624, 0.10911]
100%	[0.06477, 0.12489]	[0.09241, 0.12915]

Table 1.11. Input uncertainty information for the Rosenbrock function

Variable	Distribution	Uncertainty information
x_1	Uniform	[-2.048, 2.048]
x_2	Normal	$(N[0.215, 0.04])$
x_3	Epistemic	Source 1: [-3.7, 2.0] 50%, [1.5, 4.5] 50% Source 2: [0.0, 2.5] 33.34%, [-5.0, -1.7] 33.33%, [3.7, 5.0] 33.33% Source 3: [1.25, 4.15] 35%, [-2.9, 1.4] 65%

7. DEMONSTRATION OF MIXED UQ USING EVIDENCE THEORY

7.1. Rosenbrock Function. Before the mixed UQ approach is demonstrated on a CFD problem, we test the conclusions for the selection of optimum number of subintervals on a numerical problem, which includes the Rosenbrock function as the response. It is a smooth non-linear function for which the generalized formulation is given as:

$$f(\vec{x}) = \sum_{i=1}^{n-1} [(1-x_i)^2 + 100(x_{i+1} - x_i^2)^2], \tag{1.24}$$

where n represents the number of uncertain variables ($n = 3$). The uncertainty information is as given below in Table 1.11:

A fourth-order chaos expansion was chosen to model the uncertainty propagation with the NIPC response surface. The number of original function evaluations required were 70, evaluated using Eq. (1.7) with an OSR of 2. The DSTE analysis results obtained with the mixed UQ approach for the Rosenbrock function are given in Fig. 1.10. With the objective to demonstrate the convergence, Tables 1.12 and 1.13 list the different cases considered in terms of number of subintervals and compares the response intervals at two different levels: 2.5% and 97.5%. The percent differences between successive iterations

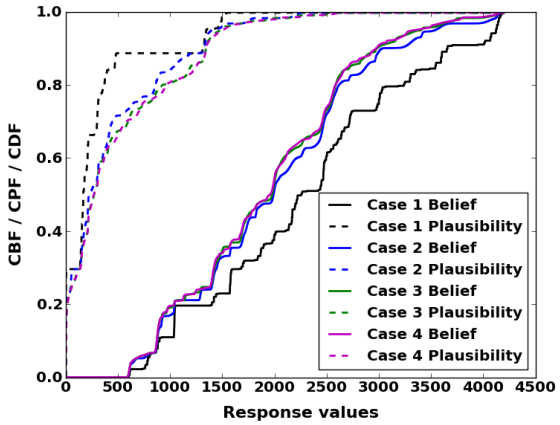

Figure 1.10. Mixed UQ results for Rosenbrock function

Table 1.12. Discretization cases for the aleatory variables

Discretization			
Case	Normal	Uniform	No. of Combinations
1	5	5	175
2	15	15	1575
3	**20**	**30**	4200
4	25	35	6125

give an overview of the convergence as one moves towards the optimum number of intervals for the case of 2 aleatory variables ($N_{opt} = 50$). Case (3) seems to provide comparable results with case (4) and the number of combinations are also decreased from 6125 to 4200. Thus, choosing the optimum number of intervals as explained in Section 6-6.2 and 6-6.4 does provide the uncertainty results with desired accuracy and efficiency.

7.2. Transonic Flow Over RAE 2822 Airfoil. To demonstrate the mixed UQ approach based on DSTE and stochastic expansions on a high fidelity CFD problem, a steady, two-dimensional, viscous, turbulent flow over RAE 2822 airfoil subject to mixed (aleatory and epistemic) input uncertainties is studied. Witteveen et al. [24] have previously

Table 1.13. Mixed UQ convergence results for Rosenbrock function analysis

Response intervals at different levels				
Case	2.5%	% Difference	97.5%	% Difference
1	$[0.816, 759.42]$	-	$[1489.86, 4149.45]$	-
2	$[1.181, 613.60]$	$[36.55, 21.24]$	$[1748.01, 4050.18]$	$[15.94, 2.42]$
3	$[1.376, 611.43]$	$[15.25, 0.35]$	$[1808.07, 3720.43]$	$[3.38, 8.49]$
4	$[1.456, 611.25]$	$[5.65, 0.029]$	$[1852.79., 3696.77]$	$[2.44, 0.64]$

compared Stochastic Collocation (SC) method based on Gauss quadrature to Simplex Elements Stochastic Collocation (SESC) method for transonic flow UQ analysis over RAE 2822. This paper will focus on using the mixed UQ with DSTE approach through interval discretization for the aleatory variables with NIPC as the surrogate model for the response variables of interest. The CFD code used in this study for numerical solution of steady Reynolds-Averaged-Navier-Stokes (RANS) equations is ANSYS FLUENT 13.0 [25]. The Mach number and the angle of attack have been treated as aleatory uncertainties. One of the closure coefficients used in the Spalart-Allmaras [26] turbulence model is treated as an epistemic uncertainty with multiple sources of information.

7.2.1. CFD model and grid convergence. The geometry of RAE 2822 airfoil is defined by the design airfoil coordinates tabulated in Cook et al. [27]. A suitable computational mesh size for stochastic simulations is selected by performing a grid convergence study. The grid convergence analysis is performed for the flow conditions corresponding to Case 6 in Cook et al. [27] with $M_\infty = 0.725$, $\tilde{\alpha} = 2.92^\circ$ and $Re = 6.5$ million (wind tunnel corrected values are $M_\infty = 0.729$ and $\tilde{\alpha} = 2.31^\circ$). A second order spatial discretization is used along with Roe flux difference splitting scheme. The iterative convergence is achieved through the reduction of the residuals of the governing equations by 6 orders of magnitude. 4 grid levels are generated for the grid convergence. The finest grid (level 4) consists of

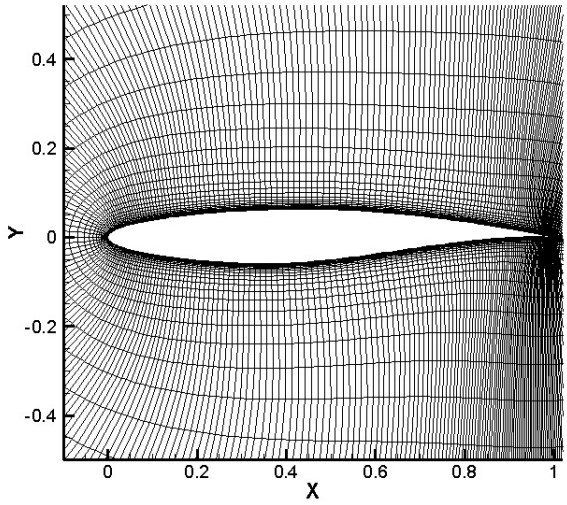

Figure 1.11. Grid around the airfoil (grid level 3)

86,400 quadrilateral cells with a mesh size of 721×121. The chord length for the airfoil is 1.0ft with 589 points on the airfoil surface and 66 in the wake region. The far-field is 27ft away from the trailing edge and the ratio of outer boundary distance to the wake distance is 0.75. The coarser grids (levels 3, 2 and 1) are obtained by halving the number of points in the stream-wise and normal direction. Thus, grid levels 3, 2 and 1 are represented by 361×61, 181×31 and 91×16 mesh sizes, respectively. Figure 1.11 shows the 3^{rd} grid level selected after the convergence study, which is used for further analysis.

The pressure distribution of the deterministic simulations for all the grid levels is compared with the experimental results of Case 6 in Figure 1.12 along with the estimation of the discretization error for the drag coefficient calculated by the Richardson extrapolation technique explained by Hosder et al. [28].

7.2.2. Stochastic problem description. For this study, the Mach number (M) and the angle of attack ($\tilde{\alpha}$) have been treated as aleatory variables with uncertainty in the form of normal distributions with the mean values corresponding to the experimental conditions

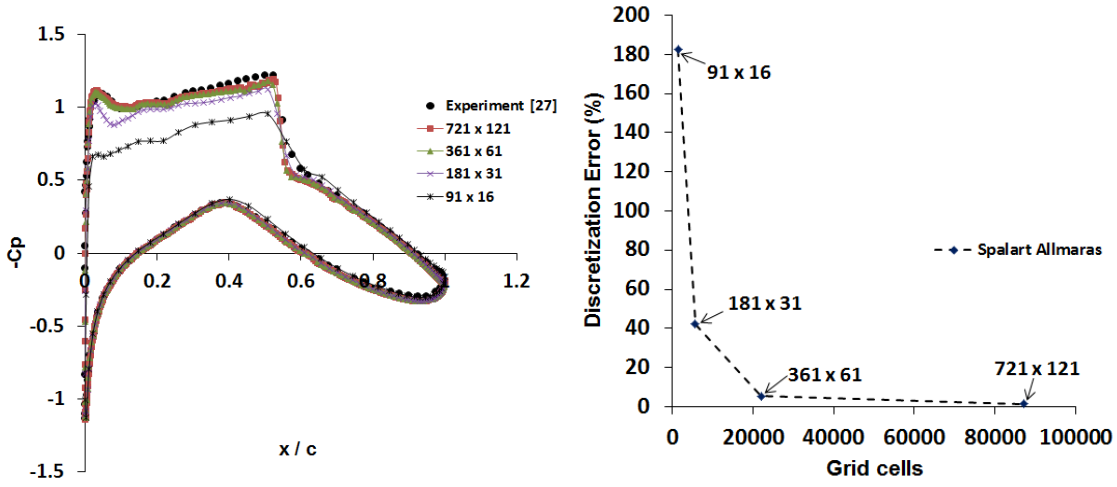

(a) Pressure distribution comparison (b) Discretization error for the drag coefficient

Figure 1.12. Grid convergence results

for Case 6 in Cook et al. [27] whereas the standard deviations as $\sigma_M = 0.005$ and $\sigma_{\tilde{\alpha}} = 0.1$, respectively. One of the closure coefficients used in the Spalart-Allmaras turbulence model is treated as an epistemic uncertainty.

The standard form of the Spalart-Allmaras model consists of various closure coefficients such as C_{b1}, C_{b2}, C_{v1}, σ_{SA}, C_{w2} and C_{w3}, detailed description of which can be found in Spalart and Allmaras [26]. The variation in these parameters has been studied in detail by many researchers. Recently, Kato and Obayashi [29] proposed an approach for uncertainty in turbulence modeling based on assimilation technique. They claim that the original values proposed by the model proposer were statistically accurate for the closure coefficients. Godfrey and Cliff [30] derived the sensitivity equations for turbulent flow simulations for different turbulence models. In their study, Spalart-Allamaras model analysis showed that the most influential coefficients in order of decreasing sensitivity magnitude are C_{v1}, C_{b1}, σ_{SA} and C_{w2}. Coefficients C_{b2} and C_{w3} had minimal effect on the output quantity studied.

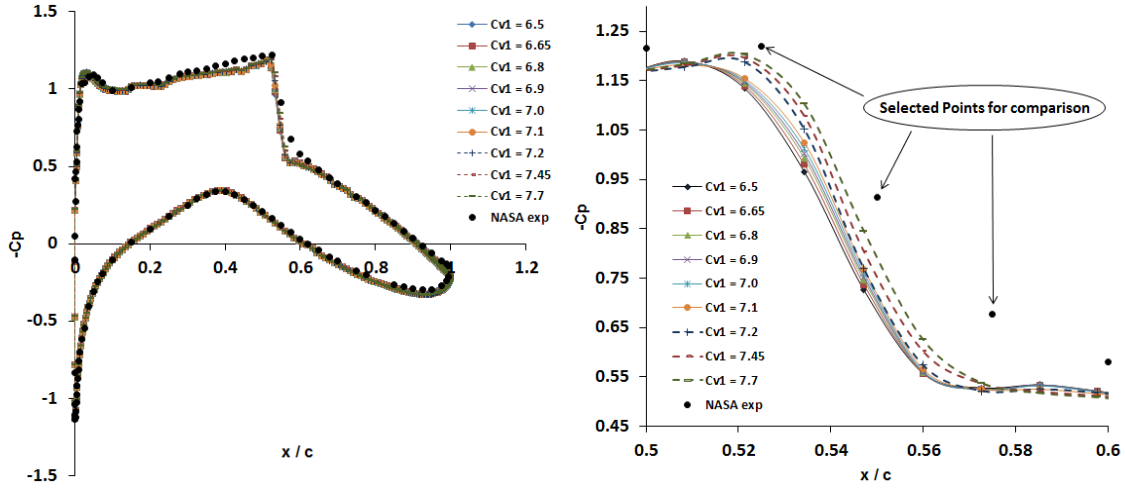

(a) Pressure distribution comparison

(b) Pressure distribution at the shock region

Figure 1.13. Variation in C_p due to variation in C_{v1} in Spalart-Allmaras turbulence model

In this work, top three sensitive parameters were tested using the wind tunnel corrected conditions within the bounds obtained with a Coefficient of Variance (CoV) of approximately 9% from their baseline values (i.e. $C_{v1} = 7.1$, $C_{b1} = 0.1355$ and $\sigma_{SA} = \frac{2}{3}$). The variation in closure coefficients was mainly based on the ranges adopted in previous research work by Rhee [31] and Cheung et al. [32]. Pressure coefficient on the airfoil surface was monitored for all the simulations and the results showed that the shock region on the upper surface was the most critical region being affected by the variation in closure coefficients (See Figure 1.13). Apart from C_{v1}, none of the other parameters seemed to have considerable effect on the flow properties in the flow field. Therefore, C_{v1} coefficient is retained as the epistemic uncertain parameter in the CFD problem along with aleatory variables Mach number and the angle of attack. The input uncertainty information for RAE 2822 transonic airfoil case is given in (Table 1.14).

Table 1.14. Uncertainty information for RAE 2822: transonic airfoil case

Variable	Uncertainty type	Uncertainty information
M	Aleatory	$N(0.725, 0.005)$
C_{v1}	Epistemic	[6.5, 7.7]
α	Aleatory	$N(2.92, 0.1)$

7.2.3. Determination of DSTE structure for the epistemic variable. The information for the epistemic variable can have different sources like an expert opinion who believes that the value of a particular variable will lie within a single interval or multiple intervals. Another source of information can be the data obtained from experiments. Evidence theory provides the tools required to incorporate the information from different sources. In the present analysis, evidence (uncertainty information) for C_{v1} is acquired from two different sources: (1) expert opinion from the literature and (2) the comparison of numerical simulations to the selected experimental data.

Spalart and Allmaras [26] preferred the value of C_{v1} as 7.1 instead of Mellor and Herring's [33] 6.9, which they believe yields a low intercept for the log law. The proposed value of C_{v1} is validated by different researchers to be accurately calibrated using different methods, especially for boundary layer flows. Based on these analyses, for demonstration purposes the epistemic interval in Table 1.14 is segregated into 3 sub-intervals: [6.5, 6.85], [6.85, 7.15] and [7.15, 7.7]. Note that the sub-intervals do not need to be continuous but can also be overlapping or discontinuous in the application of the Evidence theory. As the values of 6.9 and 7.1 both lie within the 2^{nd} interval, 100% BPA is assigned to that particular interval on the basis of expert opinion from literature review.

The second source of information regarding the uncertain parameter has been obtained from the comparison of the CFD simulations with different values of C_{v1} in the

selected intervals to the available experimental data. The following procedure is adopted in order to derive an error-based BPA assignment for each sub-interval k where $k = 1, 2, \ldots, N_{int}$ ($N_{int} = 3$ in present study):

1. Three different C_{v1} values have been chosen from each sub-interval (two values close to the upper & lower bounds and the third value approximately at the mean of that particular interval). Let j denote the index of the CFD simulation for each sub-interval where $j = 1, 2, \ldots, N_{CFD}$ with $N_{CFD} = 3$ for each interval in present analysis.

2. As the maximum deviation is observed in the shock region, 3 points ($\frac{x}{c} = 0.525, 0.55,$ 0.575) are selected for comparison with the experimental results as shown in Figure. 1.13(2). Let i denote the index for the number of points selected to be compared with the experimental results for each sub-interval where $i = 1, 2, \ldots, N_{exp}$ ($N_{exp} = 3$ in present analysis).

3. Error ε_k as a function of coefficient of pressure Cp on the upper surface at the selected points for comparison can be given by:

$$\varepsilon_k = \frac{1}{N_{CFD}} \left\{ \sum_{j=1}^{N_{CFD}} \sqrt{\frac{\sum_{i=1}^{N_{exp}} [((Cp_{exp})_{ij})_k - ((Cp_{CFD})_{ij})_k]^2}{N_{exp}}} \right\}. \tag{1.25}$$

4. Weights (ω_k) are assigned to each sub-interval on the basis of error value evaluated, $\omega_k = \frac{1}{\varepsilon_k}$.

5. BPA's can now be assigned to each sub-interval by normalizing the weights with the cumulative weight which can be mathematically expressed as:

Table 1.15. Uncertainty information for the epistemic variable C_{v1}

Source	**BPA**		
	[6.5, 6.85]	[6.85, 7.15]	[7.15,7.7]
1	29.40%	31.68%	38.91%
2		100%	

$$BPA_k = \frac{\omega_k}{\sum_{k=1}^{N_{int}} \omega_k}. \tag{1.26}$$

The DSTE structure for the epistemic variable C_{v1} obtained through the stepwise procedure explained above is outlined in Table 1.15:

7.2.4. UQ results. Following the observations made in Section 6, the aleatory variables were discretized into 50 sub-intervals in the mixed UQ analysis of this CFD problem. Three output quantities have been monitored in the airfoil case study, namely; coefficient of pressure (C_p) on the airfoil surface, coefficient of lift (c_l) and coefficient of drag (c_d). NIPC response surface is used as a surrogate for each output quantity and DSTE results in the form of belief and plausibility have been derived. The surrogate model was created with a 1^{st}, 2^{nd} and 3^{rd} order NIPC expansion with an over sampling ratio of 2, which required 8, 20 and 40 deterministic CFD evaluations, respectively.

The convergence of NIPC expansion orders in terms of uncertainties in lift and drag coefficient are shown in Figure 1.14. They can be interpreted as lower (plausibility) and upper (belief) bounds similar to the second order probability analysis for each polynomial order. For example, the probability of $c_l \leq 0.82$ is between 0.25 (indicated by 3^{rd} order CBF) and 0.4 (indicated by 3^{rd} order CPF). These quantities are not affected much by the epistemic parameter C_{v1} which is evident from the width of the probability box (region

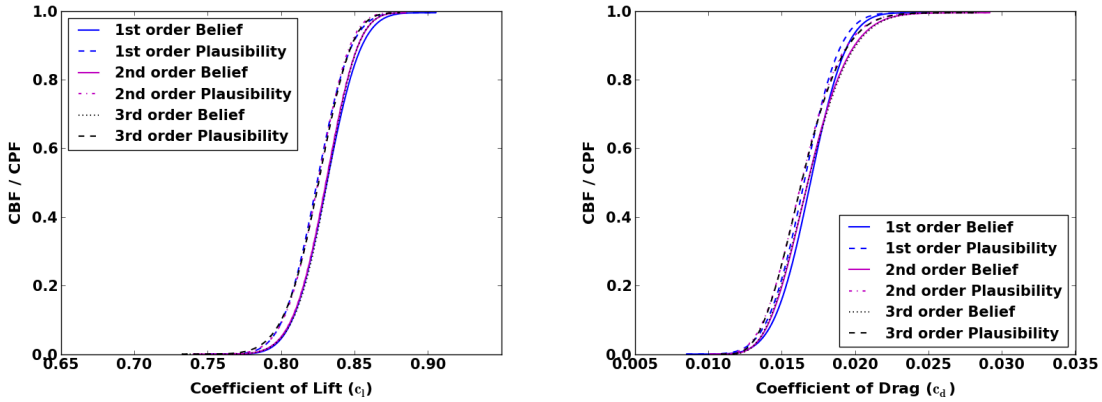

(a) Uncertainty in c_l (b) Uncertainty in c_d

Figure 1.14. UQ using mixed DSTE results for c_l and c_d

between the belief and plausibility curves). This is in accordance with the turbulence model parameter studies which show that the closure coefficient, C_{v1} does not significantly affect the flow properties at lower angles of attack where there is minimal separation of flow. Evidently, the results may be different if the analysis is performed at higher angles of attack.

In case of C_p, uncertainty is represented in terms of error bars which is similar to the documentation standards for experimental data, using a 3^{rd} order NIPC expansion at each point. The 3^{rd} order expansion is created at 296 different points on the airfoil surface using the same 40 deterministic function evaluations i.e. CFD runs utilized in the analysis of c_l and c_d for each surface pressure coefficient. Belief and plausibility curves are generated at each point using the corresponding surrogate model. The 95% CI is obtained using the response value at 2.5% plausibility level and 97.5% belief level as shown in Figure 1.15.

It is clear that the maximum uncertainty is in the shock region and the changing shock wave location varies the pressure distribution denoted by the length of uncertainty

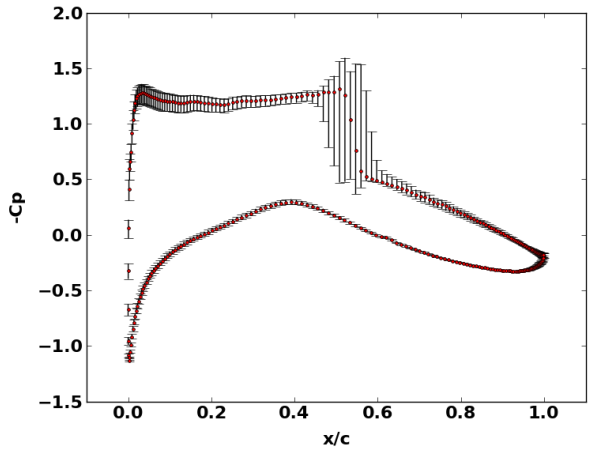

Figure 1.15. UQ using mixed DSTE results for C_p

bars. Note that the local oscillations in the shock region are likely due to the global polynomial approximation of the large gradients present in the flow field. Hence application of local approximation methods can also be considered for uncertainty quantification in regions of discontinuity.

Further, to quantify the individual contribution of each uncertain parameter to the uncertainty in c_l and c_d, Sobol indices [34] were evaluated. The basic procedure to calculate Sobol Index for a particular variable is explained in Appendix. The sensitivity results for c_l and c_d for NIPC orders 1, 2 and 3 are provided in Table 1.16. As expected, the angle of attack ($\tilde{\alpha}$) is the highest contributor followed by Mach number (M) and C_{v1} in terms of coefficient of lift whereas the Mach number contributes more towards the uncertainty in coefficient of drag as compared to $\tilde{\alpha}$. The variation in Sobol indices for the epistemic parameter C_{v1} for both output quantities are in accordance with the uncertainty plots in Figure 1.15 with the uncertainty range being wider for c_l as compared to c_d.

Table 1.16. Sobol indices for the uncertain input parameters for coefficient of lift and drag

Uncertain Parameter	**Coefficient of Lift (c_l)**			**Coefficient of Drag (c_d)**		
	1^{st} order NIPC	2^{nd} order NIPC	3^{rd} order NIPC	1^{st} order NIPC	2^{nd} order NIPC	3^{rd} order NIPC
Mach number (M)	0.1149	0.1042	0.1002	0.7514	0.7505	0.7450
C_{v1}	0.0145	0.0107	0.0188	0.0011	0.00085	0.00047
Angle of Attack ($\tilde{\alpha}$)	0.8706	0.8891	0.8951	0.2475	0.2650	0.2766

8. CONCLUSIONS

In this paper, an approach for mixed UQ with evidence theory and stochastic expansions is presented. The aleatory variables are discretized into sets of intervals with appropriate BPA's according to their probability distributions. They are treated as well characterized epistemic variables in the DSTE analysis. Also, the Point-Collocation NIPC has been implemented for construction of a stochastic surrogate model with the overall objective of reducing original function evaluations and achieving computational efficiency.

A detailed analysis is carried out in order to quantify the optimum number of subintervals required to accurately represent an aleatory domain. In this study, the focus is on normal and uniform distributions for the aleatory variables. A minimum number of subintervals in case of 1, 2, 4, 6 and 8 aleatory variables in a specific problem have been recommended as 75, 50, 40, 18 and 12 intervals per aleatory variable, respectively. Also, the effect of distributions on the number of intervals required has been discussed.

The mixed UQ using NIPC based DSTE approach and verification of the proposed minimum number of intervals for aleatory discretization is demonstrated using 2 examples: (1) 3 variable Rosenbrock function and (2) transonic flow over RAE 2822 airfoil. The first model problem (Rosenbrock function) was modeled with multiple sources of uncertainty

for the epistemic variable. A 4^{th} order chaos expansion was chosen for propagation of input uncertainty using DSTE analysis. The normal variable was modeled with 20 intervals whereas the uniform variable with 30 intervals (a total of 50 intervals) representing the aleatory domain for the model problem. This was found to be in accordance with the numerical analysis carried out for optimum number of subintervals.

For the 2^{nd} model problem, the mixed UQ approach is demonstrated on the transonic CFD study of the airfoil (RAE 2822). Mach number and angle of attack are treated as aleatory and the closure coefficient C_{v1} in Spalart-Allmaras turbulence model is treated as the epistemic uncertainty. A method to derive BPA's for the epistemic variable based on expert opinion and comparison between experimental data and CFD simulations is demonstrated. Since both aleatory variables are normally distributed, 50 intervals are used to discretize the aleatory domain. The epistemic parameter did not have a major contribution in the output uncertainty which was clear from the Sobol indices and is also in accordance with the previous findings that variation in C_{v1} has minimal effect at lower angles of attack.

Overall, the examples demonstrated that the NIPC based evidence theory is capable of capturing mixed uncertainty in case of multiple sources of uncertainty for epistemic variables. It was also shown that global bound approximation for the epistemic variable by neglecting the sources of uncertainty with beliefs can lead to overestimation of the output uncertainty. Future research will include application of the proposed approach for large scale problems by implementing the sensitivity analysis based dimension reduction techniques.

ACKNOWLEDGMENT

This research was supported by NASA Jet Propulsion Laboratory under a Small Business Technology Transfer Phase II project grant no. NNX11CC60C (Lee D. Peterson, program manager).

APPENDIX

Global Sensitivity Analysis with Sobol Indices. In a system where multiple uncertain variables are present, it is often useful to demonstrate and rank the relative importance of each input uncertain variable to the overall output quantity of interest using a global sensitivity analysis approach. In the current study, Sobol [34] indices are used to perform this analysis. Sobol indices can be derived via *Sobol Decomposition* which is a variance-based global sensitivity analysis method. First, the total variance (D) can be written in terms of the PCE as follows:

$$D = \sum_{j=1}^{P} \alpha_j^2(t,\vec{x}) \left\langle \Psi_j^2(\vec{\xi}) \right\rangle. \tag{1.27}$$

Next, as shown by Sudret [35] and Crestaux et al. [36], the total variance can be decomposed as:

$$D = \sum_{i=1}^{i=n} D_i + \sum_{1\le i<j\le n}^{i=n-1} D_{i,j} + \sum_{1\le i<j<k\le n}^{i=n-2} D_{i,j,k} + \cdots + D_{1,2,\ldots,n}, \tag{1.28}$$

where the partial variances ($D_{i_1,\ldots,i_s}$) are given by:

$$D_{i_1,\ldots,i_s} = \sum_{\beta\in\{i_1,\ldots,i_s\}} \alpha_\beta^2 \left\langle \Psi_\beta^2(\vec{\xi}) \right\rangle, \quad 1 \le i_1 < \ldots < i_s \le n. \tag{1.29}$$

The Sobol indices ($S_{i_1\cdots i_s}$) are defined by Eq. (1.30) which satisfy Eq. (1.31):

$$S_{i_1\cdots i_s} = \frac{D_{i_1,\ldots,i_s}}{D}, \tag{1.30}$$

$$\sum_{i=1}^{i=n} S_i + \sum_{1\le i<j\le n}^{i=n-1} S_{i,j} + \sum_{1\le i<j<k\le n}^{i=n-2} S_{i,j,k} + \cdots + S_{1,2,\ldots,n} = 1.0. \tag{1.31}$$

The Sobol indices provide a sensitivity measure due to individual contribution from each input uncertain variable (S_i), as well as the mixed contributions ($\{S_{i,j}\}, \{S_{i,j,k}\}, \cdots$). As shown by Sudret [35] and Ghaffari et al. [37], the total (combined) effect (S_{T_i}) of an input parameter i is defined as the summation of the partial Sobol indices that include the particular parameter:

$$S_{T_i} = \sum_{L_i} \frac{D_{i_1,\ldots,i_s}}{D}; \;\; L_i = \{(i_1,\ldots,i_s) : \exists\, k,\; 1 \leq k \leq s,\; i_k = i\}\,. \tag{1.32}$$

For example, with $n = 3$, the total contribution to the overall variance from the first uncertain variable ($i = 1$) can be written as:

$$S_{T_1} = S_1 + S_{1,2} + S_{1,3} + S_{1,2,3}. \tag{1.33}$$

From these formulations, it can be seen that the Sobol indices can be used to provide a relative ranking of each input uncertainty to the overall variation in the output with the consideration of non-linear correlation between input variables and output quantities of interest.

BIBLIOGRAPHY

[1] Oberkamp, W. L., Diegert, K., V., Alvin, K., F., and Rutherford, B., M., "Variability, Uncertainty and Error in Computational Simulation," *ASME Proceedings of the* 7^{th} *AIAA/ASME Joint Thermophysics and Heat Transfer Conference*, Vol. HTD-vol. 357-2, 1998, pp. 259-72

[2] Shafer, G., *A Mathematical Theory of Evidence*, Princeton University Press, Princeton, NJ, 1976.

[3] Zadeh, L. A., "Review of Books: A Mathematical Theory of Evidence," *The AI Magazine*, Vol 5, No. 3, 1984, pp. 81-83.

[4] Zadeh, L. A., "A Simple View of the Dempster Shafer Theory of Evidence and its Implication for the Rule of Combination," *The AI Magazine*, Vol 7, 1986, pp. 85-90.

[5] Yager, R., "Arithmetic and Other Operations on Dempster Shafer Structures," *International Journal of Man-Machine Studies*, Vol. 25, 1986, pp. 357-366.

[6] Helton, J. C., Johnson, J. D., and Oberkampf, W. L., "An Exploration of Alternative Approaches to the Representation of Uncertainty in Model Predictions," *Reliability Engineering and System Safety*, Vol. 85, 2004, pp. 39-71.

[7] Oberkampf, W. L., Helton, J. C., Joslyn, C. A., Wojtkiewicz, S. F., and Ferson, S., "Challenge Problems: Uncertainty in System Response Given Uncertain Parameters," *Reliability Engineering and System Safety*, Vol. 85, No. 1-3, 2004, pp. 11-19.

[8] Bae, H., Grandhi, R. V., and Canfield, R. A., "An Approximation Approach for Uncertainty Quantification Using Evidence Theory," *Reliability Engineering and System Safety*, Vol. 86, 2004, pp. 215-225.

[9] Bae, H., Grandhi, R. V., and Canfield, R. A., "Epistemic Uncertainty Quantification Techniques Including Evidence Theory for Large-Scale Structures," *Reliability Engineering and System Safety*, Vol. 82, 2004, pp. 1101-1112.

[10] Agarwal, H., Renaud, J. E., and Padmanabhan, D., "Uncertainty Quantification Using Evidence Theory in Multidisciplinary Design Optimization," *Reliability Engineering and System Safety*, Vol. 85, 2004, pp. 281-294.

[11] Eldred, M. S., and Swiler, L. P., "Efficient Algorithms for Mixed Aleatory-Epistemic Uncertainty Quantification with Application to Radiation-Hardened Electronics ," Sandia National Laboratories SAND2009-5805, Albuquerque, NM, September 2009.

[12] Eldred, M. S., Swiler, L. P., and Tang, G., "Mixed Aleatory-Epistemic Uncertainty Quantification with Stochastic Expansions and Optimization-Based Interval Estimation," *Reliability Engineering and System Safety*, Vol. 96, 2011, pp. 1092-1113.

[13] Hosder, S., Walters, R. W., and Balch, M., "Efficient Sampling for Nonintrusive Polynomial Chaos Applications with Multiple Input Uncertain Variables," 9^{th} *AIAA Non-Deterministic Approaches Conference*, AIAA Paper 2007-1939, Honolulu, HI, April 2007.

[14] Hosder, S., Walters, R. W., and Balch, M., "Point-Collocation Nonintrusive Polynomial Chaos Method for Stochastic Computational Fluid Dynamics," *AIAA Journal*, Vol. 48, No. 12, December 2010, pp. 2721-2730.

[15] Bettis, B. R., Hosder, S., and Winter T., "Efficient Uncertainty Quantification in Multidisciplinary Analysis of a Reusable Launch Vehicle," 17*th AIAA International Space Planes and Hypersonic Systems and Technologies Conference*, AIAA Paper 2011-2393, San Francisco, CA, April 2011.

[16] Hosder, S., "Stochastic Response Surfaces Based on Nonintrusive Polynomial Chaos for Uncertainty Quantification ," *International Journal of Mathematical modeling and Numerical Optimization*, Vol. 3, No. 1-2, January 2012, pp. 117-139.

[17] Hosder, S., and Bettis, B. R., "Uncertainty and Sensitivity Analysis for Reentry Flows with Inherent and Model-Form Uncertainties," *Journal of Spacecraft and Rockets*, Vol. 49, No. 2, March-April 2012, pp. 193-206.

[18] Oberkampf, W. L., Helton, J. C., and Sentz, K., "Mathematical Representation of Uncertainty," 3^{rd} *Non-Deterministic Approaches Forum*, AIAA Paper 2001-1645, Seattle, WA, April 2001.

[19] Nikolaidis, E., Ghiocel, D. M., and Singhal, S., *Engineering Design Reliability Handbook*, 1^{st} ed., CRC Press, July 2004, Chapter 10.

[20] Sentz, K., and Ferson, S., "Combination of Evidence in Dempster Shafer Theory," Sandia National Laboratories SAND2002-0835, Albuquerque, NM, April 2002.

[21] Akram, F., Prior, M. A., and Mavris, D. N., "A Comparison Between Monte Carlo and Evidence Theory Approaches for Technology Portfolio Planning," *Infotech@Aerospace 2011*, AIAA Paper 2011-1412, St. Louis, MO, March 2011.

[22] Helton, J. C., Johnson, J. D., Oberkampf, W. L., and Storlie, C., B., "A Sampling-Based Computational Strategy for the Representation of Epistemic Uncertainty in Model Predictions with Evidence Theory," Sandia National Laboratories SAND2006-5557, Albuquerque, NM, October 2006.

[23] R. H. Byrd, P. Lu and J. Nocedal., "A Limited Memory Algorithm for Bound Constrained Optimization," *SIAM Journal on Scientific and Statistical Computing* , Vol. 16, No. 5, 1995, pp. 1190-1208.

[24] Witteveen, J. A. S., Doostan, A., Chantrasmi, T., Pecnik, R., and Iaccarino, G., "Comparison of Stochastic Collocation Methods for Uncertainty Quantification of the Transonic RAE 2822 Airfoil," Workshop on Quantification of CFD Uncertainties, Vrije Universiteit Brussel, Brussels, Belgium.

[25] *ANSYS FLUENT user manual*.

[26] Spalart, P. R. and Allmaras, S. R., "A One-Equation Turbulence Model for Aerodynamic Flows," 30^{th} *Aerospace Sciences Meeting and Exhibit*, AIAA Paper 92-0439, Reno, NV, January 1992.

[27] Cook, P. H., McDonald, M. A., and Firmin, M. C. P., "Aerofoil RAE 2822 - Pressure Distributions, Boundary Layer and Wake Measurements," *Experimental Database for Computer Program Assessment*, AGARD Report AR 138, 1979.

[28] Hosder, S., Grossman, B., Haftka, R. T., Mason, W. H. and Watson, L. T., "Quantitative Relative Comparison of CFD Simulation Uncertainties for a Transonic Diffuser Problem," *Computers & Fluids*, Vol. 35, 2006, pp. 1444-1458.

[29] Kato, H. and Obayashi, S., "Approach for Uncertainty of Turbulence Modeling Based on Data Assimilation Technique," *Computers & Fluids*, Vol. 85, 2013, pp. 2-7.

[30] Godfrey, A. G. and Cliff, E. M., "Sensitivity Equations for Turbulent Flows," 39^{th} *Aerospace Sciences Meeting and Exhibit*, AIAA Paper 2001-1060, Reno, NV, January 2001.

[31] Rhee, M., "Evaluation of Grid Convergence and Turbulence model Constant Changes for the Airfoil Flow Simulation," 45^{th} *AIAA Aerospace Sciences Meeting and Exhibit*, AIAA Paper 2007-1082, Reno, NV, January 2007.

[32] Cheung, S. H., Oliver, T. A., Prudencio, E. E., Prudhomme, S. and Moser, R. D., "Bayesian Uncertainty Analysis with Applications to Turbulence Modeling," *Reliability Engineering and System Safety*, Vol. 96, 2011, pp. 1137-1149.

[33] Mellor, G. L. and Herring, H. J., "Two Methods of Calculating Turbulent Boundary Layer Behavior Based on Numerical Solution of the Equations of Motion," Proc. Conf. Turb. Boundary Layer Pred., Stanford, 1968.

[34] Sobol, I., "Global Sensitivity Indices for Nonlinear Mathematical Models and their Monte Carlo Estimates," *Mathematics & Computers in Simulation*, Vol. 55, 2001, pp. 271-280.

[35] Sudret, B., "Global Sensitivity Analysis Using Polynomial Chaos Expansion," *Reliability Engineering and System Safety*, Vol. 93, No. 7, July 2008, pp. 964-979.

[36] Crestaux, T., Maitre, O. L, and Martinez, J. M., "Polynomial Chaos Expansion for Sensitivity Analysis," *Reliability Engineering and System Safety*, 2009.

[37] Ghaffari, S., Magin, T. and Iaccarino, G., "Uncertainty Quantification of Radiative Heat Flux Modeling for titan Atmospheric Entry," 48^{th} *AIAA Aerospace Sciences Meeting*, AIAA Paper 2010-239, Orlando, FL, January 2010.

II. QUANTIFICATION OF MARGINS AND MIXED UNCERTAINTIES USING EVIDENCE THEORY AND STOCHASTIC EXPANSIONS

Harsheel Shah[1], Serhat Hosder[1] and Tyler Winter[2]

[1]Missouri University of Science & Technology, Rolla, MO, 65409, USA
[2]M4 Engineering Inc., Long Beach, CA, 90807, USA

ABSTRACT

The objective of this paper is to implement Dempster-Shafer Theory of Evidence (DSTE) in the presence of mixed (aleatory and multiple sources of epistemic) uncertainty to the reliability and performance assessment of complex engineering systems through the use of Quantification of Margins and Uncertainties (QMU) methodology. This study focuses on quantifying the simulation uncertainties, both in the design condition and the performance boundaries along with the determination of margins. To address the possibility of multiple sources and intervals for epistemic uncertainty characterization, DSTE is used for uncertainty quantification. An approach to incorporate aleatory uncertainty in Dempster-Shafer structures is presented by discretizing the aleatory variable distributions into sets of intervals. In view of excessive computational costs for large scale applications and repetitive simulations needed for DSTE analysis, a stochastic response surface based on point-collocation Non-intrusive Polynomial Chaos (NIPC) has been implemented as the surrogate for the model response. The technique is demonstrated on a model problem with non-linear analytical functions representing the outputs and performance boundaries of two coupled systems. Finally, the QMU approach is demonstrated on a multi-disciplinary analysis of a High Speed Civil Transport (HSCT).

NOMENCLATURE

M	margin
U	uncertainty
FU	upper boundary performance
U_{FU}	uncertainty in FU
FL	lower boundary performance
U_{FL}	uncertainty in FL
F	performance at design condition
U_F	uncertainty in F
M_{UP}	upper margin
M_{LW}	lower margin
$\tilde{M}$	Mach number
$\tilde{\alpha}$	angle of attack
λ	taper ratio
Λ	sweep angle
n	number of random variables
N_S	number of samples
n_p	over-sampling ratio
p	order of polynomial chaos
$\vec{\xi}$	standard input random variable vector
N_t	number of terms in a total-order expansion
ψ	random basis function
α	coefficient in polynomial chaos expansion
α^*	stochastic function

Bel	Belief
Pl	Plausibility
$\mathbb{U}$	Universal set
$\mathscr{U}$	set of focal elements of $\mathbb{U}$
BPA	basic probability assignment
$m(\varepsilon)$	BPA corresponding to subset ε of $\mathscr{U}$
P	belief / plausibility / probability level
γ	confidence level

1. INTRODUCTION

The objective of this paper is to implement Dempster-Shafer Theory of Evidence (DSTE) in the presence of mixed (aleatory and multiple sources of epistemic) uncertainty to the reliability and performance assessment of complex engineering systems through the use of Quantification of Margins and Uncertainties (QMU) methodology. Specifically, *Uncertainty Quantification* (UQ) has been used as a tool of *certification* to decide whether a system is likely to perform safely and reliably within design specifications. The unique contributions of the current study to the system reliability and safety research can be summarized as follows: The current work focuses on the creation of a novel QMU framework in terms of Dempster-Shafer structures (belief & plausibility) for the characterization of uncertainty in system design performance as well as the performance boundaries to obtain uncertainty and margin metrics to evaluate the system safety and reliability. Specifically, DSTE is used for uncertainty quantification to address the possibility of multiple sources and intervals for epistemic uncertainty characterization. Furthermore, the DSTE is utilized

for mixed uncertainty quantification by discretizing the aleatory probability distributions into optimum sets of intervals and treating them as well-characterized epistemic variables. In addition, the response quantities of interest for design performance and boundaries are represented with stochastic surrogates based on non-intrusive polynomial chaos to reduce the computational expense of implementing DSTE for uncertainty quantification of high-fidelity complex system models.

To review the previous work and contrast with the current study, the following section gives a detailed literature review on QMU methodology, epistemic and aleatory uncertainty considerations in QMU, and DSTE for epistemic and mixed uncertainty representation. Section 3 briefly discusses different types of uncertainties present in a computational model. Section 4 gives an overview of basics of point-collocation Non-intrusive Polynomial Chaos (NIPC) methodology. In Section 5, the mathematical framework for Dempster-Shafer Theory of Evidence for mixed uncertainty quantification using NIPC response surface has been presented. Section 6 describes the incorporation of uncertainty measures of evidence theory into QMU. The newly developed QMU approach is demonstrated in Section 7 on a model problem with non-linear analytical functions representing the outputs and performance boundaries of two coupled systems. In Section 8, the proposed QMU methodology is demonstrated on a multi-disciplinary analysis of a supersonic civil transport. Section 9 concludes the paper by summarizing the findings of the current study.

2. LITERATURE REVIEW

2.1. QMU Methodology and Confidence Ratio. QMU is a methodology developed to facilitate analysis and communication of confidence for certification of complex systems, which is performed with quantified uncertainty and margin metrics obtained for

various system responses and performance parameters. In the recent years, a number of studies were reported on the theoretical development and the application of the QMU concept in the certification of reliability and safety of nuclear weapons stockpile [1, 2, 3, 4, 5]. The description of the key elements of a QMU framework that can be used to address risk and risk mitigation for the certification of nuclear weapons was presented by Sharp and Wood-Schultz [1]. Eardley et al. [3] described QMU as a formalism dealing with the reliability of complex technical systems and the confidence that can be placed in estimates of reliability. They also investigated the main components (performance gates, margins, and uncertainties) of the QMU methodology. Key ideas underlying the concept of QMU were defined by Pilch et al. [6]. They claimed that QMU provides input for a risk-informed decision making process and constitutes a decision-support methodology for complex technical decisions that are made under conditions of uncertainty.

Pepin et al. [7] presented a practical QMU metric for the certification of complex systems in terms of the ratio of *Margin* (M) and *Uncertainty* (U), known as Confidence Ratio (*CR*) or confidence factor. The metric allowed uncertainty both on the operating region and the performance requirement and was not restrictive to a probabilistic definition of the uncertainty. A study by Lucas et al. [8] utilized the QMU methodology to study the reliability of a ring structure. According to the author, if U denotes a suitable measure of uncertainties and has been quantified accurately, the confidence ratio may be taken as a rational basis for certification. Also, a QMU approach based on confidence ratio was used for the characterization of the operation limits of the supersonic combustion engine of a hypersonic air-breathing vehicle by Iaccarino et al. [9]. Some previous work have expressed a concern for the use of confidence ratio as the sole indicator of confidence [10]. Pilch et al. [6] expressed dissatisfaction with the confidence ratio metric being deceptively simple and involving significant loss of information.

Compared to the previous work, the current study is expected to contribute to the QMU methodology by efficient implementation of DSTE for the calculation of margins and uncertainties, which is the primary focus of the paper. Following some previous studies, the current work also utilizes confidence ratio as a measure of system safety in the demonstration of the UQ and QMU methodologies developed, however more sophisticated measures utilizing the UQ methodology introduced in this paper could be investigated and integrated to the QMU framework in future studies.

2.2. Epistemic and Aleatory Uncertainty Considerations in QMU. As implied in the previous section where the QMU methodology is reviewed, one should not forget that *uncertainty quantification* (determination of output uncertainty resulting from uncertainty in inputs) is a broad research area on which the QMU process is dependent. Uncertainties in engineering systems can be characterized mainly as aleatory (inherent or irreducible) uncertainty and epistemic (reducible) uncertainty originating due to lack of knowledge. Pilch et al. [6] emphasized the need to separate aleatory and epistemic uncertainty in QMU. Helton [11] presented a comprehensive study on QMU, which included a detailed analysis of the QMU concept with different representations of uncertainty. Oberkampf et al. [12] have described various methods for estimating total uncertainty by identifying all possible sources of variability, uncertainty and error in computational simulations. Urbina et al. [13] proposed a methodology to quantify the margins and uncertainty in presence of mixed uncertainties through a framework based on Bayes networks and further developed a QMU metric in terms of probability of failure. A new formalism based on Bayesian inference, known as probabilistic QMU or pQMU, was introduced by Wallstrom [14], which was fully probabilistic and showed how QMU may be interpreted within the framework of system reliability theory. Epistemic uncertainty was represented using a Bayesian approach by transforming the bounds to probability density functions. Many have expressed concern

about modeling epistemic uncertainty via probability density functions due to the assumption of a higher resolution of knowledge than what is really present [15]. Owhadi et al. [16] introduced a rigorous framework for UQ (Optimal Uncertainty Quantification) that did not implicitly impose inappropriate assumptions on the characterization of uncertainty, which has been the weakness of most of the UQ methods. They further compared the framework with different UQ methods like Monte Carlo strategies, stochastic expansion methods, sensitivity analysis and Bayesian inference. However, the paper did not specifically discuss methods for different representation of epistemic uncertainty such as possibility theory, interval analysis or evidence theory.

2.3. DSTE for Epistemic and Mixed Uncertainty Representation. As an alternative to Bayesian approach, formulation of mathematical structures like the evidence theory [17, 18, 19] has been an attractive approach for appropriate representation of epistemic uncertainty due to the fact that it does not make assumptions regarding the distribution of the variables described by intervals. DSTE approach is particularly useful when the uncertain variables are defined by more than one interval (i.e., multiple sources or expert opinions on uncertainty ranges). Probability theory and evidence theory were introduced as possible mathematical structures for the representation of the epistemic uncertainty associated with the performance of safety systems by Helton et al. [20]. The results suggested that evidence theory provided a valuable representational tool for the display of the implications of significant epistemic uncertainty in the inputs of complex systems. Furthermore, Helton et al. [21] explained the use of evidence theory as an alternative to the use of probability theory for the representation of epistemic uncertainty in QMU-type analyses. Swiler et al. [22] studied various approaches like interval analysis and DSTE in order to characterize epistemic uncertainty in the calculation of margins.

In previous years, extensive research has been dedicated to improve the practical application of the Dempster-Shafer theory to complex models due to the excessive computational cost associated with the required number of simulations [23, 24, 25]. A sampling based computational strategy for the representation of epistemic uncertainty in model predictions with evidence theory was introduced by Helton et al. [15] to reduce the computational cost of crude Monte Carlo method. In the present paper, a stochastic response surface constructed using point-collocation NIPC [26, 27, 28, 29, 30] has been implemented as a response surrogate in uncertainty analysis in order to reduce the computational cost.

Recently, Eldred et al. [31] have demonstrated mixed UQ using different methods like interval optimization, second-order probability [19, 28, 30, 32] and DSTE. They investigated the use of nested sampling for mixed UQ, where each sample taken from the epistemic distributions at the outer loop results in an inner loop sampling over the aleatory probability distributions. In order to demonstrate the accuracy and efficiency over crude nested sampling, the mixed UQ results obtained through local gradient based and global non-gradient based optimization on the outer epistemic loop within nested sampling approach were compared. Recently, Sentz and Ferson [33] proposed the use of probability bound analysis coupled with Dempster-Shafer theory for treating mixed uncertainty, as one of the tools relevant for QMU. In their work, the p-boxes [34] for aleatory uncertain parameters were discretized into 100 equiprobability levels in order to be represented as Dempster-Shafer structures. In the current paper, the use of DSTE procedure has been proposed for mixed UQ by discretizing the aleatory probability distributions into optimum sets of intervals (explained mathematically in Section 5) and treat them as well-characterized epistemic variables. For accurate representation in terms of Dempster-Shafer structures, these parameters are discretized into an optimum number of sets of intervals based on a previous study by Shah et al. [35]. This approach enables us to represent mixed uncertainty

in terms of Dempster-Shafer structures for uncertainty analysis with multiple sources of uncertainty.

3. TYPES OF UNCERTAINTY

Uncertainties are assigned to the specification of input physical parameters that are required for computational models. Two types of uncertainties exist in analyses of complex systems: aleatory uncertainty and epistemic uncertainty. Many contributions have been dedicated to emphasize the importance of characterization and treatment of uncertainties in Performance Assessments (PAs) for complex systems [36, 37, 38, 39, 40, 41]. Helton [42] illustrates the use of the Kaplan/Garrick ordered triple representation for risk in maintaining a distinction between aleatory (stochastic) and epistemic (subjective) uncertainty.

3.1. Aleatory Uncertainty. Aleatory uncertainty, also known as probabilistic uncertainty, arises due to inherent physical variability present in the system being analyzed. It is not strictly due to lack of knowledge and is irreducible. Conducting additional experiments might provide more description of the variability but cannot be eliminated completely. For example, the Mach number can be treated as an aleatory uncertain variable in the computational aerodynamics analysis of airfoils or wings.

3.2. Epistemic Uncertainty. The epistemic uncertainty arises due to lack of knowledge and is reducible by using, for example, a combination of calibration, inference from experimental observations and improvement of the physical models. One source of epistemic uncertainty is the set of assumptions introduced in the derivation of mathematical models of the physical phenomena. This type of uncertainty cannot be defined in a probabilistic framework unless a specific distribution is assumed, which may lead to inaccurate results as shown by Oberkampf et al. [43]. Thus, epistemic variables are often modeled using intervals derived from experimental data or expert judgment with specified lower and

the upper bounds. Turbulence modeling parameters (e.g., closure coefficients) in Computational Fluid Dynamics (CFD) simulations present a good example for epistemic uncertainty.

4. POINT-COLLOCATION NON-INTRUSIVE POLYNOMIAL CHAOS

Polynomial Chaos is an uncertainty propagation approach which has been used in many recent UQ studies. In this work, the focus is on generalized polynomial chaos using the Wiener-Askey scheme, which is explained in detail by Xiu and Karniadakis [44]. In previous years, many researchers have utilized polynomial chaos theory in stochastic computations [26, 27, 28, 35, 45, 46]. In non-intrusive Polynomial Chaos Expansion (PCE), simulations are used as black boxes and the calculation of chaos expansion coefficients is based on a set of simulation response evaluations. The point-collocation NIPC is derived from the polynomial chaos theory, which is based on spectral representation of uncertainty [47]. An important aspect of the spectral representation of uncertainty is that a stochastic response function can be decomposed into deterministic and stochastic components. Thus, for any stochastic response function α^*, one can write,

$$\alpha^*(\vec{x},\vec{\xi}) \approx \sum_{j=0}^{P} \alpha_j(\vec{x})\psi_j(\vec{\xi}) \tag{1.34}$$

where $\alpha_j(\vec{x})$ is the deterministic component and ψ_j is the random basis function corresponding to j^{th} mode. Generally, α^* is a function of deterministic variable vector $\vec{x}$ and the n-dimensional independent standard random variable vector $\vec{\xi} = (\xi_1, \ldots, \xi_n)$. In theory, the expansion given in Eq. (1.34) is an infinite series. However, in practice this series is truncated at a finite number of terms (hence the approximation sign used in Equation 1) based on a selected expansion order and finite number of uncertain variables. The PCE can

be created on a complete order. In this case, the total number of output modes (N_t) for an expansion order of p and n random variables is given by

$$N_t = P + 1 = \frac{(n+p)!}{n!p!} \tag{1.35}$$

An alternative approach as indicated by Eldred et al. [48] is to employ a "tensor-product expansion", in which polynomial order bounds are applied on a per-dimension basis including all combinations of the one-dimensional polynomials. In this work, a total-order expansion has been implemented for creating the polynomial chaos response surfaces. The basis functions used in Eq. (1.34) are optimal polynomials that are orthogonal with respect to a weight function over the support region of the input random variable vector. In terms of L^2 convergence of the statistics, the Hermite polynomial is optimal for normal distribution whereas the Laguerre and Legendre polynomials are used for exponential and uniform input uncertainty distributions, respectively. The detailed description of the orthogonal polynomials for different input uncertainty distributions (e.g., uniform, normal, exponential, etc.) and the associated weight functions are given by Hosder [29], Xiu and Karniadakis [44], and Eldred et al. [48].

The collocation based NIPC starts with replacing uncertain variables of interest with their polynomial expansions derived from Eq. (1.34). Next, $P+1$ (N_t) vectors $(\vec{\xi}_j = \{\xi_1, \xi_2, \ldots, \xi_n\}_j, j = 0, 1, 2, \ldots, P)$ are sampled from the uncertainty space defined by the bounds of the uncertain variables with Latin Hypercube (LH) sampling for a given polynomial chaos expansion with number of modes determined from Eq. (1.35). The deterministic model (e.g., Computational Fluid Dynamics Model, Finite Element Model, etc.) is evaluated at these points. With the left hand side of Eq. (1.34) known from the solutions of the deterministic model evaluations at the sample points, a linear system of equations can be obtained:

$$\begin{pmatrix} \psi_0(\vec{\xi}_0) & \psi_1(\vec{\xi}_0) & \dots & \psi_P(\vec{\xi}_0) \\ \psi_0(\vec{\xi}_1) & \psi_1(\vec{\xi}_1) & \dots & \psi_P(\vec{\xi}_1) \\ \vdots & \vdots & \ddots & \vdots \\ \psi_0(\vec{\xi}_P) & \psi_1(\vec{\xi}_P) & \dots & \psi_P(\vec{\xi}_P) \end{pmatrix} \begin{pmatrix} \alpha_0 \\ \alpha_1 \\ \vdots \\ \alpha_P \end{pmatrix} = \begin{pmatrix} \alpha^*(\vec{x}, \vec{\xi}_0) \\ \alpha^*(\vec{x}, \vec{\xi}_1) \\ \vdots \\ \alpha^*(\vec{x}, \vec{\xi}_P) \end{pmatrix} \tag{1.36}$$

Eq. (1.36) represents a linear system of equations which needs to be solved in order to determine the spectral modes $\alpha_j (j = 0, 1, \dots, P)$ for the stochastic function α^*. Eq. (1.35) is considered as the minimum number of deterministic samples required to solve the linear system of equations. However, if more number of deterministic samples (N_S) are available, the over-determined system is solved using a least squares approach. The term, over-sampling ratio denoted by n_p is related to Eq. (1.35) in the following manner:

$$N_S = n_p \times \frac{(n+p)!}{n!p!} \tag{1.37}$$

Thus, an n_p of 1 corresponds to the minimum number of deterministic samples required. Hosder et al. [26] demonstrated through different stochastic model problems that an n_p of 2 is the optimum value for most problems, which has also been implemented in the current study.

5. AN APPROACH FOR MIXED UQ USING EVIDENCE THEORY

This section summarizes the evidence theory traditionally used for pure epistemic analysis and extends this idea to perform mixed UQ analysis by converting the aleatory uncertain variables into Dempster-Shafer structures.

5.1. Fundamentals of Evidence Theory. Evidence theory introduces two new measures of uncertainty, Belief (Bel) i.e., lower limit of probability and Plausibility (Pl)

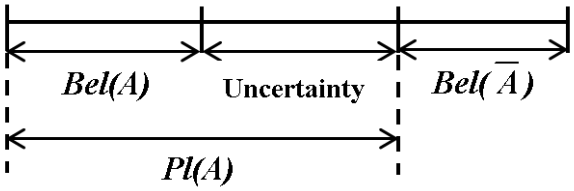

Figure 1.1. Schematic of belief and plausibility

i.e., upper limit of probability. Evidence theory application involves the specification of $(\mathbb{U}, \mathscr{U}, m)$ where $\mathbb{U}$ denotes the universal set, $\mathscr{U}$ denotes the collection of subsets or set of focal elements of $\mathbb{U}$ and m is the Basic Probability Assignment (BPA), which can be viewed as the belief of the user of how likely it is that the uncertain input falls within the specified interval. BPA, a value between 0 and 1, can be assigned for any possible subset of the universal set based on experimentation or expert opinion. The advantage of this theory is that it does not assume any particular value within the interval and nor does it assign a specific distribution to the interval. Also, Figure 1.1 illustrates that the axiom of additivity is not imposed, as the evidential measure for the occurrence and negation of an event does not have to sum to unity $(Bel(A) + Bel(\bar{A}) \leq 1, Pl(A) + Pl(\bar{A}) \geq 1, Bel(A) + Pl(\bar{A}) = 1)$ where $\bar{A}$ represents the negation of event A.

According to the definition, $m(\varepsilon)$ denotes the BPA corresponding to subset ε of $\mathscr{U}$. Any additional evidence supporting the claim that the uncertain variable lies within a subset of ε, say $B \subset \varepsilon$, must be assigned another non-zero BPA $m(B)$. $m(\varepsilon)$ should satisfy following axioms of evidence theory:

- $m(\varepsilon) > 0$ for any $\varepsilon \in \mathscr{U}$
- $m(\varepsilon) = 0$ if $\varepsilon \subset \mathbb{U}$ and $\varepsilon \ni \mathscr{U}$
- $m() = 0$ where denotes an empty set

- $\sum m(\varepsilon) = 1$ for all $\varepsilon \in \mathscr{U}$

In case of multiple sources of uncertainty per variable, the Dempster rule of combination has been extensively used with a strong assumption that there is some degree of consistency or agreement among the opinions of different sources. It has been proved by Yager [49] that the Dempster's rule completely ignores the conflict among different sources. Zadeh [50] in his review of Shafer's book, *A Mathematical Theory of Evidence*, pointed out that using Dempster's rule with conflicting evidences results in erroneous analysis. In this study, the mixing or averaging rule has been adopted which generalizes the averaging operation used for probability distributions. The mathematical formulation is given by:

$$m_{1\ldots n}(A) = \frac{1}{n}\sum_{j=1}^{n} w_j m_j(A) \tag{1.38}$$

where $m'_j s$ are the BPAs for belief structures being aggregated and $w'_j s$ are the weights assigned according to the reliability of the sources. There is abundant literature dedicated to combination rules for the evidence theory [51, 52] which is beyond the scope of this paper.

Once the uncertainty associated with the domain is characterized by an evidence space in the form of BPAs, an input sample space is constructed. For example, if $y = f(\vec{x})$ where $\vec{x} = [x_1, x_2, \ldots, x_n]$ with the evidence space defined as $(\mathbb{X}_i, \mathscr{X}_i, m_i)$ for each input uncertainty, the input sample space is given by

$$\mathbb{X} = \{x : x = [x_1, x_2, \ldots, x_n] \in \mathbb{X}_1 \times \mathbb{X}_2 \times \ldots \times \mathbb{X}_n\} \tag{1.39}$$

Further for $\vec{x}$, the evidence space can be defined by $(\mathbb{X}, \mathscr{X}, m_X)$ where $\mathscr{X}$ is developed from the sets contained in Eq. (1.40).

$$\mathscr{C} = \{\varepsilon : \varepsilon = [\varepsilon_1, \varepsilon_2, \ldots, \varepsilon_n] \in \mathscr{X}_1 \times \mathscr{X}_2 \times \ldots \times \mathscr{X}_n\} \tag{1.40}$$

Under the assumption that the x_i are independent, m_X is defined as:

$$m_X(\varepsilon) = \begin{cases} \prod_{i=1}^{n} m_i(\varepsilon_i) & \text{if} \quad \varepsilon = \varepsilon_1 \times \varepsilon_2 \times \ldots \times \varepsilon_n \in \mathscr{X} \\ 0 & \text{otherwise} \end{cases} \tag{1.41}$$

for subsets ε of $\mathbb{X}$.

Once the BPAs for input sample space in Eq. (1.39) are defined by Eq. (1.41), belief and plausibility for the output y can be evaluated as:

$$Bel_Y(\varepsilon) = \sum_{\mathscr{S} | \mathscr{S} \subseteq f^{-1}(\varepsilon)} m_X(\mathscr{S}) \tag{1.42}$$

$$Pl_Y(\varepsilon) = \sum_{\mathscr{S} | \mathscr{S} \cap f^{-1}(\varepsilon) \neq} m_X(\mathscr{S}) \tag{1.43}$$

As no assumptions were made to calculate these measures, *Bel* and *Pl* provide a more realistic uncertainty structure consistent with the given evidences. The evidence theory statistics can be summarized in terms of Cumulative Belief and Plausibility Functions (CBF and CPF) and Complementary Cumulative Belief and Plausibility Functions (CCBF and CCPF) as shown in Figure 1.2.

These measures are calculated on the basis of minimum and maximum response values for each combination in the input sample space. Interval optimization approach (mathematical formulation given in Eq. (1.44)) can be implemented to provide accurate results for both, the original function or the response surface based on point-collocation NIPC, which is used as a surrogate of the original function in this work.

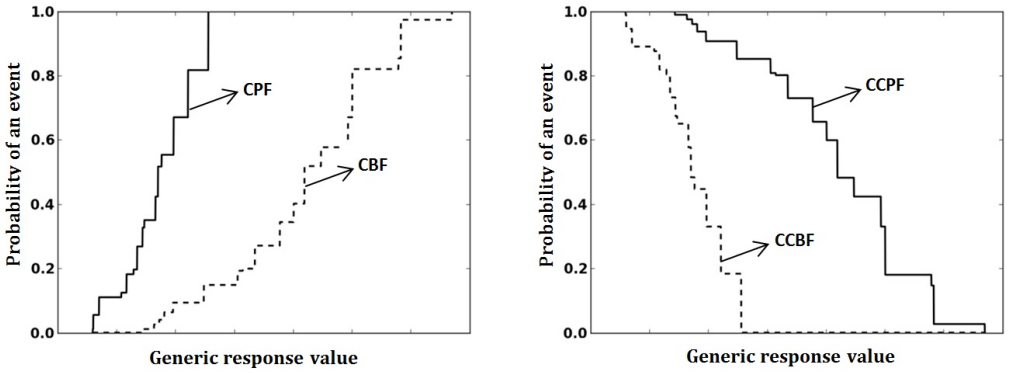

Figure 1.2. Example of cumulative and complementary cumulative belief and plausibility functions

$$\begin{aligned} &\underset{x}{\text{minimize/maximize}} && f(\vec{\xi}) \\ &\text{subject to} && \vec{\xi}_L \leq \vec{\xi} \leq \vec{\xi}_U \end{aligned} \tag{1.44}$$

where $f(\vec{\xi})$ is the required response value, $\vec{\xi}_L$ and $\vec{\xi}_U$ correspond to lower and upper bounds of the standard random variables. The final step is to calculate the belief and plausibility structures using the minimum and maximum response values according to Eqs. (1.42) and (1.43).

Now, if the uncertainty in output y is characterized by $(\mathbb{Y}, \mathscr{Y}, m_Y)$, the output uncertainty is summarized using CBF, CPF, CCBF and CCPF given by Eqs. (1.45),(1.46),(1.47) and (1.48).

$$CBF = [\rho, Bel_X(f^{-1}(\mathbb{Y}_\rho^c))], \rho \in \mathbb{Y} \tag{1.45}$$

$$CCBF = [\rho, Bel_X(f^{-1}(\mathbb{Y}_\rho))], \rho \in \mathbb{Y} \tag{1.46}$$

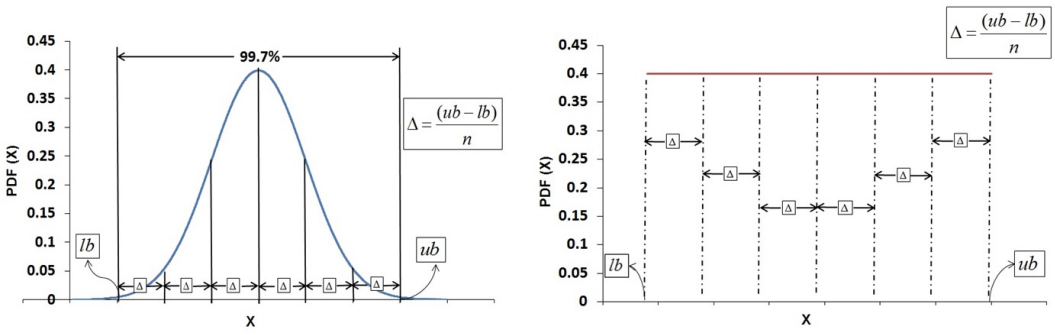

Figure 1.3. Discretization of a normally and uniformly distributed variable

$$CPF = [\rho, Pl_X(f^{-1}(\mathbb{Y}_\rho^c))], \rho \in \mathbb{Y} \tag{1.47}$$

$$CCPF = [\rho, Bel_X(f^{-1}(\mathbb{Y}_\rho))], \rho \in \mathbb{Y} \tag{1.48}$$

where $\mathbb{Y}_\rho = \{y : y \in \mathbb{Y} \quad \text{and} \quad y > \rho\}$ and $\mathbb{Y}_\rho^c = \{y : y \in \mathbb{Y} \quad \text{and} \quad y \leq \rho\}$. Detailed explanation of the evidence theory with numerical examples has been provided by Oberkampf et al. [43], Helton et al. [53] and Nikolaidis et al. [54].

5.2. Aleatory Uncertainty Representation in Terms of Demspter-Shafer Structures. Although Dempster-Shafer theory is primarily used for epistemic uncertainty representation, there may be instances when aleatory uncertainties are present in the model along with the epistemic. In that case, one may choose to segregate the aleatory uncertainties and treat them within an inner loop of nested sampling. The end result may be multiple belief and plausibility structures, as shown by Eldred et al. [31]. As an alternative, one may choose to discretize the aleatory variables into sets of intervals according to their respective probability distributions. Figure 1.3 shows an example of the discretization process for the normal (left plot) and uniform (right plot) distributions.

In this paper, the focus is on the latter option of discretizing the aleatory variables into sets of intervals and assign BPA's to each interval corresponding to the probability distribution. Shah et al. [35] gave a detailed description of the methodology of aleatory uncertainty representation in terms of Dempster-Shafer structures. For example, a random variable with uniform distribution can be divided into n number of intervals with an equal BPA of 1/n assigned to each sub-interval as can be seen in the right hand side plot of Figure 1.3. Suppose x_1 is a uniformly distributed variable with lower and upper bounds as $[0.1, 0.7]$ and the same is discretized into 5 sub-intervals ($n = 5$). The Dempster-Shafer structure for x_1 can be given by:

$$x_1 = ([0.1, 0.22], m_1), ([0.22, 0.34], m_2), ([0.34, 0.46], m_3), ...$$
$$([0.46, 0.58], m_4), ([0.58, 0.7], m_5)$$
$$\text{where} \quad m_i = \frac{1}{n} = \frac{1}{5} \quad (i = 1, 2, .., 5)$$

In order to discretize a random variable with normal distribution, one needs to characterize the same with a lower bound and an upper bound. Consider the left plot in Figure 1.3 which shows a standard normal distribution i.e., with 0 mean ($\mu = 0$) and 1 standard deviation ($\sigma = 1$). As per the theory, for a normally distributed random variable with mean μ and σ as the standard deviation, 99.7% of the area under the curve is within $\mu \pm 3\sigma$. Hence, this can be treated as a benchmark for bounding all the normal variables in any analysis. However, the BPA should be assigned to each sub-interval according to the Gaussian distribution by solving the definite integral in Eq. (1.49):

$$P(a < X < b) = \int_a^b f(X), dx \quad \text{where} \quad f(X) = \frac{1}{\sigma\sqrt{2\pi}} \exp \frac{-(X-\mu)^2}{2\sigma^2} \tag{1.49}$$

where a and b denote the upper and lower bound of the sub-interval and $P(a < X < b)$ denotes the probability of X between a and b.

Suppose x_2 is a normally distributed variable with a mean value of 0.5 ($\mu = 0.5$) and standard deviation of 0.01 ($\sigma = 0.01$). The lower and upper bounds for x_2 using $\mu \pm 3\sigma$ are $[0.47, 0.53]$ and discretized into 3 intervals. The Dempster-Shafer structure for x_2 can be given by:

$$x_2 = ([0.47, 0.49], m_1), ([0.49, 0.51], m_2), ([0.51, 0.53], m_3)$$
$$\text{where} \quad m_1 = 0.1573, m_2 = 0.6827 \quad \text{and} \quad m_3 = 0.1573$$

In the current study, the interval discretization is based upon the convergence study performed by the authors [35] for the minimum number of intervals required to accurately capture the aleatory uncertainty in a model problem. The discretization process mainly depends upon the amount of information needed by the Dempster-Shafer structures to accurately cover the uncertainty domain.

6. QMU BASED ON EVIDENCE THEORY

6.1. Key Measures Required for QMU. The key measures of the QMU framework to be developed are shown in Figure 1.4. In this QMU framework, for the whole engineering system (e.g., aircraft or spacecraft) or for each sub-system, the first step will be to determine performance metrics (system outputs) relevant to the systems modeling, which should ideally be functions of all input parameters including the operating conditions. Then these metrics will be evaluated at a design condition determined for the safe and reliable operation of the engineering system. Each of these metrics F will typically

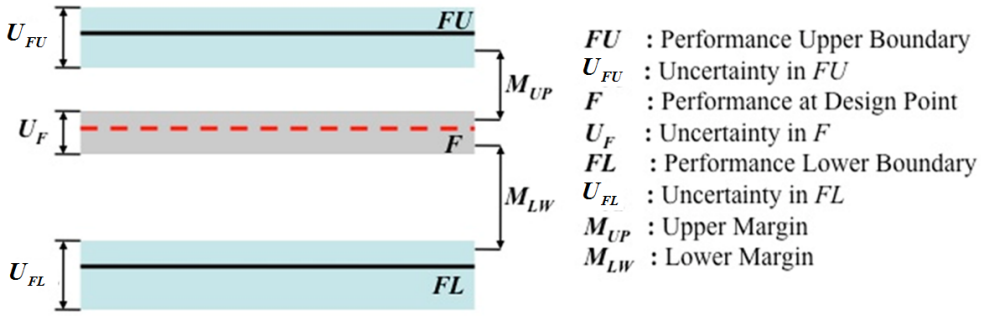

Figure 1.4. Schematic of key measures used in a QMU framework

involve some amount of uncertainty U_F due to the inherent real-life variation of parameters used in physical models as well as the epistemic uncertainties. The safe and reliable operation region of the spacecraft or aircraft (performance gates) will be bounded with a lower bound FL and an upper bound FU for each metric (i.e., metrics evaluated at the off-design boundaries), which will also include some uncertainty (U_{FL} for FL and U_{FU} for FU) due to the aforementioned uncertainty sources.

A measure of the distance between the design value of each performance metric and the lower boundary including the effect of uncertainties U_F and U_{FL} will give the lower margin M_{LW} and the distance between the upper boundary and the design value of each performance metric including the effect of uncertainties U_{FU} and U_F will give the upper margin M_{UP}. The margins must significantly exceed any associated uncertainty in order to avoid failure. Using the uncertainty (U) and the margin (M) information, a QMU metric has to be developed to quantify and certify the confidence for the safe operation of the system or each sub system (e.g., confidence ratio, CR) which is given by:

$$CR = \frac{M}{U} \tag{1.50}$$

where M is a measure of the margin and U represents a measure of the uncertainty. The confidence ratio can be used as a degree to which the operation of a system or each sub-system is considered to lie within 'safe' bounds. As mentioned earlier, margins should exceed any associated uncertainty thereby stating that a CR sufficiently larger than 1 indicates safe and reliable conditions.

Since there exist two performance gates for each performance metric (upper and lower bound), the evaluation of margin and uncertainty will result in two confidence ratios; (1) confidence ratio with respect to lower boundary CR_{LW} and (2) confidence ratio with respect to the upper boundary CR_{UP}. However, it is important to note that the CR is calculated for each system, sub-system and / or component of a sub-system in a particular QMU analysis. The system confidence ratio CR_{system} is represented by the minimum CR which replicates the worst case scenario as far as system safety is concerned. Theoretically speaking, there is a family of confidence ratios in a problem with mixed uncertainties due to the presence of multiple cumulative distribution functions (CDFs) per p-box. The bounding CDFs (lowest & highest) of the p-box are used to calculate the 95% confidence interval in uncertainty quantification [29]. Similar methodology is used to calculate the confidence ratio for the lower and upper boundary, respectively. Further, the minimum value of the two CRs $(CR_{LW}$ & $CR_{UP})$ will result in the worst case scenario and a reliable value to carry out the performance assessment and certification.

Mathematically, the two confidence ratios can be formulated as follows:

$$CR_{LW} = \frac{M_{LW}}{U_{LW}} \quad \text{and} \quad CR_{UP} = \frac{M_{UP}}{U_{UP}} \tag{1.51}$$

In Eq. (1.51), similar to the measure of the margins, U_{UP} is a function of performance metric and upper boundary uncertainties i.e. U_F and U_{FU} whereas U_{LW} is a function of performance metric and lower boundary uncertainties i.e. U_F and U_{FL}. The system

confidence ratio can be chosen to be the smallest out of the two performance gates. Thus, the minimum confidence ratio from among CR_{LW} and CR_{UP} is likely to tend towards the failure region and can be considered as the confidence ratio for the system.

6.2. QMU Framework Based on Evidence Theory. This section formulates the QMU framework in terms of evidence theory uncertainty measures, belief and plausibility. The usage of DSTE for QMU is preferred especially in situations where multiple sources of uncertainties are encountered for epistemic variables. If this is not the case and pnly single source of uncertainty exists for both probabilistic and epistemic variables, then one can consider to perform mixed uncertainty quantification using methods like second order probability. When a problem formulation consists of probabilistic distributions along with Dempster-Shafer structures for epistemic variables, the discretization procedure as mentioned in Section 5.2 should be used for representing aleatory variables in terms of well-characterized epistemic variables.

Based on this discussion, four cases are presented for the formulation of uncertainty (U) and margin (M) calculations; 1) no uncertainty, 2) pure epistemic uncertainty, 3) pure aleatory uncertainty and 4) mixed (aleatory-epistemic) uncertainty. As this paper focuses on QMU using evidence theory for mixed UQ, the epistemic variables will be considered with Dempster-Shafer structures. Thus, the pure epistemic and mixed uncertainty analysis results will be quantified in terms of CBF and CPF as explained in Section 5.1. For pure aleatory analysis, the response surface is sampled over a large number of Latin Hypercube samples and the uncertainty is quantified in terms of Cumulative Distribution Functions (CDFs).

The uncertainty calculation parameters with respect to upper and lower boundaries are provided in Tables 1.1 and 1.2, Eqns. (1.52) and (1.53), respectively.

Table 1.1. Formulations for uncertainty calculation with respect to upper boundary

Type of uncertainty	$U_{UP1}(FU)$	$U_{UP2}(FU)$	$U_{UP3}(F)$	$U_{UP4}(F)$
No Uncertainty	FU	FU	F	F
Pure Epistemic	$Bel_{P=0.5}$	$Pl_{P=\frac{1-\gamma}{2}}$	$Bel_{P=\frac{1+\gamma}{2}}$	$Pl_{P=0.5}$
Pure Aleatory	$FU_{P=0.5}$	$FU_{P=\frac{1-\gamma}{2}}$	$F_{P=\frac{1+\gamma}{2}}$	$F_{P=0.5}$
Mixed aleatory-epistemic	$Bel_{P=0.5}$	$Pl_{P=\frac{1-\gamma}{2}}$	$Bel_{P=\frac{1+\gamma}{2}}$	$Pl_{P=0.5}$

Table 1.2. Formulations for uncertainty calculation with respect to lower boundary

Type of uncertainty	$U_{LW1}(FL)$	$U_{LW2}(FL)$	$U_{LW3}(F)$	$U_{LW4}(F)$
No Uncertainty	FL	FL	F	F
Pure Epistemic	$Pl_{P=0.5}$	$Bel_{P=\frac{1+\gamma}{2}}$	$Pl_{P=\frac{1-\gamma}{2}}$	$Bel_{P=0.5}$
Pure Aleatory	$FL_{P=0.5}$	$FL_{P=\frac{1+\gamma}{2}}$	$F_{P=\frac{1-\gamma}{2}}$	$F_{P=0.5}$
Mixed aleatory-epistemic	$Pl_{P=0.5}$	$Bel_{P=\frac{1+\gamma}{2}}$	$Pl_{P=\frac{1-\gamma}{2}}$	$Bel_{P=0.5}$

$$U_{UP} = \sqrt{(U_{UP1} - U_{UP2})^2 + (U_{UP3} - U_{UP4})^2} \tag{1.52}$$

$$U_{LW} = \sqrt{(U_{LW1} - U_{LW2})^2 + (U_{LW3} - U_{LW4})^2} \tag{1.53}$$

$$M_{UP} = |M_{UP1} - M_{UP2}| \quad \text{and} \quad M_{LW} = |M_{LW1} - M_{LW2}| \tag{1.54}$$

Table 1.3 indicates the metric (for the design condition or the off-design boundaries) to be adopted corresponding to the type of uncertainty encountered for the calculation of upper and lower margins. Mathematical formulations for M_{UP} and M_{LW} are given

Table 1.3. Formulations for margin calculation

Type of uncertainty	$M_{UP1}(FU)$	$M_{UP2}(F)$	$M_{LW1}(F)$	$M_{LW2}(FL)$
No Uncertainty	FU	F	F	FL
Pure Epistemic	$Pl_{P=\frac{1-\gamma}{2}}$	$Bel_{P=\frac{1+\gamma}{2}}$	$Pl_{P=\frac{1-\gamma}{2}}$	$Bel_{P=\frac{1+\gamma}{2}}$
Pure Aleatory	$FU_{P=\frac{1-\gamma}{2}}$	$F_{P=\frac{1+\gamma}{2}}$	$F_{P=\frac{1-\gamma}{2}}$	$FL_{P=\frac{1+\gamma}{2}}$
Mixed aleatory-epistemic	$Pl_{P=\frac{1-\gamma}{2}}$	$Bel_{P=\frac{1+\gamma}{2}}$	$Pl_{P=\frac{1-\gamma}{2}}$	$Bel_{P=\frac{1+\gamma}{2}}$

in Eq. (1.54). The subscript P corresponds to the belief / plausibility / probability level whichever is applicable and γ is the specified confidence level (for e.g., $\gamma = 0.95$).

The confidence ratio for the system can then be evaluated using Eqs. (1.51), (1.52), (1.53) and (1.54).

$$CR_{system} = min\{CR_{LW}, CR_{UP}\} = min\{\frac{M_{LW}}{U_{LW}}, \frac{M_{UP}}{U_{UP}}\} \tag{1.55}$$

7. ANALYTICAL QMU MODEL PROBLEM

In order to demonstrate the implementation of evidence theory for mixed UQ using stochastic expansions in QMU methodology, a model problem is presented for coupled systems (System 1 and System 2, see Figure 1.5) represented by analytical non-linear functions. This section will be segregated into 3 subsections; first section will describe the design condition for both systems, second section will describe the boundaries / performance gates for System 1 and the third section will describe the boundaries / performance gates for System 2.

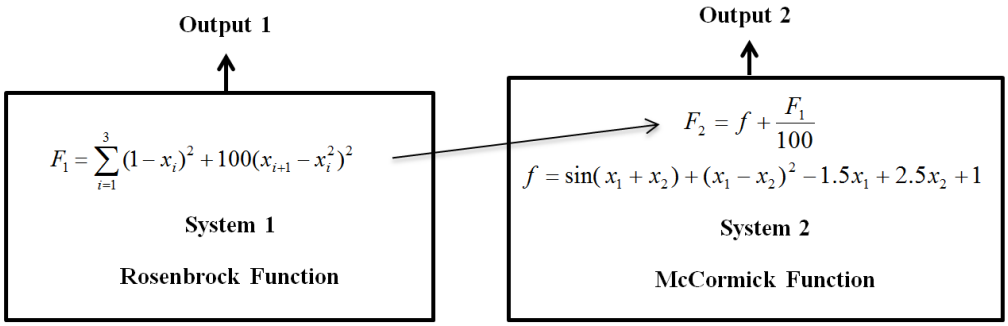

Figure 1.5. Mathematical QMU problem

Table 1.4. Uncertainty information for the mathematical QMU problem

Variable	Distribution	Uncertainty information
x_1	Uniform	[-0.5, 0.8]
x_2	Epistemic	Source 1: [-0.5, -0.1] 50%, [0.1, 0.4] 50% Source 2: [0.0, 0.5] 33.34%, [-0.4, 0.2] 33.33%, [-0.1, 0.1] 33.33% Source 3: [0.25, 0.35] 35%, [-0.45, -0.29] 65%
x_3	Normal	$N(0.25, 0.03)$
x_4	Epistemic	Source 1: [0.2, 1.0] 30%, [-1.0, 0.4] 70% Source 2: [-0.2, 0.3] 33.34%, [-0.5, -0.15] 33.33%, [0.15, 0.9] 33.33%

7.1. UQ for Design Condition of the QMU Model Problem. The mathematical structure of the design condition for Systems 1 and 2 is shown in Figure 1.5. Here, F_1 and F_2 represent the outputs for System 1 and 2, respectively. System 1 comprises of Rosenbrock function with 4 uncertain variables $(x_i, i = 1, 2, 3, 4)$ and System 2 is the McCormick function which has shared input variables x_1 and x_2 with System 1. The mixed uncertainty information for all the variables is given in Table 1.4.

It is clear that one needs to propagate mixed uncertainty using DSTE through discretization procedure described in Section 5.2. A fourth-order chaos expansion was

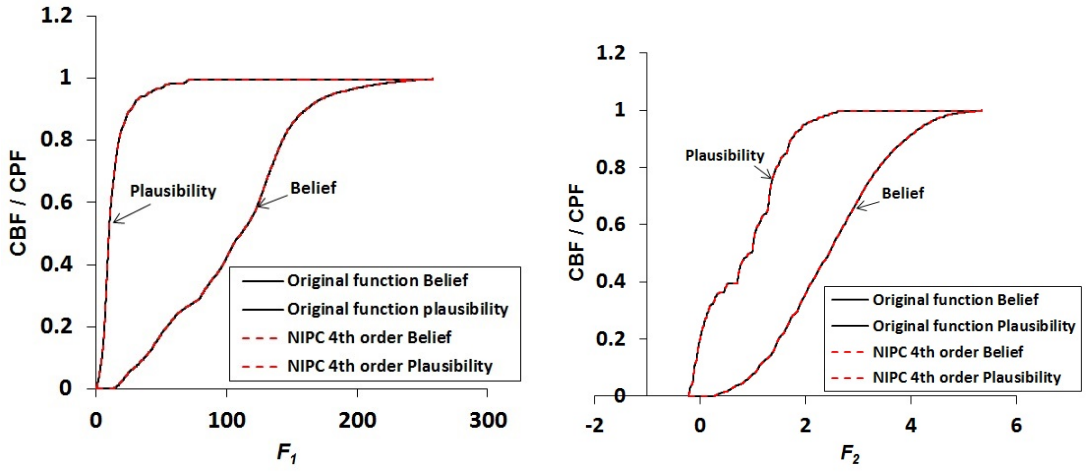

(a) System 1: Design condition

(b) System 2: Design condition

Figure 1.6. Design condition for the QMU model problem

chosen to model the uncertainty propagation with the NIPC method. With an over-sampling ratio of 2 and number of uncertain variables of 4, 140 original function evaluations are required for an accurate stochastic response surface according to Eq. (1.37). The inexpensive response surface replaces the deterministic model which proves to be computationally efficient in view of repetitive simulations required for DSTE analysis. This advantage is substantial for large scale computational models such as aerospace simulations including high fidelity models.

Based on the analysis presented by Shah et al. [35] for aleatory uncertainty discretization, the uniformly distributed variable x_1 is segregated into 30 different intervals with an equal BPA of 1/30 for each sub-interval and the normally distributed variable is discretized into 20 intervals with BPA assigned to each sub-interval according to the Gaussian distribution shown in Eq. (1.49). The DSTE analysis is carried out with the composite Dempster-Shafer structure for mixed UQ for the design condition (See Figure 1.6).

Table 1.5. Input uncertainty information for the performance limits of System 1

Lower Boundary: Single parameter with $N(-100.0, 5.5)$		
		Upper Boundary
Variable	**Distribution**	**Uncertainty information**
y_1	Normal	$N(30.0, 2.5)$
x_2	Epistemic	Source 1: [-0.5, -0.1] 50%, [0.1, 0.4] 50% Source 2: [0.0, 0.5] 33.34%, [-0.4, 0.2] 33.33%, [-0.1, 0.1] 33.33% Source 3: [0.25, 0.35] 35%, [-0.45, -0.29] 65%

7.2. Performance Gates and UQ for System 1. In this example problem, System 1 is considered to be bounded by both, upper and lower boundaries. The lower boundary consists of a normally distributed parameter, treated as a pure aleatory limit which provides a single CDF and the upper boundary for System 1 is represented by a 2 variable Booth function which is given by:

$$FU_{sys1} = (y_1 + 2x_2 - 7)^2 + (2y_1 + x_2 - 5)^2 \tag{1.56}$$

where FU_{sys1} denotes the upper boundary for System 1. As can be seen from Eq. (1.56), the upper boundary has a shared input variable in the form of x_2. The input uncertainty information for the performance gates is given in Table 1.5.

As the variable x_2 is an epistemic variable with a Dempster-Shafer structure and y_1 represents aleatory uncertainty, uncertainty is quantified using DSTE with discretization process for the aleatory variable. In this case, normally distributed variable y_1 is discretized into 75 intervals to carry out the DSTE analysis for the composite Dempster-Shafer structure using a 2^{nd} order chaos expansion (see Figure 1.7). Thus, only 12 original function evaluations were required with an over-sampling ratio of 2.

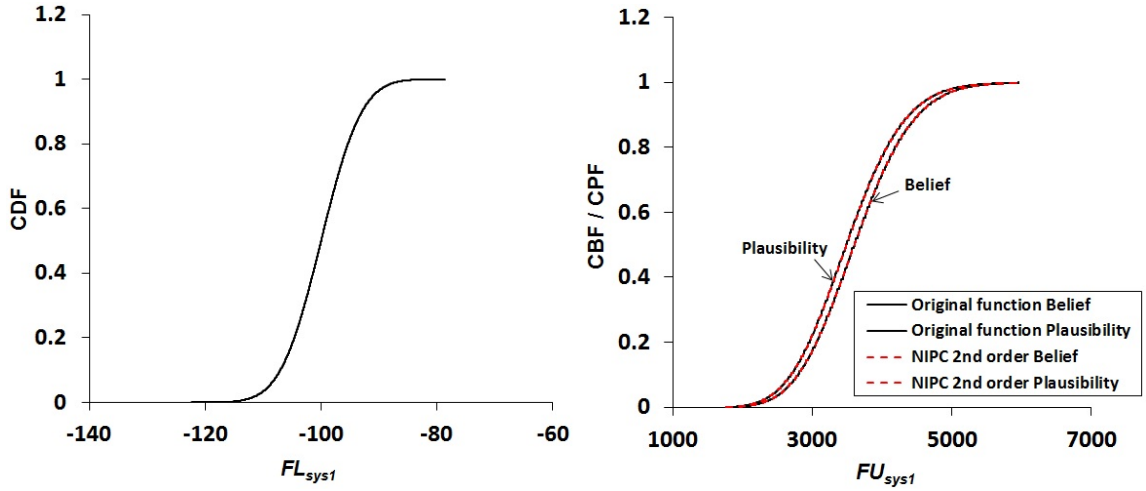

(a) System 1: Lower bound (b) System 1: Upper bound

Figure 1.7. Performance gates for System 1

7.3. Performance Gates and UQ for System 2. There exists an upper boundary for System 2 in the form of Dakota textbook problem [55] with 2 uncertain variables which is given by:

$$FU_{sys2} = (x_1 - 1)^4 + (z_2 - 1)^4 \tag{1.57}$$

Eq. (1.57) represents the same scenario as in the upper boundary for System 1. It shares an input variable x_1 with the design condition, uncertainty data for which is shown in Table 1.4. z_2 is an epistemic variable with a Dempster-Shafer structure from a single source as listed in Table 1.6.

As the upper boundary for System 2 is also characterized by mixed uncertainty, DSTE analysis is carried out by segregating the uniformly distributed variable x_1 into 75 intervals with an equal BPA to each sub-interval (see Figure 1.8). A 4^{th} order chaos expansion with over-sampling ratio of 2 required 30 original function evaluations.

Table 1.6. Uncertainty Information for Upper Boundary of System 2

Variable	Distribution	Uncertainty
x_1	Uniform	[-0.5, 0.8]
z_2	Epistemic	[6.0, 6.5] 50%, [6.3, 6.75] 30%, [5.9, 6.2] 20%

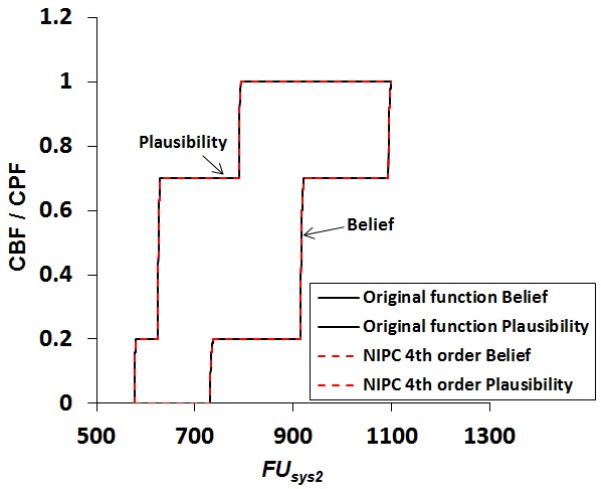

Figure 1.8. Performance gate for System 2: Upper Bound

Table 1.7. Computational efficiency of NIPC methodology

Performance metric	**Polynomial order**	**Original Function evaluations**	**Original Function evaluations using NIPC**
Design Point: System 1	4	47967	140
Upper Bound: System 1	2	560	12
Design Point: System 2	4	39219	140
Upper Bound: System 2	4	180	30

Table 1.8. System 1: QMU Analysis Metrics

Performance Gate	**Margin**	**Uncertainty**	*CR*
Lower	91.3959	109.859	0.8319
Upper	2124.765	1292.169	1.6443

The surrogate models for each metric, including the performance gates, are compared to the original function output statistics in Figures 1.6, 1.7 and 1.8. It is evident that the NIPC response surfaces are accurate. Computational efficiency is also achieved in terms of original function evaluations which can be compared in Table 1.7.

7.4. Quantification of Margins and Uncertainties for QMU Model Problem. A confidence level of $\gamma = 0.95$ is chosen for the QMU model problem. For better understanding, Figure 1.9 gives a pictorial presentation for calculation of uncertainties and margins for System 1 with the specified confidence level. For System 1, QMU analysis based on upper and lower boundaries is summarized in Table 1.8.

Similarly for System 2, QMU analysis is solely based on the upper boundary which is summarized in Table 1.9. Thus, the system confidence ratio can be given as $CR_{system} = min\{CR_{sys1}, CR_{sys2}\} = 0.8319$. We see that the confidence ratio for the whole system is

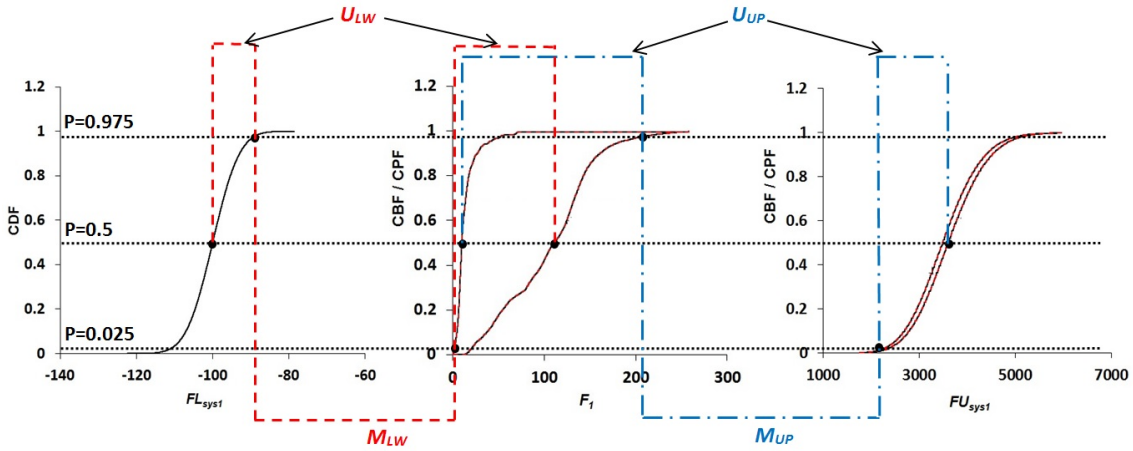

Figure 1.9. Demonstration for calculation of uncertainties and margins for System 1 (Note that the figures are not drawn to scale to increase the clarity)

Table 1.9. System 2: QMU Analysis Metrics

Performance Gate	**Margin**	**Uncertainty**	*CR*
Upper	571.9426	339.7115	1.6836

governed by that of System 1, in particular the confidence ratio related to the lower performance boundary and associated uncertainties including the design point. The parameter *CR* basically helps the decision-maker in risk assessment and risk mitigation. Post analysis may be carried out on the basis of the confidence ratio parameter to make the design robust, which will be measured by the improvement in the confidence ratio.

8. MULTIDISCIPLINARY ANALYSIS OF A SUPERSONIC CIVIL TRANSPORT

A multidisciplinary analysis system for the High Speed Civil Transport (HSCT) was selected as the 2^{nd} model problem in order to demonstrate QMU using DSTE with stochastic expansions. The Integrated Multidisciplinary Optimization Object System (IMOO) [56],

analysis tool used for this model problem, is a tool set designed to address many issues for next generation vehicle applications. It utilizes an object-oriented integration framework that allows users to efficiently link high fidelity analysis modules. The problem setup time is significantly reduced by simplifying the definition of interdisciplinary coupling, allowing the creation of complex data objects and eliminating laborious manual data conversion. The IMOO system succeeds in sharing complex data by utilizing an object-oriented approach in which upstream modules create objects that are used by downstream modules on demand. Both the data and the methods reside in the object and downstream modules may request the data when needed. An example of this is mesh generation. IMOO implements automatic mesh generation and morphing through advanced parametric geometry and grid technology for multidisciplinary modeling [57]. M4 Engineering has developed a parametric grid morphing tool, Geometry Manipulation by Automatic Parameterization (GMAP [58]), and a parametric Finite Element Analysis (FEA) model generator for internal structures (RapidFEM [59]). These tools are integrated into the framework environment to quickly analyze FEA / CFD cases, morph geometry, re-mesh, apply loads, and generate useful results. Thus, the IMOO system allows configurations to be rapidly assessed and different numerical optimization techniques be used to help determine the optimal design.

8.1. Description of the Deterministic Model. For the current study, the analysis configuration selected is the HSCT [60] as shown in Figure 1.10. The design variables used in the IMOO system model of the HSCT include the wing area, aspect ratio, sweep angle, taper ratio, span-wise location of break chord, leading edge position of break, break chord, and tip chord ratio (Figure 1.11).

For the QMU demonstration, a modified version of the supersonic vehicle design process was chosen (shown in Figure 1.12). The five modules considered are: 1. Geometry, 2. Aerodynamics, 3. Propulsion, 4. Structures and 5. Range Performance (Brequet Range).

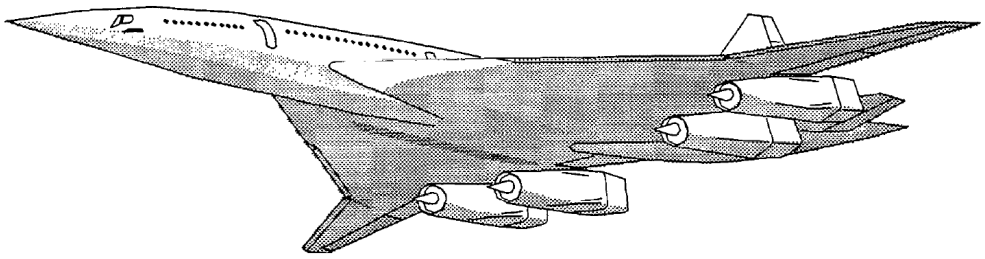

Figure 1.10. Generic HSCT configuration

- **High Speed Civil Transport (HSCT)**
- **Geometric Design Variables**
  - S (wing projected area)
  - AR (aspect ratio)
  - Sweep
  - Taper
  - Omega
  - Eta
  - Theta

Non-dimensional representation of wing break

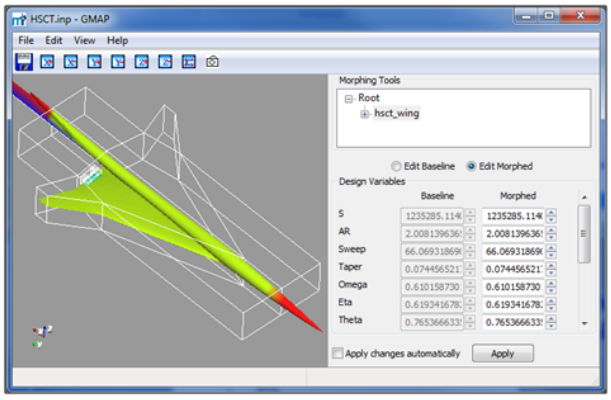

Figure 1.11. HSCT with geometric design variables

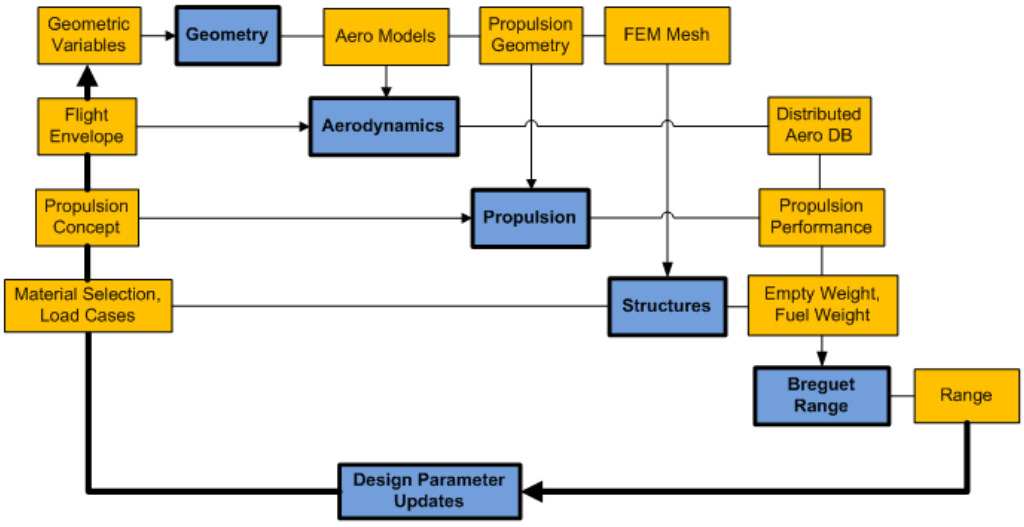

Figure 1.12. Supersonic vehicle design structure matrix

The standard design structure matrix shows the analysis modules as blue boxes on the diagonal of the matrix, and the data items used by or generated by the modules are shown as yellow boxes. The far left column of yellow boxes represents inputs to the entire process, and the far right column represents outputs from the process. The outputs from a particular module are placed on the same row as the module, and the inputs are in the same column (for example, Propulsion Performance is an output of the Propulsion Module and an input to the Breguet Range Module). In general, module execution is shuffled to get as much information as possible into the upper-right triangle of the matrix, which represents a feed-forward path, where the module generating the data is executed prior to the module using the data. Feedback paths are possible, but require special consideration (e.g., iteration to convergence) and hence, will not be included in this demonstration.

In this process, the geometry Module takes the geometric variables and generates (through GMAP) an updated CFD model (via mesh morphing), a FEM mesh (through parametric geometry & meshing), and information for the propulsion module. Figure 1.13(a)

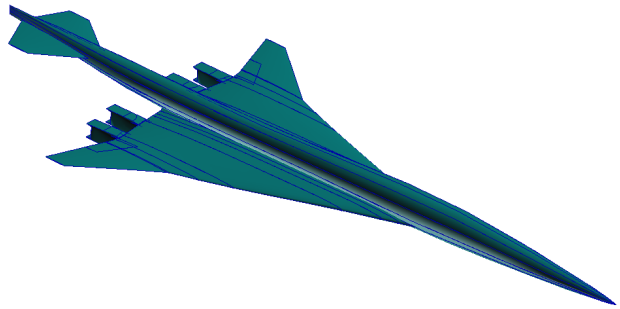

(a) HSCT Base Geometry (shown without vertical tail)

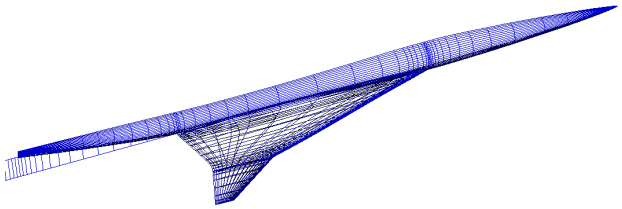

(b) HSCT PANAIR Model (Wing Body Wake)

Figure 1.13. HSCT: Geometry & Aerodynamics model

shows the initial geometry used to develop the baseline aerodynamic and structural meshes. The baseline geometry is analyzed using different modules as explained below.

The aerodynamics module calculates the vehicle aerodynamic coefficients and distributed pressures at various flight conditions for use in performance simulation and load calculations. In order to expedite aerodynamic analyses, the current implementation of the aerodynamics module utilizes Panair [61] to compute aerodynamic loads. Panair (Panel Aerodynamics) solves the linearized potential flow problem for subsonic and supersonic regimes using a higher-order panel method [62, 63, 64]. Figure 1.13(b) shows the half model used for aerodynamic analysis.

The second module (propulsion) utilizes the Numerical Propulsion System Simulation (NPSS) [65] to calculate the propulsion performance (specific fuel consumption etc.) for use in the Breguet Range module. NPSS is a comprehensive propulsion simulation

Table 1.10. HSCT Uncertain Parameters

Variable	Distribution	Uncertainty information
Mach Number ($\tilde{M}$)	Normal	$N(2.0, 0.02)$
Angle of Attack ($\tilde{\alpha}$)	Epistemic	Source 1: [2.4, 2.45] 20%, [2.43, 2.56] 50%, [2.51, 2.6] 30% Source 2: [2.58, 2.6] 10%, [2.5, 2.55] 60%, [2.45, 2.49] 30%
Wing Sweep Angle (Λ)	Normal	$N(68.0, 1.0)$
Wing Taper ratio (λ)	Uniform	[0.06, 0.1]

tool capable of accurately predicting aerothermodynamic behavior of jet engines in various flight regimes.

The structural module, using a NASTRAN optimization, calculates loads and structural sizing to estimate the takeoff gross weight (TOGW). The design load case simulated corresponds to a 1.5-g pull up (consistent with FAR part 25 criteria). The Breguet Range Module computes the range performance for the supersonic vehicle based upon the outputs from the upstream modules.

8.2. Description of the Stochastic Model. This section describes the stochastic model problem chosen to demonstrate the proposed QMU methodology based on DSTE measures.

8.2.1. Design condition. For the HSCT model problem, two modules (Geometry and Aerodynamics) have been chosen to include uncertain input parameters. The schematic of the stochastic model for the HSCT problem is shown in Figure 1.14. The geometry module has 2 uncertain input parameters: wing sweep angle and the wing taper ratio. The Mach number and the angle of attack, being the two important parameters in aerodynamic analysis, have been chosen as the source of uncertainty for the design of supersonic vehicle. The uncertainty information for all the parameters is summarized in Table 1.10.

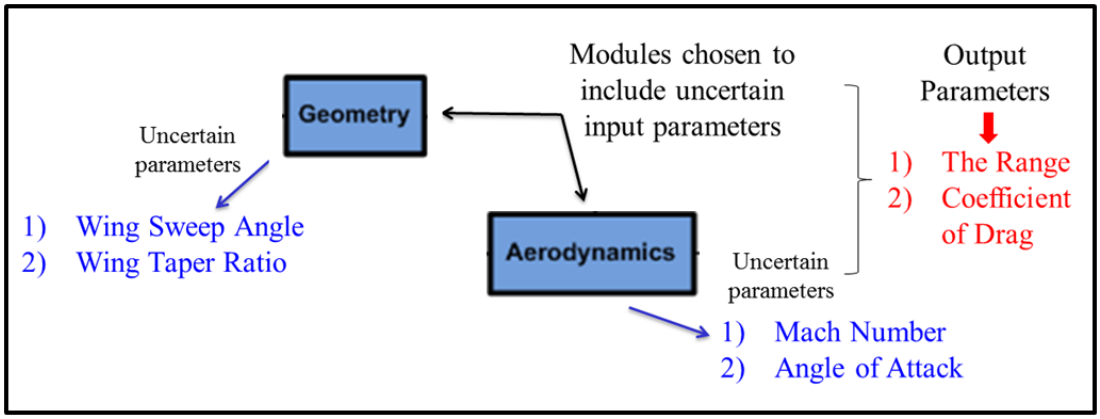

Figure 1.14. Stochastic model for HSCT

Given the input uncertainty, the range and the drag coefficient are considered as the performance metrics which are related to multiple systems, each subject to inherent and epistemic uncertainties. The Range plays an important role in the design of a civil transport vehicle and coefficient of drag is one of the key design parameters that affects the vehicle performance.

8.2.2. Performance gates for the Range. In an aircraft design, a minimum value of range for which the aircraft should fly, is specified. For demonstration purposes, a lower boundary for the range is selected as 2700 nautical miles (nmi) with no uncertainty.

8.2.3. Performance gates for the coefficient of Drag. In aircraft design, a maximum value of drag coefficient may be used as a criteria to limit engine selection size and reduce fuel economy. In present analysis, drag coefficient is constrained by an upper limit of 0.0085 with no uncertainty.

8.3. Uncertainty Quantification using DSTE. This section summarizes the uncertainty quantification results for the supersonic civil transport.

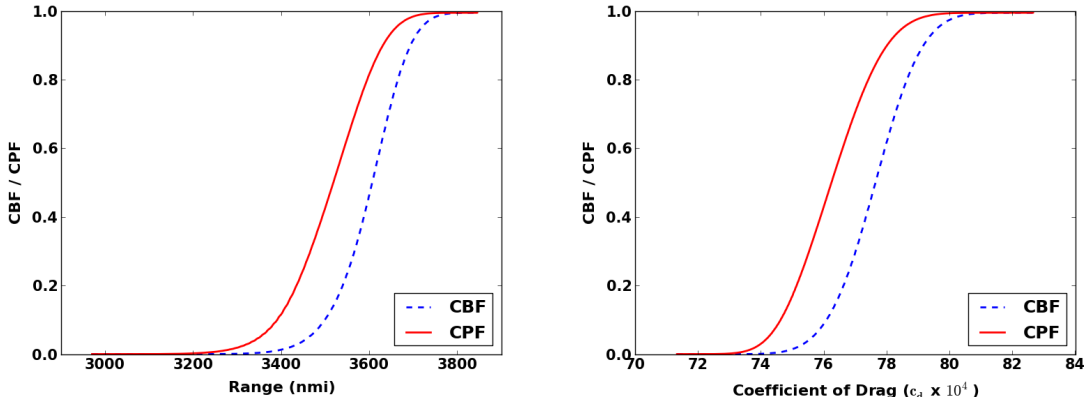

(a) HSCT: Range

(b) HSCT: Coefficient of drag

Figure 1.15. UQ for HSCT using DSTE

8.3.1. Design condition. UQ analysis for the HSCT design condition is carried out using the DSTE approach with stochastic expansions. As there are 4 uncertain variables in the system, according to Eq. (1.35), 30 deterministic evaluations were required with a n_p of 2 for a second order PCE. The taper ratio was discretized into 23 sub-intervals and the Mach number and sweep angle were discretized into 22 sub-intervals each to obtain the belief and plausibility measures. The CBF and CPF for the output quantities, range and coefficient of drag are shown in Figure 1.15.

To assess the accuracy of the response surface for range and coefficient of drag, 10 sample points were chosen in the uncertainty domain at which the difference between the actual model and the surrogate (i.e. the response surface) were calculated. It was found that, the surrogate models for the range and coefficient of drag, based on a second order PCE, were accurate with the highest mean error being approximately 0.05%. As a result of this error analysis, the QMU analysis was performed using the second order expansion.

Table 1.11. HSCT Range: QMU Analysis Metrics

Performance Gate	**Margin**	**Uncertainty**	*CR*
Lower	611.951	289.347	2.1149

Table 1.12. HSCT Drag Coefficient: QMU Analysis Metrics

Performance Gate	**Margin**	**Uncertainty**	*CR*
Upper	5.085×10^{-4}	3.947×10^{-4}	1.289

8.3.2. Performance limits. As mentioned before, no uncertainty was considered in case of performance gates for both the output quantities. Thus, they are treated as being constant which will correspond to the row with "No uncertainty" in Tables 1.1, 1.2 and 1.3.

8.4. Quantification of Margins and Uncertainties for HSCT. Now that the uncertainties are quantified in the design condition, the next step is to perform the QMU analysis on HSCT. Similar to the previous example problem, a confidence level of $\gamma = 0.95$ is chosen for the HSCT problem. The design metric for the range of the supersonic vehicle is represented by mixed uncertainty whereas the lower performance limit is attributed with no uncertainty. Using the equations and tables given in Section 6.2, the uncertainty and margin calculations are performed and summarized in Table 1.11 in terms of *CR*.

Similarly, the drag coefficient is also represented with mixed uncertainty whereas the upper performance limit has no uncertainty. The QMU analysis results are summarized in Table 1.12.

Using Eq. (1.55), system wide confidence ratio is the minimum *CR* from among the two output quantities under consideration. The minimum value is chosen as it indicates the weakest link in the system design. In present analysis, the system wide confidence ratio is obtained as 1.289 for coefficient of drag, indicating that the margins are greater than

the uncertainties. In case the uncertainties are greater than or equal to the margins (i.e. $CR \leq 1$), a re-design of the system, performance limits or both may be required to make the system more reliable.

9. CONCLUSION

The objective of this paper is to implement Dempster-Shafer Theory of Evidence (DSTE) in the presence of mixed uncertainty to the system reliability and performance assessment of complex engineering systems through the use of Quantification of Margins and Uncertainties (QMU) methodology. Specifically, *uncertainty quantification* (UQ) has been used as a tool of *certification* to decide whether a system is likely to perform safely and reliably within design specifications. Importance and contribution of the current study lies in creation of a novel QMU framework in terms of Dempster-Shafer structures (belief & plausibility) which can be used for performance assessment of a system under uncertainty. Specifically, DSTE is used for uncertainty quantification to address the possibility of multiple sources and intervals for epistemic uncertainty characterization. Furthermore, the DSTE is utilized for mixed uncertainty quantification by discretizing the aleatory probability distributions into optimum sets of intervals and treating them as well-characterized epistemic variables. In addition, the response quantities of interest for design performance and boundaries are represented with stochastic surrogates based on Non-intrusive Polynomial Chaos (NIPC) to reduce the computational expense of implementing DSTE for uncertainty quantification of high-fidelity complex system models.

The first QMU model problem consisted of a complex system of nonlinear functions which are typically used in numerical optimization studies. The QMU methodology using the evidence theory is demonstrated on the coupled analytical system of equations, which have shared inputs with their respective performance boundaries. In order to demonstrate

the usage of evidence theory in propagating mixed uncertainties, different combinations of performance metrics and limits were adopted in the QMU analysis.

The second model problem was multi-disciplinary analysis of a high speed civil transport for the demonstration of the QMU methodology for complex engineering systems in aerospace applications. The drag coefficient and the Range performance were studied as the output quantities which are considered critical during an aircraft design process. Second order NIPC expansions were used as surrogates for both performance metrics, which proved to be computationally efficient in quantifying the margins and uncertainties using evidence theory.

Overall, the proposed approach outlined a computationally efficient framework for quantifying margins and uncertainties with DSTE and stochastic expansions. Two model problems were utilized to demonstrate the QMU methodology, which included various types of uncertainty representations for the performance metrics and limits. The results indicate the potential of the proposed QMU approach for the evaluation of safety and reliability of complex engineering systems in terms of efficiency and effectiveness.

ACKNOWLEDGMENT

Funding for this research was provided by NASA Jet Propulsion Laboratory under a Small Business Technology Transfer Phase II project grant no. NNX11CC60C (Dr. Lee D. Peterson, program manager).

BIBLIOGRAPHY

[1] Sharp, D. H., and Wood-Schultz, M. M., "QMU and Nuclear Weapons Certification. What's Under the Hood," Los Alamos Science, Number 28, 2003, pp: 47-53.

[2] Goodwin, B. T., and Juzaitis, R. J., National certification methodology for the nuclear weapon stockpile. Draft working paper;2003.

[3] Eardley, D. (Study Leader), "Quantification of Margins and Uncertainties (QMU)," Technical Report, JSR-04-330 (JASON), March 2005.

[4] U.S. GAO (U.S.Government Accountability Office). Nuclear weapons: NNSA needs to refine and more effectively manage its new approach for assessing and certifying nuclear weapons. GAO-06-261. Washington, DC: U.S. Government Accountability Office; 2006.

[5] NAS/NRC (National Academy of Science/National Research Council). Evaluation of Quantification of Margins and Uncertainties for Assessing and Certifying the Reliability of the Nuclear Stockpile. Washington, DC: National Academy Press; 2008.

[6] Pilch, M., Trucano, T. G., and Helton, J. C., "Ideas Underlying the Quantification of Margins and Uncertainties," *Reliability Engineering and System Safety*, Vol. 96, 2011, pp. 965-975.

[7] Pepin, J. E., Rytherford, A. C., and Hemez, F. M., "Defining a Practical QMU Metric," 49^{th} *AIAA/ASME/ASCE/AHS/ASC Structures, Structural Dynamics and Materials Conference*, AIAA Paper 2008-1717, Schaumburg, IL, April 2008.

[8] Lucas, L. J., Owhadi, H., and Ortiz, M., "Rigorous Verification, Validation, Uncertainty Quantification and Certification Through Concentration-of-Measure Inequalities," *Computer Methods in Applied Mechanics and Engineering*, Vol. 197, Issues 51-52, October 2008, pp. 4591-4609.

[9] Iaccariono, G., Pecnik, R., Glimm, J., and Sharp, D., "A QMU Approach for Characterizing Operability Limits of Air-Breathing Hypersonic Vehicles," LANL Report, LA-UR 09-01863, 2009.

[10] National Research Council evaluation of quantification of margins and uncertainties methodology for assessing and certifying the reliability of the nuclear stockpile. Washington, DC: The National Academies Press; 2009.

[11] Helton, J. C., "Quantification of Margins and Uncertainties: Conceptual and Computational Basis," *Reliability Engineering and System Safety*, Vol. 96 (9), 2011, pp. 976-1013.

[12] Oberkampf, W. L., DeLand, S. M., Rutherford, B. M., Diegert, K. V., and Alvin, K. F., "Error and Uncertainty in Modeling and Simulation," *Reliability Engineering and System Safety*, Vol. 75, 2002, pp. 333-357.

[13] Urbina, A., Mahadevan, S., and Paez, T. L., "Quantification of Margins and Uncertainties of Complex Systems in the Presence of Aleatory and Epistemic Uncertainty ," *Reliability Engineering and System Safety*, Vol. 96, 2011, pp. 1114-1125.

[14] Wallstrom, T. C., "Quantification of Margins and Uncertainties: A Probabilistic Framework," *Reliability Engineering and System Safety*, Vol. 96, 2011, pp. 1053-1062.

[15] Helton, J. C., Johnson, J. D., Oberkampf, W. L., and Storlie, C. B., "A Sampling-Based Computational Strategy for the Representation of Epistemic Uncertainty in Model Predictions with Evidence Theory" *Computational Methods in Applied Mechanics and Engineering*, Vol. 196 (37-40), 2007, pp. 3980-3998.

[16] Owhadi, H., Scovel, C., Sullivan, T. J., McKerns, M., and Ortiz, M., "Optimal Uncertainty Quantification" *SIAM Review*, Vol. 55 (2), 2013, pp. 271-345.

[17] Shafer, G., *A Mathematical Theory of Evidence*, Princeton University Press, Princeton, NJ, 1976.

[18] Pereira, L. C., Guimaraes, L. J. N., Horowitz, B., and Sanchez, M., "Coupled Hydro-Mechanical Fault Reactivation Analysis Incorporating Evidence Theory for Uncertainty Quantification", *Computers and Geotechnics*, Vol. 56, 2014, pp. 202-215.

[19] Helton, J. C., Johnson, J. D., Oberkampf, W. L., and Sallaberry. C. J., "Representation of Analysis Results Involving Aleatory and Epistemic Uncertainty" *International Journal of General Systems*, Vol. 39(6), 2010, pp. 605-646.

[20] Helton, J. C., Oberkampf, W. L., and Johnson, J. D., "Competing Failure Risk Analysis Using Evidence Theory" *Risk Analysis*, Vol. 25 (4), 2005, pp. 973-995.

[21] Helton, J. C., and Johnson, J. D., "Quantification of Margins and Uncertainties: Alternative Representations of Epistemic Uncertainty," *Reliability Engineering and System Safety*, Vol. 96 (9), 2011, pp. 1034-1052.

[22] Swiler, L. P., Paez, T. L., Mayes, R. L., and Eldred, M. S., "Epistemic Uncertainty in the Calculation of Margins," 50^{th} *AIAA/ASME/ASCE/AHS/ASC Structures, Structural Dynamics and Materials Conference*, AIAA Paper 2009-2249, Palm Springs, CA, May 2009.

[23] Bae, H., Grandhi, R. V., and Canfield, R. A., "An Approximation Approach for Uncertainty Quantification Using Evidence Theory," *Reliability Engineering and System Safety*, Vol. 86, 2004, pp. 215-225.

[24] Bae, H., Grandhi, R. V., and Canfield, R. A., "Epistemic Uncertainty Quantification Techniques Including Evidence Theory for Large-Scale Structures," *Reliability Engineering and System Safety*, Vol. 82, 2004, pp. 1101-1112.

[25] Agarwal, H., Renaud, J. E., and Padmanabhan, D., "Uncertainty Quantification Using Evidence Theory in Multidisciplinary Design Optimization," *Reliability Engineering and System Safety*, Vol. 85, 2004, pp. 281-294.

[26] Hosder, S., Walters, R. W., and Balch, M., "Efficient Sampling for Non-intrusive Polynomial Chaos Applications with Multiple Input Uncertain Variables," 9^{th} *AIAA Non-Deterministic Approaches Conference*, AIAA Paper 2007-1939, Honolulu, HI, April 2007.

[27] Hosder, S., Walters, R. W., and Balch, M., "Point-Collocation Non-intrusive Polynomial Chaos Method for Stochastic Computational Fluid Dynamics," *AIAA Journal*, Vol. 48, No. 12, December 2010, pp. 2721-2730.

[28] Bettis, B. R., Hosder, S., and Winter T., "Efficient Uncertainty Quantification in Multidisciplinary Analysis of a Reusable Launch Vehicle," 17*th AIAA International Space Planes and Hypersonic Systems and Technologies Conference*, AIAA Paper 2011-2393, San Francisco, CA, April 2011.

[29] Hosder, S., "Stochastic Response Surfaces Based on Non-intrusive Polynomial Chaos for Uncertainty Quantification ," *International Journal of Mathematical modeling and Numerical Optimization*, Vol. 3, No. 1-2, January 2012, pp. 117-139.

[30] Hosder, S., and Bettis, B. R., "Uncertainty and Sensitivity Analysis for Reentry Flows with Inherent and Model-Form Uncertainties," *Journal of Spacecraft and Rockets*, Vol. 49, No. 2, March-April 2012, pp. 193-206.

[31] Eldred, M. S., Swiler, L. P., and Tang, G., "Mixed Aleatory-Epistemic Uncertainty Quantification with Stochastic Expansions and Optimization-Based Interval Estimation," *Reliability Engineering and System Safety*, Vol. 96, 2011, pp. 1092-1113.

[32] Helton, J. C., Johnson, J. D., and Sallaberry, C. J., "Quantification of Margins and Uncertainties: Example Analyses from Reactor Safety and Radioactive Waste Disposal Involving the Separation of Aleatory and Epistemic Uncertainty," *Reliability Engineering and System Safety*, Vol. 96 (9), 2011, pp. 1014-1033.

[33] Sentz, K., and Ferson, S., "Probabilistic Bounding Analysis in the Quantification of Margins and Uncertainties," *Reliability Engineering and System Safety*, Vol. 96, 2011, pp. 1126-1136.

[34] Ferson, S., Kreinovich, V., Ginzburg, L., Meyers, D. S., and Sentz, K., "Constructing probability boxes and Dempster Shafer structures," Sandia National Laboratories SAND2002-4015, Albuquerque, NM, 2002.

[35] Shah, H. R., Hosder, S., and Winter, T., "A Mixed Uncertainty Quantification Approach with Evidence Theory and Stochastic Expansions," *AIAA SciTech 2014*, AIAA Paper 2014-0298, National Harbor, MD, January 2014.

[36] Parry, G. W., and Winter, P. W., "Characterization and Evaluation of Uncertainty in Probabilistic Risk Analysis" *Nuclear Safety*, Vol. 22 (1), 1981, pp. 28-42.

[37] Parry, G. W., "The Characterization of Uncertainty in Probabilistic Risk Assessments of Complex Systems" *Reliability Engineering and System Safety*, Vol. 54(2-3), 1996, pp. 119-126.

[38] Pate-Cornell, M. E., "Uncertainties in Risk Analysis: Six Levels of Treatment" *Reliability Engineering and System Safety*, Vol. 54(2-3), 1996, pp. 95-111.

[39] Hoffman, F. O., and Hammonds, J. S., "Propagation of Uncertainty in Risk Assessments: The Need to Distinguish Between Uncertainty Due to Lack of Knowledge and Uncertainty Due to Variability" *Risk Analysis*, Vol. 14(5), 1994, pp. 707-712.

[40] Helton, J. C., and Burmaster, D. E., "Guest Editorial: Treatment of Aleatory and Epistemic Uncertainty in Performance Assessments for Complex Systems" *Reliability Engineering and System Safety*, Vol. 54 (2-3), 1996, pp. 91-94.

[41] Helton, J. C., "Uncertainty and Sensitivity Analysis in the Presence of Stochastic and Subjective Uncertainty" *Journal of Statistical Computation and Simulation*, Vol. 57 (1-4), 1997, 3-76.

[42] Helton J. C., "Treatment of Uncertainty in Performance Assessments for Complex Systems" *Risk Analysis*, Vol. 14 (4), 1994, pp. 483-511.

[43] Oberkampf, W. L., Helton, J. C., and Sentz, K., "Mathematical Representation of Uncertainty," 3^{rd} *AIAA Non-Deterministic Approaches Forum*, AIAA Paper 2001-1645, Seattle, WA, April 2001.

[44] Xiu, D., and Karniadakis, G. E., "The Wiener-Askey Polynomial Chaos for Stochastic Differential Equations" *SIAM Journal on Scientific Computing*, Vol. 24(2), 2003, pp. 619-644.

[45] Xiu, D., and Karniadakis, G. E., "Modeling Uncertainty in Flow Simulations Via Generalized Polynomial Chaos" *Journal of Computational Physics*, Vol. 187(1), 2003, pp. 137-167.

[46] Najm, H. N., "Uncertainty Quantification and Polynomial Chaos Techniques in Computational Fluid Dynamics" In. Annual Review of Fluid Mechanics. Vol. 41, 2009: 35-52.

[47] Ghanem, R.G., and Spanos, P., *Stochastic Finite Elements: A Spectral Approach*, Springer, Berlin, 1991.

[48] Eldred, M.S., Webster, C.G. and Constantine, P.G., "Evaluation of non-intrusive approaches for Wiener-Askey generalized polynomial chaos," 10^{th} *AIAA Non-Deterministic Approaches Forum*, AIAA-Paper 2008-1892, Schaumburg, IL, April 2008.

[49] Yager, R., "Arithmetic and Other Operations on Dempster Shafer Structures," *International Journal of Man-Machine Studies*, Vol. 25, 1986, pp. 357-366.

[50] Zadeh, L. A., "Review of Books: A Mathematical Theory of Evidence," *The AI Magazine*, Vol 5, No. 3, 1984, pp. 81-83.

[51] Sentz, K., and Ferson, S., "Combination of Evidence in Dempster-Shafer Theory," Sandia National Laboratories SAND2002-0835, Albuquerque, NM, April 2002.

[52] Zadeh, L. A., "A Simple View of the Dempster-Shafer Theory of Evidence and its Implication for the Rule of Combination," *The AI Magazine*, Vol 7, 1986, pp. 85-90.

[53] Helton, J. C., Johnson, J. D., and Oberkampf, W. L., "An Exploration of Alternative Approaches to the Representation of Uncertainty in Model Predictions," *Reliability Engineering and System Safety*, Vol. 85, 2004, pp. 39-71.

[54] Nikolaidis, E., Ghiocel, D. M., and Singhal, S., *Engineering Design Reliability Handbook*, 1^{st} ed., CRC Press, July 2004, Chapter 10.

[55] Adams, B. M., Ebeida, M. S., Eldred, M. S., Jakeman, J. D., Swiler, L. P., Bohnnhoff, W. J., Dalbey, K. R., Eddy, J. P., Hu, K. T., Vigil, D. M., Bauman, L. E., and Hough P. D., "Dakota, A Multilevel Parallel Object-Oriented Framework for Design Optimization, Parameter Estimation, Uncertainty Quantification, and Sensitivity Analysis," Sandia National Laboratories SAND2010-2183, Albuquerque, NM, Updated March 6, 2014.

[56] Doyle, S., PMP, K. A., Winter T., "Developing the Aerodynamics Module for the Integrated Multidisciplinary Optimization Object System," 49^{th} *AIAA Aerospace Sciences Meeting including the New Horizons Forum and Aerospace Exposition*, AIAA Paper 2011-8, Orlando, FL, January 2011.

[57] Raymondson, C., Baker, M., Doyle, S., Young, S. and Tejtel, D., "Geometry Manipulation by Automatic Parameterization (GMAP)," *AIAA MDAO Conference*, September 2008.

[58] Dahlin, Andrew and Baker, Myles L., "GMAP Mesh User's Manual s.1," *M4 Engineering*, 2010.

[59] Stuewe, Daniel and Baker, Myles L, "RapidFEM User's Manual," *M4 Engineering*, 2010.

[60] *High Speed Research Program HSR II âĂŞ Airframe Task 20, Task 2.1 âĂŞ Technology Integration, Sub-task 2.1.1.2 Refine Technology Concept Airplane: Configuration Description Document.* April 1996.

[61] Saaris, G. R., Tinoco, E. N., Lee, J. L. and Rubbert, P. E, "User's Guide PAN AIR Technology Program for Solving Potential Flow about Arbitrary Configurations," 1992.

[62] Johnson, F. T. and Rubbert, P. E., "Advanced Panel-Type Influence Coefficient Methods Applied to Subsonic Flows. s.l.," *AIAA 75-50*, January 1975.

[63] Ehlers, F. E., Johnson, F. T. and Rubbert, P. E., "A Higher Order Panel Method for Linearized Supersonic Flow. s.l. ," *AIAA 76-381*, July 1976.

[64] Ehlers, F.E., Epton, M.A., Johnson F.T., Magnus A.E., and Rubbert, P.E., "A Higher Order Panel Method for Linearized Supersonic Flow," *NASA Contractor Report 3062*, 1979.

[65] Claus, R.W., Evans, A.L., Lylte, J.K., Nichols, L.D., "Numerical Propulsion System Simulation. 4," *Computing Systems in Engineering*, Vol. 2, 1991, pp. 357-364.

III. MULTI-FIDELITY ROBUST AERODYNAMIC DESIGN OPTIMIZATION UNDER MIXED UNCERTAINTY

Harsheel Shah[1], **Serhat Hosder**[1]

Slawomir Koziel[2], **Yonatan A. Tesfahunegn**[3], **and Leifur Leifsson**[4]

[1]Missouri University of Science & Technology, Rolla, MO, 65409, USA
[2]Gdansk University of Technology, 80-233 Gdansk, Poland
[3]Reykjavik University, Menntavegur 1, 101 Reykjavik, Iceland
[4]Iowa State University, Ames, Iowa, 50011, USA

ABSTRACT

The objective of this paper is to present a robust optimization algorithm for computationally efficient airfoil design under mixed (inherent and epistemic) uncertainty using a multi-fidelity approach. This algorithm exploits stochastic expansions derived from the Non-Intrusive Polynomial Chaos (NIPC) technique to create surrogate models utilized in the optimization process. A combined NIPC expansion approach is used, where both the design and the mixed uncertain parameters are the independent variables of the surrogate model. To reduce the computational cost, the high-fidelity Computational Fluid Dynamics (CFD) model is replaced by a suitably corrected low-fidelity one, the latter being evaluated using the same CFD solver but with a coarser mesh. The model correction is implemented to the low-fidelity CFD solutions utilized for the construction of stochastic surrogate by using multi-point Output Space Mapping (OSM) technique. The proposed algorithm is applied to the design of NACA 4-digit airfoils with four deterministic design variables (the airfoil shape parameters and the angle of attack), one aleatory uncertain variable (the Mach number) and one epistemic variable (β, a geometry parameter) to demonstrate robust optimization under mixed uncertainties. In terms of computational cost, the proposed technique outperforms the conventional approach that exclusively uses the high-fidelity model

to create the surrogates. The design cost reduces to only 34 equivalent high-fidelity model evaluations versus 168 obtained with the conventional method.

NOMENCLATURE

n	number of design variables
N	number of random variables
p_d	deterministic state variable vector
SR	support region of random input variable
n_p	oversampling ratio
p	order of polynomial chaos
ξ	standard input random variable vector
$p(\xi)$	probability density function of $\vec{\xi}$
ψ	random basis function
a	coefficient in polynomial chaos expansion
a^*	stochastic function
μ	mean
σ	standard deviation
N_t	number of terms in a total-order expansion
C_l	coefficient of lift
C_d	coefficient of drag
M	Mach number
α	angle of attack in degrees
β	geometry parameter in thickness distribution formula for NACA 4-digit airfoils
Re	Reynolds number

N_h number of high-fidelity CFD simulations

N_f number of low-fidelity CFD simulations

N_{cost} total design cost

LF low-fidelity

HF high-fidelity

CLF corrected low-fidelity

1. INTRODUCTION

Robust Design is a design methodology for improving the quality of a product by minimizing the impact of uncertainties on the product performance. The objective of robust design is to optimize the mean performance while minimizing the variation of performance caused by various uncertainties. In the context of aerodynamic shape optimization, robust design implies that the performance (such as coefficient of drag, the lift-to-drag ratio, etc.) of the final configuration should be insensitive to the uncertainties in the operating conditions (e.g., free-stream Mach number) and the geometry (e.g., manufacturing uncertainties). An important component of robust design is Uncertainty Quantification (UQ), which may significantly increase the computational expense of the design process compared to the computational effort of deterministic optimization. This is particularly the case when high-fidelity analysis tools are involved in the design process in order to ensure sufficient accuracy. Therefore, it is important to develop and implement computationally efficient robust design methodologies while keeping the desired accuracy level in the optimization process.

Two types of input uncertainty should be considered in robust aerodynamic design studies: inherent (aleatory) uncertainty and epistemic uncertainty [1, 2]. Aleatory uncertainty, which is probabilistic and irreducible, describes the inherent variation associated with the physical system (e.g., the operating conditions). Epistemic uncertainty[3] is reducible and described as lack of knowledge or information in any phase or operation of a design process (e.g., turbulence models used in CFD simulations). These two types of uncertainties usually co-exist (e.g., mixed uncertainties) in real-world systems. In mathematical terms, aleatory uncertainties are characterized by probability density functions with sufficient information on the type of the distribution. In order to characterize epistemic uncertainty, probabilistic methods are not suitable due to insufficient information about the uncertainty. One possible approach to model the epistemic uncertainty is to characterize it with intervals. For mixed uncertainty quantification, formulations that combine probabilistic methods and interval approach are usually sought. The aerodynamic response (e.g., the drag coefficient) should be in the form of the combination of probability distribution due to the effect of aleatory input uncertainty and interval distribution which indicate the effect of epistemic uncertainty.

This paper attempts to further reduce the computational cost of the robust design procedure introduced in Zhang et al.[4] and builds upon the recent study by the authors[5], which focused on robust optimization under inherent uncertainties only. The proposed approach is based on replacing the computationally expensive High-Fidelity (HF) CFD model by its inexpensive representation referred to as the Corrected Low-Fidelity (CLF) model. The Low-Fidelity (LF) model is evaluated using the same CFD solver but with a coarser mesh and relaxed convergence criteria. The misalignment between LF and HF models is reduced by means of Output Space Mapping (OSM) [6, 7, 8, 9]. The OSM technique has traditionally been used as an auxiliary response correction method in the context of design

optimization, with the LF model being corrected at each iteration using the HF model data accumulated during the process. In the proposed approach, the correction can only be performed once, for the points used for constructing the stochastic surrogate model based on Non-Intrusive Polynomial Chaos (NIPC) technique. Moreover, the CLF model has to be aligned sufficiently well with the HF model in the entire design space to be considered in the construction of the surrogate model subsequently utilized in the optimization process. Such an alignment is obtained by using design-variable-dependent multiplicative OSM set up with sufficient number of HF training samples.

In the next section, different robustness measures and objective function formulation for robust design depending on the input uncertainty type are given. The UQ approach, which is the point-collocation NIPC based stochastic expansions is described in Section 3. Further, the multi-fidelity approach involving the construction of the CLF model based on the HF model using OSM strategy is explained in Section 4. To demonstrate the multi-fidelity robust optimization methodology under mixed uncertainties, a CFD example is presented in Section 5 with Mach number considered as aleatory uncertainty and β (geometry) parameter as the epistemic uncertainty. The NACA airfoil shape parameters and the angle of attack are treated as deterministic design variables. Section 6 concludes the paper with important interpretations of the results obtained.

2. PROBLEM FORMULATION FOR ROBUST OPTIMIZATION

2.1. Deterministic Design. In general, the goal of Aerodynamic Shape Optimization (ASO) is to find a shape such that one or more performance metrics are optimized for a given operating condition(s), while at the same time fulfilling a set of constraints. Mathematically, the ASO problem consists of determining values of design variables $\mathbf{x} \in R^n$, such that the objective function $J : R^n \rightarrow R$ is minimized,

$$min \quad J(\mathbf{x}, \mathbf{Q}), \tag{1.58}$$

subject to constraint equations,

$$\mathbf{g}(\mathbf{x}, \mathbf{Q}) \leq 0, \tag{1.59}$$

where $\mathbf{Q}$ denotes the vector of conservative flow variables, and $\mathbf{g} : R^n \rightarrow R^m$ is a vector function containing m constraints. The flow variables must satisfy the governing flow equations, $\mathbf{R}$,

$$\mathbf{R}(\mathbf{x}, \mathbf{Q}) = 0. \tag{1.60}$$

The functions J and $\mathbf{g}$ are assumed to be continuous and differentiable over the design space of interest.

The problem formulation (1.58)-(1.60) is general and can be applied to different design approaches. The one-point and one-objective approach is widely adopted, where the aerodynamic surface is optimized for one operating condition with a single merit function. The most common example for this type of optimization is the lift-constrained drag minimization problem. Here, the goal is to improve the aerodynamic efficiency while maintaining a required lift. The objective function is set as

$$J = C_d, \tag{1.61}$$

where C_d is the drag coefficient and the lift constraint is

$$g = C_l^* - C_l \leq 0, \tag{1.62}$$

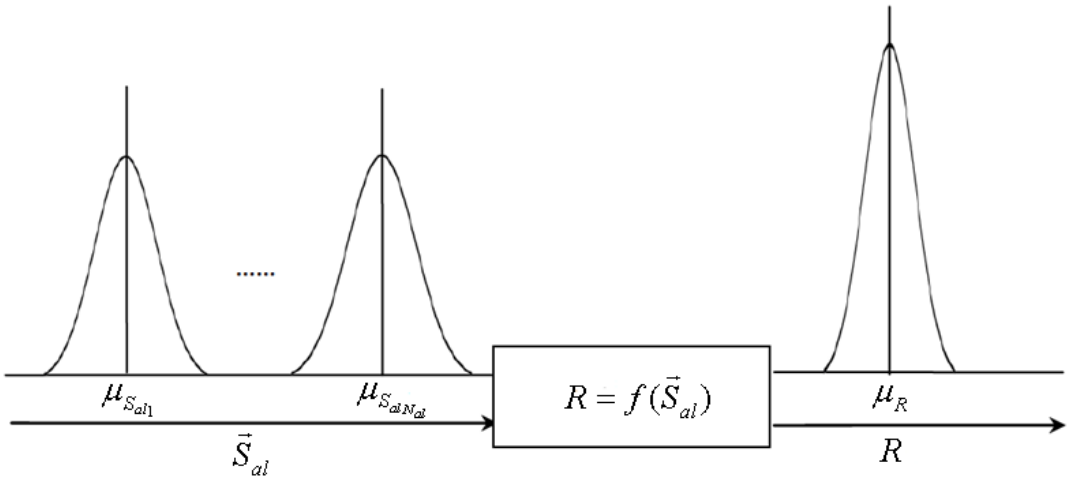

Figure 1.1. Robustness estimation of response in presence of aleatory uncertainties.

where C_l is the lift coefficient obtained for design $\mathbf{x}$, and C_l^* is the required lift coefficient. Parameters of the operating condition include the Mach number, M_∞, the Reynolds number, Re, and the angle of attack, α (which can be set as a design variable or it can be considered a state variable that is adjusted during the flow solution to satisfy (1.60)). Formally, one can say that the lift and drag coefficients are a function of the design variables, $\mathbf{x}$, and the state variables, $\mathbf{p} = [M_\infty \; Re \; \alpha]^T$, i.e., $C_d = C_d(\mathbf{x}, \mathbf{p})$ and $C_l = C_l(\mathbf{x}, \mathbf{p})$.

2.2. Robust Design with Aleatory Uncertainty. Aleatory uncertainty, which is probabilistic and irreducible, describes the inherent variation associated with the physical system (e.g., the operating conditions). Aleatory uncertainties are mathematically characterized by probability density functions when there is enough information on the type of the distribution. In this case, the robustness measure can be based on the mean and the variance (or standard deviation) of the model response. Figure 1.1 shows the propagation of input aleatory uncertainties through the simulation code and the uncertainty of the response, $R = f(S_{al})$.

Based on this, the objective for robust aerodynamic design optimization under pure aleatory uncertainty can be formulated as

$$J = \mu_{C_d} + \sigma_{C_d}, \tag{1.63}$$

where μ_{C_d} is the mean drag coefficient and σ_{C_d} is the standard deviation. The lift constraint can be formulated as

$$g = C_l^* - \mu_{C_l} \leq 0, \tag{1.64}$$

where μ_{C_l} is the mean lift coefficient.

In the above formulation, the drag and lift coefficients are a function of the deterministic design variable vector $\mathbf{x}$, the deterministic state variable vector p_d and the aleatory input uncertainty vector $\mathbf{S}_{al}$, i.e., $C_d = C_d(\mathbf{x}, \mathbf{p_d}, \mathbf{S}_{al})$ and $C_l = C_l(\mathbf{x}, \mathbf{p_d}, \mathbf{S}_{al})$. The input uncertainty vector is defined as $\mathbf{S}_{al} = (S_{al_1}, S_{al_2}, ...S_{al_{N_{al}}})$ where N_{al} is the number of aleatory uncertainties. Note that, in this case, input uncertainty vector may also contain uncertain state variables such as the free-stream Mach number.

For probabilistic output uncertainty, the mean can be calculated by

$$\mu_{C_d} = E(C_d) = \int_{SR} C_d(\mathbf{x}, \mathbf{p_d}, \mathbf{S}_{al}) P(\mathbf{S}_{al}) d\mathbf{S}_{al}, \tag{1.65}$$

and the variance as

$$\sigma_{C_d}^2 = E[(C_d - \mu_{C_d})^2] = \int_{SR} (C_d(\mathbf{x}, \mathbf{p_d}, \mathbf{S}_{al}) - \mu_{C_d})^2 P(\mathbf{S}_{al}) d\mathbf{S}_{al}, \tag{1.66}$$

where $P(\mathbf{S}_{al})$ represents the joint probability function (PDF) of $\mathbf{S}_{al}$ and SR stands for the support region of $\mathbf{S}_{al}$.

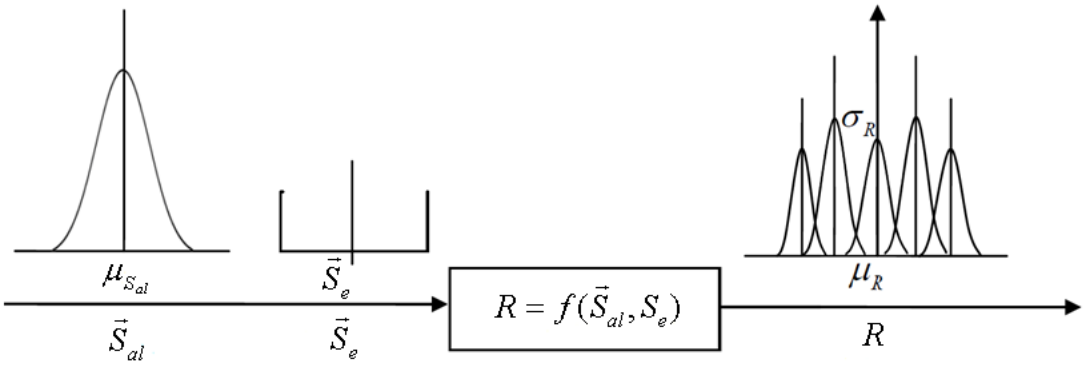

Figure 1.2. Robustness estimation of response in presence of mixed uncertainties.

2.3. Robust Design with Mixed Uncertainty. In real-world engineering systems, both aleatory and epistemic uncertainties exist - called mixed uncertainty. Epistemic uncertainty is reducible and described as lack of knowledge or information in any phase or operation of a design process [3]. For the characterization of epistemic uncertainty, the probabilistic methods are not suitable due to the lack of information about the uncertainty. One approach to model the epistemic uncertainty is to characterize it with intervals. For mixed uncertainty quantification, formulations that combine probabilistic methods and interval approach are sought. When mixed uncertainties exist as input variables, the response R becomes a function of both (aleatory and epistemic) uncertainties, $R = f(S_{al}, S_e)$ as shown in Figure 1.2.

The aerodynamic response should be in form of a combination of the probability distribution due to the effect of aleatory input uncertainty and an interval distribution indicating the effect of epistemic uncertainty. In this case, $C_d = C_d(\mathbf{x}, \mathbf{p_d}, \mathbf{S}_{al}, \mathbf{S}_e)$ and $C_l = C_l(\mathbf{x}, \mathbf{p_d}, \mathbf{S}_{al}, \mathbf{S}_e)$, where $\mathbf{S}_e = (S_{e_1}, S_{e_2}, ..., S_{e_{N_e}})$ are the epistemic uncertainties and N_e represents the number of epistemic input uncertainties. The uncertainty of C_d will consist of infinite number of probability distributions each due to the aleatory input uncertainties

at a fixed value of epistemic input uncertainty vector. The intervals at each probability level reflect the effect of epistemic uncertainties on C_d. For the mixed uncertainty case, one approach for the formulation of the objective function can be given as

$$J = w_1 \overline{\mu}_{C_d} + w_2 \overline{\sigma}_{C_d} + w_3 \delta\sigma_{C_d}, \tag{1.67}$$

where w_i $(i = 1,2,3)$ are user-assigned weights, $\overline{\mu}_{C_d}$ denotes mean value of C_d, $\overline{\sigma}_{C_d}$ represents the average standard deviation in C_d, and $\delta\sigma_{C_d}$ denotes the difference between maximum and minimum standard deviations in C_d.

The mean value of C_d will be calculated by

$$\overline{\mu}_{C_d} = \frac{1}{2}(\mu_{C_d}^{max} + \mu_{C_d}^{min}), \tag{1.68}$$

where $\mu_{C_d}^{max}$ and $\mu_{C_d}^{min}$ are the maximum and minimum means of C_d, respectively. The average value of standard deviation of C_d is obtained by

$$\overline{\sigma}_{C_d} = \frac{1}{2}(\sigma_{C_d}^{max} + \sigma_{C_d}^{min}), \tag{1.69}$$

where $\sigma_{C_d}^{max}$ and $\sigma_{C_d}^{min}$ are the maximum and minimum standard deviations of C_d, respectively. The difference between the standard deviations of C_d are given by

$$\delta\sigma_{C_d} = \sigma_{C_d}^{max} - \sigma_{C_d}^{min}, \tag{1.70}$$

The lift constraint can be formulated as

$$g = C_l^* - \overline{\mu}_{C_l} \leq 0. \tag{1.71}$$

In this study, the average standard deviation $\overline{\sigma}_{C_d}$ is used as a robustness measure

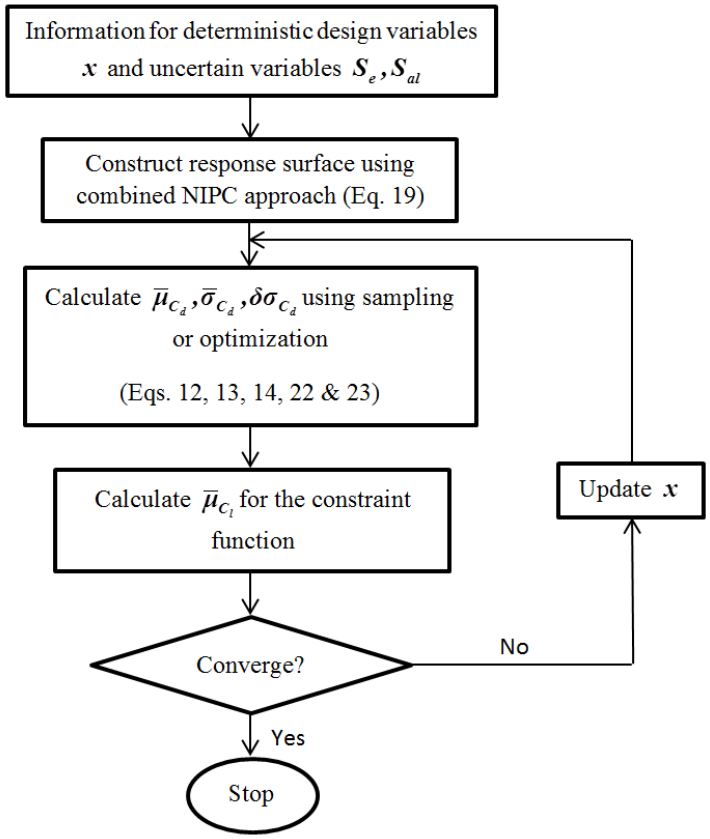

Figure 1.3. Flow chart of robust optimization process under mixed uncertainties with combined stochastic expansions.

for aleatory input uncertainties $\mathbf{S}_{al}$, whereas the difference in standard deviations $\delta\sigma_{C_d}$ is utilized as the robustness measure due to epistemic uncertainties $\mathbf{S}_e$. Both measures will be minimized along with the average C_d using a weighted objective function as given by Eq. 1.67. The flowchart of robust optimization under mixed uncertainties based on combined stochastic expansions is shown in Figure 1.3.

3. STOCHASTIC EXPANSIONS FOR SURROGATE MODELING

For the robust optimization methodology described in this paper, stochastic expansions obtained with the NIPC technique is used due to its computational efficiency and accuracy in uncertainty propagation as shown in the previous studies [10, 11]. The stochastic expansions are used as response surfaces (i.e., surrogates of the response) in the optimization procedure and are used to approximate the stochastic objective function and the constraint functions. In the robust optimization problems, the point-collocation NIPC approach has been used as explained below.

3.1. Point-Collocation Non-Intrusive Polynomial Chaos. The point-collocation NIPC is derived from polynomial chaos theory, which is based on the spectral representation of the uncertainty. An important aspect of spectral representation of uncertainty is that one may decompose a random function (or variable) into separable deterministic and stochastic components. For example, for any response variable (i.e., R) in a stochastic optimization problem, one can write:

$$R(\vec{\xi}) \approx \sum_{j=0}^{P} a_j \Psi_j(\vec{\xi}), \tag{1.72}$$

where a_j is the coefficient of each term in the expansion and $\Psi_j(\vec{\xi})$ is the random basis function corresponding to the j^{th} mode and is a function of n-dimensional random variable vector $\vec{\xi} = (\xi_1, ..., \xi_n)$, which has a specific probability distribution. In theory, the polynomial chaos expansion given by Equation 1.72 should include infinite number of terms, however in practice a discrete sum is taken over a number of output modes. For a total order expansion, the number of output modes is given by,

$$N_t = P + 1 = \frac{(N+p)!}{N!p!}, \tag{1.73}$$

which is a function of the order of polynomial chaos (p) and the number of random dimensions (n). The basis function ideally takes the form of multi-dimensional Hermite Polynomial to span the N-dimensional random space when the input uncertainty is Gaussian (unbounded), which was first used by Wiener [12] in his original work of polynomial chaos. To extend the application of the polynomial chaos theory to the propagation of continuous non-normal input uncertainty distributions, Xiu and Karniadakis [13] used a set of polynomials known as the Askey scheme to obtain the "Wiener-Askey Generalized Polynomial Chaos". The Legendre and Laguerre polynomials, which are among the polynomials included in the Askey scheme are optimal basis functions for bounded (uniform) and semi-bounded (exponential) input uncertainty distributions, respectively in terms of the convergence of the statistics.

An arbitrary polynomial chaos expansion proposed by Witeveen et al. [14] can handle arbitrary distributions of input parameters with limited statistical moments. According to the authors, the Gram-Schmidt orthogonalization algorithm can be used to compute an optimal orthogonal polynomial chaos basis for any type of input distribution. The multivariate basis functions can be obtained from the product of univariate orthogonal polynomials (See Eldred et al. [15]). If the probability distribution of each random variable is different, then the optimal multivariate basis functions can be again obtained by the product of univariate orthogonal polynomials employing the optimal univariate polynomial at each random dimension. This approach requires that the input uncertainties are independent standard random variables, which also allows the calculation of the multivariate weight functions by the product of univariate weight functions associated with the probability distribution at each random dimension. The detailed information on polynomial chaos expansions can be found in Walters and Huyse, [16] Najm, [17] and Hosder and Walters. [18]

To model the uncertainty propagation in computational simulations via polynomial chaos with the intrusive approach, all dependent variables and random parameters in the governing equations are replaced with their polynomial chaos expansions. Taking the inner product of the equations, (or projecting each equation onto jth basis) yields $P+1$ times the number of deterministic equations which can be solved by the same numerical methods applied to the original deterministic system. Although straightforward in theory, an intrusive formulation for complex problems can be relatively difficult, expensive, and time consuming to implement. To overcome such inconveniences associated with the intrusive approach, non-intrusive polynomial chaos formulations have been considered for uncertainty propagation.

The point-collocation NIPC method starts with replacing the uncertain variables of interest with their polynomial expansions given by Equation 1.72. Then, $N_t = P+1$ vectors $(\vec{\xi}_j = \{\xi_1, \xi_2, ..., \xi_N\}_j, j = 0, 1, ..., P)$ are chosen in random space for a given PC expansion with $P+1$ modes and the deterministic code is evaluated at these points. With the left hand side of Equation 1.72 known from the solutions of deterministic evaluations at the chosen random points, a linear system of equations can be obtained:

$$\begin{pmatrix} R(\overrightarrow{\xi_0}) \\ R(\overrightarrow{\xi_1}) \\ \vdots \\ R(\overrightarrow{\xi_P}) \end{pmatrix} = \begin{pmatrix} \Psi_0(\overrightarrow{\xi_0}) & \Psi_1(\overrightarrow{\xi_0}) & \cdots & \Psi_P(\overrightarrow{\xi_0}) \\ \Psi_0(\overrightarrow{\xi_1}) & \Psi_1(\overrightarrow{\xi_1}) & \cdots & \Psi_P(\overrightarrow{\xi_1}) \\ \vdots & \vdots & \ddots & \vdots \\ \Psi_0(\overrightarrow{\xi_P}) & \Psi_1(\overrightarrow{\xi_P}) & \cdots & \Psi_P(\overrightarrow{\xi_P}) \end{pmatrix} \begin{pmatrix} a_0 \\ a_1 \\ \vdots \\ a_0 \end{pmatrix} \tag{1.74}$$

The coefficients (a_j) of the stochastic expansion are obtained by solving the linear system of equations given above. The solution of the linear problem given by Equation 1.74 requires N_t deterministic function evaluations. If more than N_t samples are chosen, then

the over-determined system of equations can be solved using the Least Squares approach. Hosder et al. [19] investigated this option on model stochastic problems by increasing the number of collocation points in a systematic way through the introduction of oversampling ratio (n_p) defined as the number of samples divided by N_t. Based on the study on different model problems, they suggested an effective n_p of 2.0. The point-collocation NIPC has the advantage of flexibility on the selection of collocation points. With the proper selection of collocation points, it has been shown that point-collocation NIPC can produce highly accurate stochastic response surfaces with computational efficiency [19]. In the model problems considered in this study, Latin Hypercube sampling is implemented with an oversampling ratio of 2. The number of response evaluations will be $n_p \times N_t$ when the point-collocation NIPC is used to construct the stochastic response surface.

3.2. Combined NIPC Expansion Approach. In this work, a combined NIPC expansion approach is used to create the stochastic surrogate model, which will be a function of both the design and the uncertain variables. With the introduction of design variables $\mathbf{x}$, parameters with epistemic uncertainty $\mathbf{S}_e$, and parameters with aleatory uncertainty $\mathbf{S}_{al}$, a combined stochastic expansion of R (i.e., C_d or C_l) based on polynomial chaos can be written as

$$R(\mathbf{S}_{al}(\xi_{sal}), \mathbf{S}_e(\xi_{se}), \mathbf{x}(\xi_d)) = \sum_{j=0}^{P} a_j \Psi_j(\xi_{sal}, \xi_{se}, \xi_d). \tag{1.75}$$

In this approach, multi-dimensional basis functions Ψ_j are derived from the tensor product of one-dimensional optimum basis functions for the aleatory uncertain variables $\mathbf{S}_{al}$ selected based on the input probability distributions (e.g., Hermite polynomials for normal uncertain variables), the Legendre polynomials (basis) for the epistemic uncertainty variables, and the Legendre polynomials (basis) for the deterministic design variables. The selection of the Legendre polynomials for the epistemic uncertainties & the design variables

are due to their bounded nature ($\mathbf{x}_l \leq \mathbf{x} \leq \mathbf{x}_u$ and $\mathbf{S}_{e,l} \leq \mathbf{S}_e \leq \mathbf{S}_{e,u}$) and should not be interpreted as a probability assignment to these variables.

In Eq. (1.75), ξ_{sal} corresponds to a standard aleatory random variable vector, whereas ξ_{se} and ξ_d are the standard variables in interval [-1,1], which are mapped from the associated intervals of $\mathbf{S}_e$ and $\mathbf{x}$ via

$$\xi_{se} = \left(\mathbf{S}_e - (\frac{\mathbf{S}_{e,l}+\mathbf{S}_{e,u}}{2})\right) / \left(\frac{\mathbf{S}_{e,u}-\mathbf{S}_{e,l}}{2}\right), \tag{1.76}$$

$$\xi_d = \left(\mathbf{x} - (\frac{\mathbf{x}_l+\mathbf{x}_u}{2})\right) / \left(\frac{\mathbf{x}_u-\mathbf{x}_l}{2}\right). \tag{1.77}$$

In general, using the combined stochastic expansion and polynomial chaos theory, the mean and variance of R can be calculated by

$$\mu_R(\xi_{se},\xi_d) = \sum_{j=0}^{P} a_j \left\langle \Psi_j(\xi_{sal},\xi_{se},\xi_d)\right\rangle_{\xi_{sal}}, \tag{1.78}$$

$$\sigma_R^2(\xi_{se},\xi_d) = \left\{ \sum_{j=0}^{P}\sum_{k=0}^{P} a_j a_k \left\langle \Psi_j(\xi_{sal},\xi_{se},\xi_d)\Psi_k(\xi_{sal},\xi_{se},\xi_d)\right\rangle_{\xi_{sal}} \right\} - \mu_R^2(\xi_{se},\xi_d), \tag{1.79}$$

where the inner product expression $< .. >$ used in the above equations represent

$$\langle f(\xi)g(\xi)\rangle_\xi = \int_{SR} f(\xi)g(\xi)p(\xi)d\xi, \tag{1.80}$$

written in terms of two generic functions $f(\xi)$ and $g(\xi)$ in the support region SR of ξ with $p(\xi)$ being the weight function. Note that when the design variables are not considered as uncertain (as the case studied in this paper), the surrogates need not to be recreated at every

optimization iteration. In this case one can directly compute the output statistics (mean, standard deviation and variance) by using a single stochastic response surface created for the response quantity of interest (i.e., C_d and C_l)

4. MULTI-FIDELITY MODELING APPROACH

The robust design formulations described in Section 2 are desired to be obtained using a HF CFD model. However, accurate CFD models are computationally expensive and if the design space is large, the computational cost can be prohibitive. Therefore, to reduce the computational effort, a multi-fidelity approach is considered. In this process, the HF CFD model is replaced by a CLF model. In the following sections, the HF CFD model, LF CFD model and the CLF model construction using space mapping method is described.

4.1. High-fidelity CFD Model. The poposed design approach is demonstrated for the drag minimization of NACA 4-digit airfoils described with three geometric design variables over the range of uncertainties at transonic flow conditions. The deterministic CFD simulations were performed with the FLUENT [20] code to solve steady, 2-D, compressible, turbulent RANS equations. The fluid medium is air, assumed to be an ideal gas, with the laminar dynamic viscosity (μ) described by Sutherland's formula [21].

For modeling the turbulent kinematic eddy viscosity (ν_t), the turbulence model by Spalart and Allmaras [22] is used. The Spalart-Allmaras model, designed specifically for aerodynamic wall-bounded flows, is a one-equation model that solves a single conservation partial differential equation for the turbulent viscosity. This conservation equation contains convective and diffusive transport terms, as well as expressions for the production and dissipation of ν_t. The Spalart-Allmaras model is economical and accurate for attached wall-bounded flows, and flows with mild separation and recirculation. The flow solver and the domain used for the analsysi is as explained below.

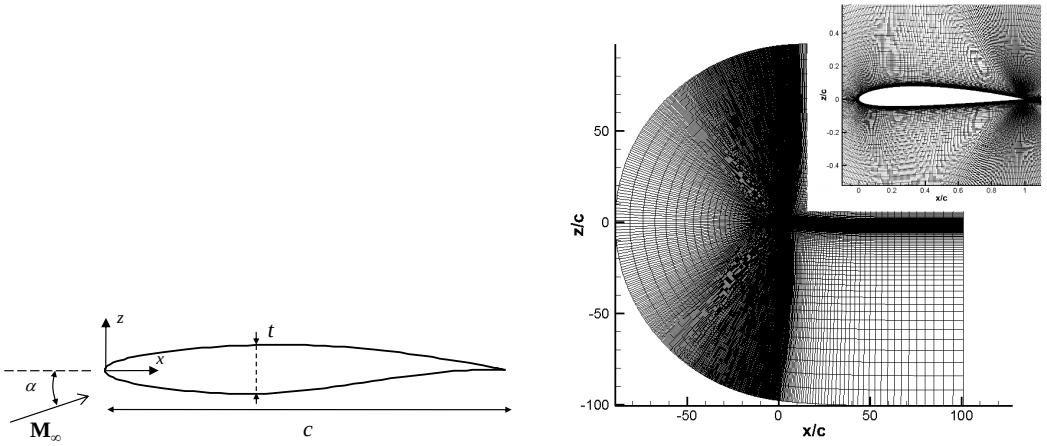

(a) (b)

Figure 1.4. A typical airfoil section and a computational grid: (a) Airfoil section is shown. The free-stream flow is at Mach number M_∞ and at an angle of attack α relative to the chord axis. (b) Example computational grid.

The solution domain boundaries are placed at 25 chord lengths in front, below and above the airfoil with front to wake ratio of one. An example computational grid along with a typical airfoil section is shown in Figure 1.4. A hyperbolic grid generator [23] is used for the mesh generation. The non-dimensional normal distance (y^+) from the wall to the first grid point is roughly one. The free-stream Mach number, angle of attack, static pressure, and the turbulent viscosity ratio are prescribed at the farfield boundary. A grid convergence study is performed using the NACA 2412 airfoil at Mach number $M = 0.75$ and angle of attack $\alpha = 1^\circ$. The study revealed that a grid level of approximately 510,000 cells are needed for mesh convergence, which is treated as the HF model for the current study.

The flow solver utilizes implicit density-based formulation and the fluxes are calculated by an upwind-biased second-order spatially accurate Roe flux scheme. Asymptotic convergence to a steady state solution is obtained for each case. In order to gradually

Table 1.1. Mesh size nomenclature and discretization error results for C_d.

Grid level	Mesh size	Cells	DE (%)
1	99×20	1980	28.83
2	199×40	7960	12.23
3	399×80	31920	5.49
4	799×160	127840	1.75
5	1599×320	511680	0.56

ramp up the Courant number and accelerate convergence, automatic solution steering is employed. Full multi-grid initialization is used to accelerate the iterative convergence. The iterative convergence of each solution is examined by monitoring the overall residuals, which is the sum (over all the cells in the computational domain) of the L^2 norm of all the governing equations solved in each cell. In addition to this, the lift and drag forces are monitored for convergence. The solution convergence criterion for the CFD runs is a reduction in the residuals by six orders of magnitude.

4.2. Low-fidelity CFD Model. The LF CFD model is constructed with the same solution and physical modeling parameters as the HF model, but with a coarser computational mesh. In the determination of the LF model, 5 grid levels (Table 1.1) have been studied. The grid levels affect the magnitude of the discretization error as it determines the spatial resolution. Richardson extrapolation [24] technique has been used to estimate the magnitude of the discretization error for C_d at each grid level and the results are summarized in Figure 1.5. In this work, two case studies are presented in terms of LF CFD models. Grid levels 2 and 3 solutions are treated as the low-fidelity models and the results are compared with the HF model, after correction.

The computational resources for all CFD simulations consisted of 3 processors with a CPU speed of 2.66 GHz. The ratio of simulation times (in seconds) of the high- and

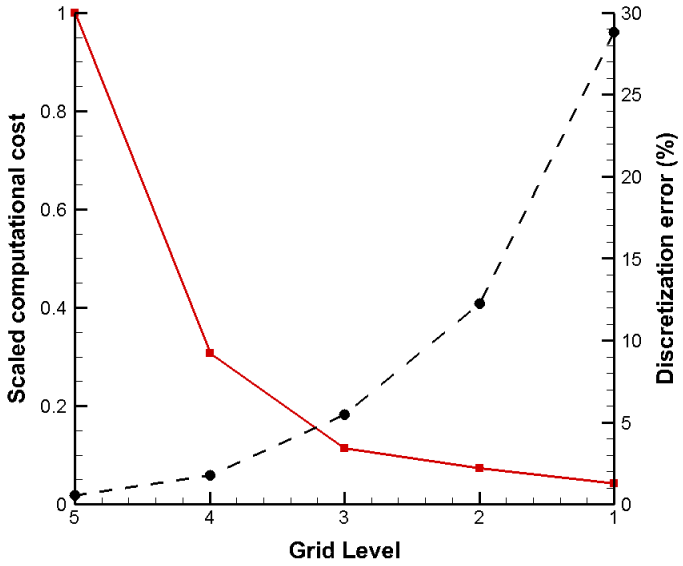

Figure 1.5. Computational cost comparison for different grid levels (left Y-axis) and grid convergence in terms of Discretization Error (DE) for C_d (right Y-axis).

low-fidelity models (for grid level 2 and 3) is around 14 and 9, respectively. Figure 1.5 also compares the computational cost of the high- and low-fidelity models in terms of simulation time (in seconds) scaled with respect to the HF model.

4.3. Corrected Low-fidelity Model Construction Using Output Space Mapping. To reduce the computational cost of the design process, the HF CFD model is replaced by a suitably corrected low-fidelity one, the latter being evaluated using the same CFD solver but with a coarser mesh. In specific, the model correction is implemented to the LF CFD sample points (solutions) utilized for the construction of stochastic surrogate based on NIPC by using Output Space Mapping (OSM) technique. The OSM correction can be obtained without costly parameter extraction procedure and ensures that the low-fidelity model represents the high-fidelity one with sufficient accuracy. The correction procedure can be outlined as follows: Define vector $\mathbf{x_c} = [\mathbf{x}\ S_{al}\ S_e]^T$ and let the HF model response be

$h(\mathbf{x_c}) = [C_{l.h}(\mathbf{x_c})\ C_{d.h}(\mathbf{x_c})]^T$, where $C_{l.h}$ and $C_{d.h}$ are (high-fidelity CFD-simulated) lift and drag coefficients. Similarly, the LF model response is $f(\mathbf{x_c}) = [C_{l.f}(\mathbf{x_c})\ C_{d.f}(\mathbf{x_c})]^T$. The CLF model is denoted as $c(\mathbf{x_c}) = [C_{l.c}(\mathbf{x_c})\ C_{d.c}(\mathbf{x_c})]^T$.

In space mapping, the corrected model is a composition of the low-fidelity model and simple, usually linear, transformations (or mappings)[6]. In this work, the correction terms are directly applied to the response components $C_{l.f}(\mathbf{x_c})$ and $C_{d.f}(\mathbf{x_c})$ of the low-fidelity model. The corrected model is defined as:

$$c(\mathbf{x_c}) = \mathbf{A}(\mathbf{x_c}) \circ f(\mathbf{x_c}) + \mathbf{D} = [a_l(\mathbf{x_c})C_{l.f}(\mathbf{x_c}) + d_l \quad a_d(\mathbf{x_c})C_{d.f}(\mathbf{x_c}) + d_d]^T, \tag{1.81}$$

where $\circ$ denotes a component-wise multiplication. The multiplicative correction term is design-variable-dependent and takes the form of

$$\mathbf{A}(\mathbf{x_c}) = [a_{l.0} + [a_{l.1}\, a_{l.2} \ldots a_{l.n}] \cdot (\mathbf{x_c} - \mathbf{x_c}^0) a_{d.0} + [a_{d.1}\, a_{d.2} \ldots a_{d.n}] \cdot (\mathbf{x_c} - \mathbf{x_c}^0)]^T, \tag{1.82}$$

where $\mathbf{x_c}^0$ is the center of the design space. Response correction parameters $\mathbf{A}$ and $\mathbf{D}$ are obtained as

$$[\mathbf{A}, \mathbf{D}] = \arg\min_{\overline{\mathbf{A}}, \overline{\mathbf{D}}} \sum_{k=1}^{K} ||h(\mathbf{x_c}^k) - (\overline{\mathbf{A}}(\mathbf{x_c}^k) \circ f(\mathbf{x_c}^k) + \overline{\mathbf{D}})||^2, \tag{1.83}$$

i.e., the response scaling is supposed to (globally) improve the matching for all training points $\mathbf{x_c}^k$, $k = 1, \ldots, K$. $2n+1$ training points (n being the number of design variables) are chosen for correcting the LF model. The correction parameters $\mathbf{A}$ and $\mathbf{D}$ can be calculated analytically as follows

$$\begin{bmatrix} a_{l.0} \\ a_{l.1} \\ \vdots \\ a_{l.n} \\ d_l \end{bmatrix} = \left(\mathbf{C}_l^T \mathbf{C}_l\right)^{-1} \mathbf{C}_l^T \mathbf{F}_l \,, \quad \begin{bmatrix} a_{d.0} \\ a_{d.1} \\ \vdots \\ a_{d.n} \\ d_d \end{bmatrix} = \left(\mathbf{C}_d^T \mathbf{C}_d\right)^{-1} \mathbf{C}_d^T \mathbf{F}_d \,, \tag{1.84}$$

$$\mathbf{C}_l = \begin{bmatrix} C_{l.f}(\mathbf{x_c}^1) & C_{l.f}(\mathbf{x_c}^1)\cdot(\mathbf{x_c}_1^1 - \mathbf{x_c}_1^0) & \cdots & C_{l.f}(\mathbf{x_c}^1)\cdot(\mathbf{x_c}_n^1 - \mathbf{x_c}_n^0) & 1 \\ C_{l.f}(\mathbf{x_c}^2) & C_{l.f}(\mathbf{x_c}^2)\cdot(\mathbf{x_c}_1^2 - \mathbf{x_c}_1^0) & \cdots & C_{l.f}(\mathbf{x_c}^2)\cdot(\mathbf{x_c}_n^2 - \mathbf{x_c}_n^0) & 1 \\ \vdots & \vdots & \ddots & \vdots & \vdots \\ C_{l.f}(\mathbf{x_c}^K) & C_{l.f}(\mathbf{x_c}^K)\cdot(\mathbf{x_c}_1^K - \mathbf{x_c}_1^0) & \cdots & C_{l.f}(\mathbf{x_c}^K)\cdot(\mathbf{x_c}_n^K - \mathbf{x_c}_n^0) & 1 \end{bmatrix}, \tag{1.85}$$

$$\mathbf{F}_l = \begin{bmatrix} C_{l.h}(\mathbf{x_c}^1) & C_{l.h}(\mathbf{x_c}^2) & \cdots & C_{l.h}(\mathbf{x_c}^K) \end{bmatrix}^T, \tag{1.86}$$

$$\mathbf{C}_d = \begin{bmatrix} C_{d.f}(\mathbf{x_c}^1) & C_{d.f}(\mathbf{x_c}^1)\cdot(\mathbf{x_c}_1^1 - \mathbf{x_c}_1^0) & \cdots & C_{d.f}(\mathbf{x_c}^1)\cdot(\mathbf{x_c}_n^1 - \mathbf{x_c}_n^0) & 1 \\ C_{d.f}(\mathbf{x_c}^2) & C_{d.f}(\mathbf{x_c}^2)\cdot(\mathbf{x_c}_1^2 - \mathbf{x_c}_1^0) & \cdots & C_{d.f}(\mathbf{x_c}^2)\cdot(\mathbf{x_c}_n^2 - \mathbf{x_c}_n^0) & 1 \\ \vdots & \vdots & \ddots & \vdots & \vdots \\ C_{d.f}(\mathbf{x_c}^K) & C_{d.f}(\mathbf{x_c}^K)\cdot(\mathbf{x_c}_1^K - \mathbf{x_c}_1^0) & \cdots & C_{d.f}(\mathbf{x_c}^K)\cdot(\mathbf{x_c}_n^K - \mathbf{x_c}_n^0) & 1 \end{bmatrix}, \tag{1.87}$$

$$\mathbf{F}_d = \begin{bmatrix} C_{d.h}(\mathbf{x_c}^1) & C_{d.h}(\mathbf{x_c}^2) & \cdots & C_{d.h}(\mathbf{x_c}^K) \end{bmatrix}^T, \tag{1.88}$$

which is a least-square optimal solution to the linear regression problems $\mathbf{C}_l\,[a_{l.0}\ a_{l.1}\ \ldots\ a_{l.n}\ d_l]^T = \mathbf{F}_l$ and $\mathbf{C}_d\,[a_{d.0}\ a_{d.1}\ \ldots\ a_{d.n}\ d_d]^T = \mathbf{F}_d$, equivalent to (1.83). An important point

to note is that the matrices $\mathbf{C}_l^T\mathbf{C}_l$ and $\mathbf{C}_d^T\mathbf{C}_d$ are non-singular for $K > n+1$, which is the case for the choice of the training set in this study.

5. DEMONSTRATION EXAMPLE

In this section, the multi-fidelity robust design approach is demonstrated on an airfoil shape optimization problem under mixed uncertainty. In particular, the accuracy and optimization cost of the proposed approach is compared with the cost of using directly the high-fidelity CFD model for creating stochastic surrogate.

5.1. Formulation and Setup. The robust airfoil optimization under mixed uncertainty is formulated as

$$min \quad w_1\overline{\mu}_{C_d} + w_2\overline{\sigma}_{C_d} + w_3\delta\sigma_{C_d}, \tag{1.89}$$

$$\begin{aligned} \textit{subject to} \quad & C_l^* - \overline{\mu}_{C_l} \leq 0, \\ & 0.005 \leq m \leq 0.05, \\ & 0.3 \leq p \leq 0.7, \\ & 0.08 \leq t/c \leq 0.14, \\ & 0.5 \leq \alpha \leq 1.5, \end{aligned}$$

where the profile drag coefficient (C_d) and the lift coefficient (C_l) are a function of deterministic design variable vector $\mathbf{x} = \{m, p, t/c, \alpha\}$, aleatory input uncertainty vector $\mathbf{S}_{al}$ and the epistemic input uncertainty vector $\mathbf{S}_e$. In particular, the NACA 4-digit parameterization method is used where the airfoil shape is defined by three parameters: m (the maximum

ordinate of the mean camber line as a fraction of chord), p (the chordwise position of the maximum ordinate as a fraction of chord) and t/c (thickness-to-chord ratio). The NACA 4-digit parameterization is explained in detail by Abbott and Doenhoff [25].

The free-stream Mach number is treated as a normally distributed aleatory (inherent) input uncertainty ($\mathbf{S}_{al} = \{M\}$) with a mean value $\mu = 0.75$ and standard deviation $\sigma = 0.015$. The equation for a modified symmetrical 4-digit NACA airfoil is given by Eq. 1.90:

$$y_t = \frac{t}{\beta}[0.2969\sqrt{\frac{x}{c}} - 0.1260\frac{x}{c} - 0.3516\frac{x^2}{c} + 0.2843\frac{x^3}{c} - 0.1036\frac{x^4}{c}]. \tag{1.90}$$

The geometry parameter β (default value of 0.2 in the nominal equation) is modeled as an epistemic input uncertainty (i.e., $\mathbf{S}_e = \{\beta\}$) with bounds [0.17, 0.23]. The range of β is chosen to mimic the epistemic uncertainty in the thickness distribution formula defining the shape of the airfoil. Figure 1.6 shows the pressure distributions of NACA 2412 airfoil at $M = 0.75$ and $\alpha = 1^\circ$ for two β values corresponding to the limits of the epistemic interval.

It can be seen that the β parameter has considerable effect on the pressure distribution including the shock location. In the optimization formulation, the mean lift coefficient limit is set to $C_l^* = 0.55$. The formulation also includes geometric constraints for the profile shape, which bound the maximum camber, maximum camber location and the thickness. In this study, equal weights ($w_1, w_2, w_3 = 1$) are assigned to each term in the objective function for demonstration purposes, however one can choose different values depending on the emphasis on each term. Besides the selection of different weights, it is also possible to normalize each term in Equation 1.67 with the statistics obtained from a reference design (e.g., initial design) to control the dominance of each term in the objective function.

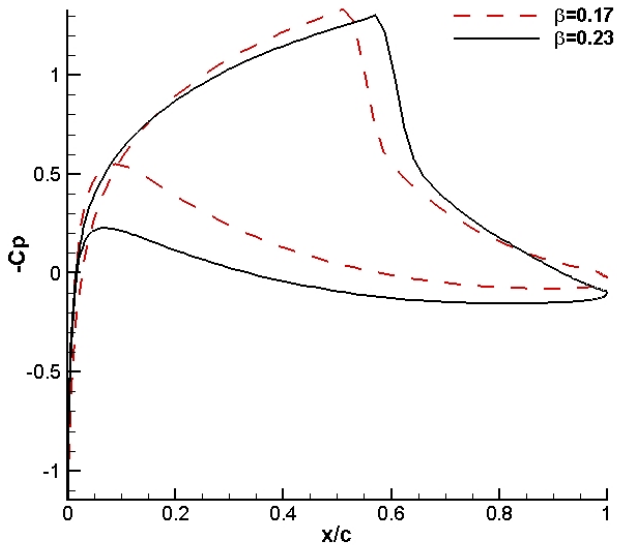

Figure 1.6. Pressure distribution for NACA 2412 at $M = 0.75$, $\alpha = 1^\circ$

5.2. Stochastic Response Surface (Surrogate Model). The robust optimization approach is based on stochastic expansions derived from the NIPC technique, which are used as surrogates in the optimization process. The combined expansion approach (see Section 3.2) used in this study makes the optimization process very efficient, since a single response surface is created as a function of both design variables and the uncertain variables. It should be noted that the combined expansion approach will be ideal for problems with fewer number of design and uncertain variables (e.g., $N_d \leq 4$ and $N_p \leq 2$). On the other hand, in optimization problems with large number of design variables, one can choose an alternative approach which is based on the expansion of polynomial chaos surface only on the uncertain (aleatory and epistemic) variables. A separate response surface should be created at each iteration, which will increase the computational cost, however the accuracy of the response surface will increases as the number of expansion variables decrease.

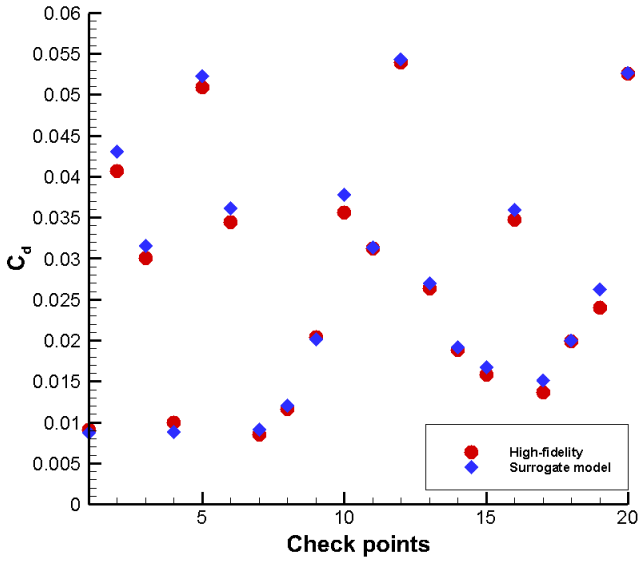

Figure 1.7. NIPC Response surface accuracy at 20 LH sample points within the domain

For this particular study, a 3^{rd} order polynomial chaos expansion is implemented with an oversampling ratio of 2, which required a total number of 168 CFD evaluations to create the response surface. In addition to the high-fidelity CFD model (grid level 5, Section 4.1), the stochastic response surfaces were also created with two low-fidelity models (grid level 2 and grid level 3, Section 4.2) and the corrected low-fidelity models (Section 4.3) to evaluate the results of the multi-fidelity approach. In order to check the accuracy of each response surface, the coefficient of drag is compared to that of CFD simulations at the same fidelity level at 20 Latin Hypercube (LH) samples chosen in the design and uncertainty space. Figure 1.7 demonstrates the accuracy of the surrogate model created with the high-fidelity CFD model (i.e., grid level 5) with a Root Mean Square Percentage Error (RMSPE) of 4.94% in C_d values, evaluated using Eqs. 1.91 and 1.92.

$$\text{Percentage Error (PE)} = \frac{(C_d^{CFD} - C_d^{NIPC})}{C_d^{CFD}} \times 100, \tag{1.91}$$

$$\text{Root Mean Square PE} = \sqrt{\frac{\sum_{i=1}^{n_{chk}} PE_i^2}{n_{chk}}}, \tag{1.92}$$

where n_{chk} represents the number of check points which is 20 in this case.

After the creation of stochastic response surfaces, the robust optimization is performed with the procedure described in Section 2.3 and outlined in Figure 1.3. For the non-linear constraint optimization, sequential least squares quadratic programming algorithm is implemented.

5.3. Optimization Results & Discussion. The objective of the optimization formulation is to reduce the average of the mean ($\overline{\mu}_{C_d}$), average standard deviation ($\overline{\sigma}_{C_d}$) and the difference in standard deviation of the drag coefficient ($\delta\sigma_{C_d}$) simultaneously in order to obtain an airfoil shape with minimum drag that is least sensitive to the change in Mach number M and the β parameter over the uncertainty range specified for each variable. Besides the geometric constraints on design variables, the optimization is performed such that the mean lift coefficient is greater than or equal to 0.55.

5.3.1. Accuracy of the corrected low-fidelity model. To demonstrate the multi-fidelity approach, the robust optimization is performed on the surrogates created by the following two CLF models with the OSM technique:

- CLF (grid level 2): OSM applied to grid level 2 as the LF model
- CLF (grid level 3): OSM applied to grid level 3 as the LF model

The stochastic response surfaces for drag and lift coefficients are created for the HF CFD model, LF CFD models and the CLF responses (i.e., CLF grid level 2 and CLF grid

Table 1.2. Optimization results using the stochastic surrogates created with the low-fidelity (LF), high-fidelity (HF) and the corrected low-fidelity (CLF) models, GL: grid level

Variable	LF (GL 2)	LF (GL 3)	CLF (GL 2)	CLF (GL 3)	HF
m	0.0189	0.0198	0.0193	0.0196	0.0195
p	0.7	0.7	0.7	0.7	0.7
t/c	0.08	0.08	0.08	0.08	0.08
α	0.5	0.5	0.5	0.5	0.5
$\overline{\mu}_{C_l}$	0.55	0.55	0.55	0.5499	0.55
$\overline{\mu}_{C_d}$	78	69	71.17	67.42	66.618
σ_{C_d}	12.6	12.9	17.26	14.99	13.55
$\delta\sigma_{C_d}$	10.7	10.5	13.301	9.268	9.523
N_f	168	168	181	181	0
N_h	0	0	13	13	168
N_{cost}	12	19	26	34	168

level 3). The optimization was performed starting with an initial airfoil geometry of NACA 2412. As can be seen from Table 1.2, the optimization runs converged to similar optimum airfoil shapes in terms of location of maximum camber ($p = 0.7$, the design variable upper bound) and the thickness ($t/c = 0.08$, the design variable lower bound). The maximum camber slightly varies for the LF and CLF models as compared to the HF model. One of the reasons for similar designs using a low-fidelity model is that the flow field around the optimal airfoil shape does not include complex flow features such as strong shocks and shock induced separation over the range of uncertain parameters, making it possible to capture the flow behavior using a lower grid resolution. Another reason is the relatively low number of design variables (i.e., shape parametrization variables) defining the NACA 4-digit airfoil, which allow only a limited number of designs to evaluate.

Although the optimized designs are comparatively similar, the difference can be attributed to the LF and HF models in terms of accuracy or convergence of statistics (for e.g., $\overline{\mu}_{C_d}, \sigma_{C_d}$ etc.). Figure 1.8(a) provides a summary of results for the average of the mean

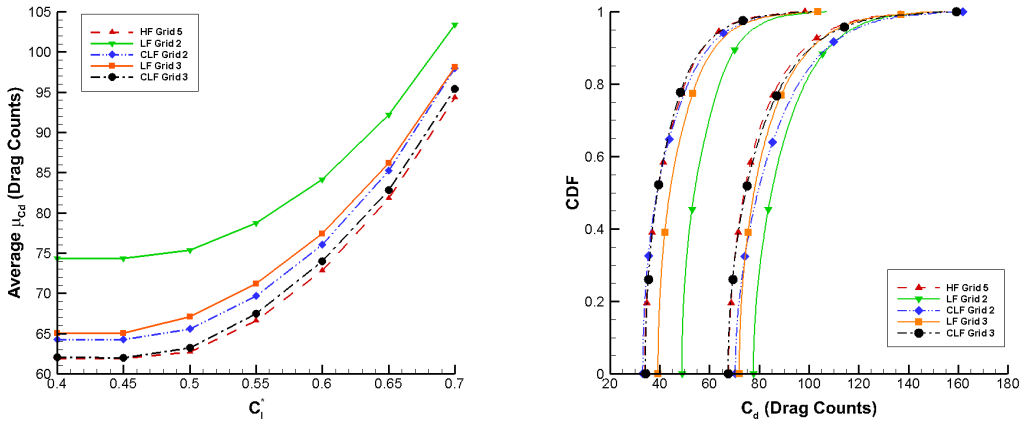

(a) (b)

Figure 1.8. (a) Average mean C_d for varying target lift coefficients, C_l^*. (b) Probability box for C_d at a target lift coeffcient of 0.55.

of the drag coefficient ($\overline{\mu}_{C_d}$) for the optimized design with varying target lift coefficient values (C_l^*). It can be inferred that the convergence of the LF model for grid levels 2 and 3 are inaccurate in terms of $\overline{\mu}_{C_d}$, the most dominant term in the objective function. The CLF model for grid level 2 does show improvement as compared to its corresponding LF model. However, the CLF model for grid level 3 approximates the HF model with considerable accuracy. For example, the $\overline{\mu}_{C_d}$ of LF model for grid levels 2 and 3 for a target lift coefficient of 0.4 are 74.5 and 64 drag counts, respectively. After the correction is applied to the LF models, the optimization process converges to 65 drag counts for CLF grid level 2 and 62 drag counts for CLF grid level 3 which exactly matches with the HF model. This behavior is expected as the grid level 3 has 32,000 mesh cells as compared to only 8,000 mesh cells for grid level 2, which corresponds to less noise and better grid resolution.

Figure 1.8(b) represents the probability box (p-box) for C_d over the uncertainty range of the Mach number (M) and the β parameter for the optimized airfoil design at a target lift coefficient $C_l^* = 0.55$. Similar to previous results, the LF model for grid level 2 inaccurately represents the uncertainty in C_d as compared to the HF model. In contrast, the difference between the HF model and the CLF model for grid level 3 is minimal. The 95% confidence interval (CI) for the LF model using grid level 2 and grid level 3 are [48.90, 124.83] and [39.32, 119.80] drag counts, respectively. Similarly, the 95% CI for CLF model using grid level 2 and grid level 3 are [33.20, 127.80] and [33.22, 120.67] drag counts, respectively as compared to [33.94, 118.33] drag counts for the HF model. As explained previously, the OSM correction can be obtained without costly parameter extraction procedure and ensures that the CLF model represents the HF model with sufficient accuracy (CLF grid level 3 in this study).

In terms of computational cost, there is a large difference between the direct HF and the multi-fidelity approach. The total computational cost (N_{cost}) of optimization varies with the number of expansion variables by a power of 3 (polynomial order 3 is used in this study), in case of using the HF model directly to create the surrogate. For the current study, as the over-sampling ratio is 2, the total cost corresponds to $n_p \times N_t = (n^3 + 6n^2 + 11n + 6)/3$. The total computational cost of optimization using the multi-fidelity approach is the sum of cost of the HF model evaluations (N_h) and LF model evaluations (N_f). The HF model is sampled $N_h = 2n + 1$ times and the LF model is sampled $N_f = n_p \times N_t + (2n + 1) = (n^3 + 6n^2 + 17n + 9)/3$. The overall cost of the multi-fidelity approach in terms of equivalent HF model evaluations can be given by $N_{cost} = N_h + N_f/r$, where r is the ratio of HF to LF simulation times. As can be seen from Table 1.2, the total cost of using the HF model directly is 168 HF simulations, whereas the multi-fidelity (CLF grid level 3) approach requires 181 LF model evaluations and 13 HF model evaluations, corresponding

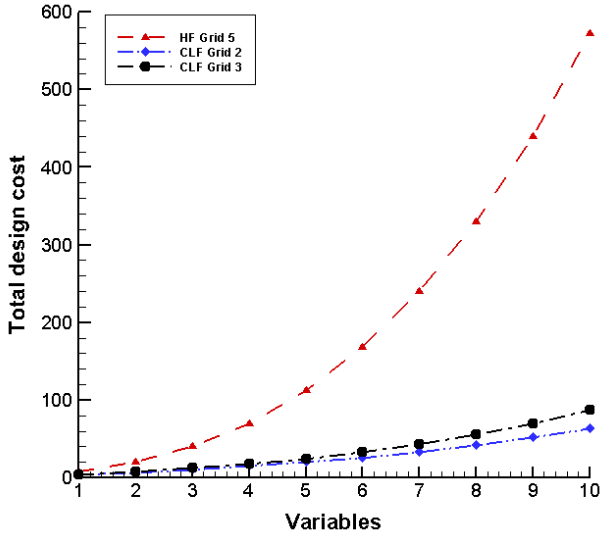

Figure 1.9. The total design cost versus the number of variables (design + uncertain variables) for optimization with different models.

to a total cost of 34 equivalent HF model evaluations. Further, a comparison of the design cost for the HF model and the CLF model is shown in Figure 1.9 up to a variable number of 10, which may include both the design variables and the uncertain parameters.

5.3.2. Robustness for the optimized design. Figures 1.10 and 1.11 present the optimization results (uncertainty for the optimized airfoil as compared to the initial airfoil design) and the convergence history of average mean ($\overline{\mu}_{C_d}$, see Figure 1.10(b)), average standard deviation ($\overline{\sigma}_{C_d}$, see Figure 1.11(a)) and the difference in standard deviation ($\delta\sigma_{C_d}$, see Figure 1.11(b)) for for a target lift coefficient of 0.55. The results correspond to an initial airfoil shape of NACA 2412 being optimized for robustness under mixed uncertainty. The p-box plot in Figure 1.10(a) demonstrates the robustness of the optimized design as compared to the initial design. The robustness of the optimized design is evaluated in the sense that it is insensitive to the variation in input parameters.

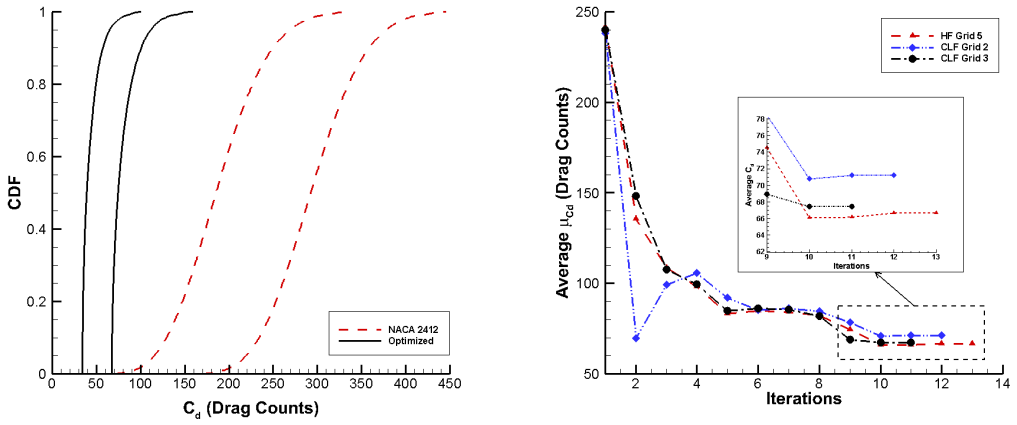

(a) Probability box for C_d (b) Average mean of C_d, $\overline{\mu}_{C_d}$

Figure 1.10. The optimization history for C_d and the average mean of C_d under mixed uncertainty with an initial airfoil geometry of NACA 2412 with $C_l^* = 0.55$.

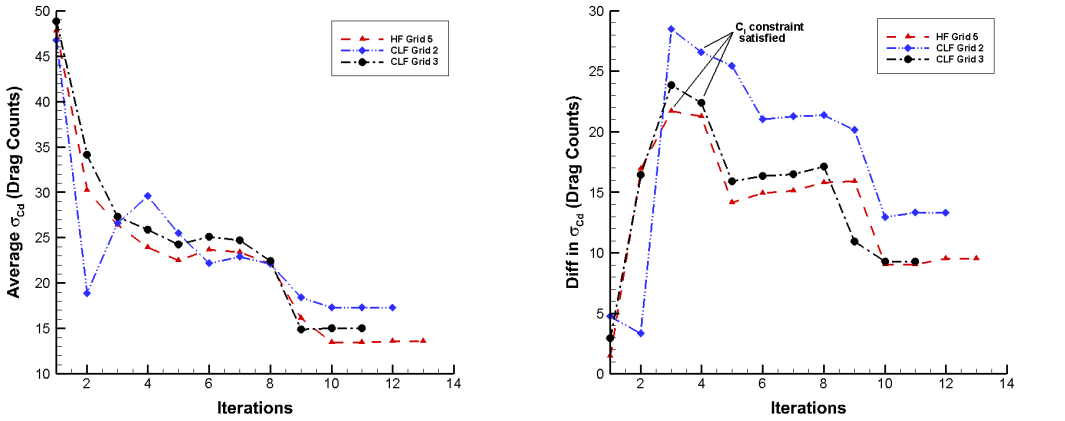

(a) Average standard deviation of C_d, $\overline{\sigma}_{C_d}$ (b) Difference in standard deviation of C_d, $\delta\sigma_{C_d}$

Figure 1.11. The optimization history for average standard deviation of C_d and difference in standard deviation of C_d under mixed uncertainty with an initial airfoil geometry of NACA 2412 with $C_l^* = 0.55$.

In specific, along with the average mean for C_d, the average standard deviation (robustness in terms of aleatory uncertainty) and the difference in standard deviation that defines the width of the p-box plot (robustness in terms of epistemic uncertainty) is also reduced simultaneously. All three quantities are reduced as compared to their starting values but the converged value is different for different models (HF and CLF). CLF using grid level 3 is a better approximation for the HF model in terms of all three quantities. The reduction in the average mean of C_d is the highest in terms of drag counts, followed by the average standard deviation and the difference in standard deviation for C_d. This is due to the fact that the average of the mean of C_d is the most dominant term in the objective function. One may also expect different convergence statistics if different weights are assigned to each term. Alternatively, the difference in standard deviation increases as compared to the initial design. However, an important point to note is that the C_l constraint is satisfied at the 3^{rd} and 4^{th} iterations for the HF and CLF models, respectively. Thereafter, the $\delta\sigma_{C_d}$ quantity reduces and converges to its optimum value. Figure 1.12 shows the surface plot of the drag coefficient over the range of Mach number (M) and the β parameter.

Both CLF models (CLF grid level 2 and 3) verify that the aerodynamic characteristics for the optimum airfoil are better as compared to the characteristics of NACA 2412. However, even in this case, the CLF using grid level 3 outperforms the one using grid level 2 in terms of accuracy with respect to the HF model. The results show that there is a significant drag rise for the CLF model using grid level 2 at high Mach numbers and lower β values. On the other hand, the drag coefficients for CLF model using grid level 3 are in good agreement with the HF model.

5.3.3. Optimization using different initial airfoils. To ensure that the optimization process does not converge to a local minimum, different initial airfoil designs have been implemented. Along with NACA 2412 as the initial airfoil shape, NACA 4412 and

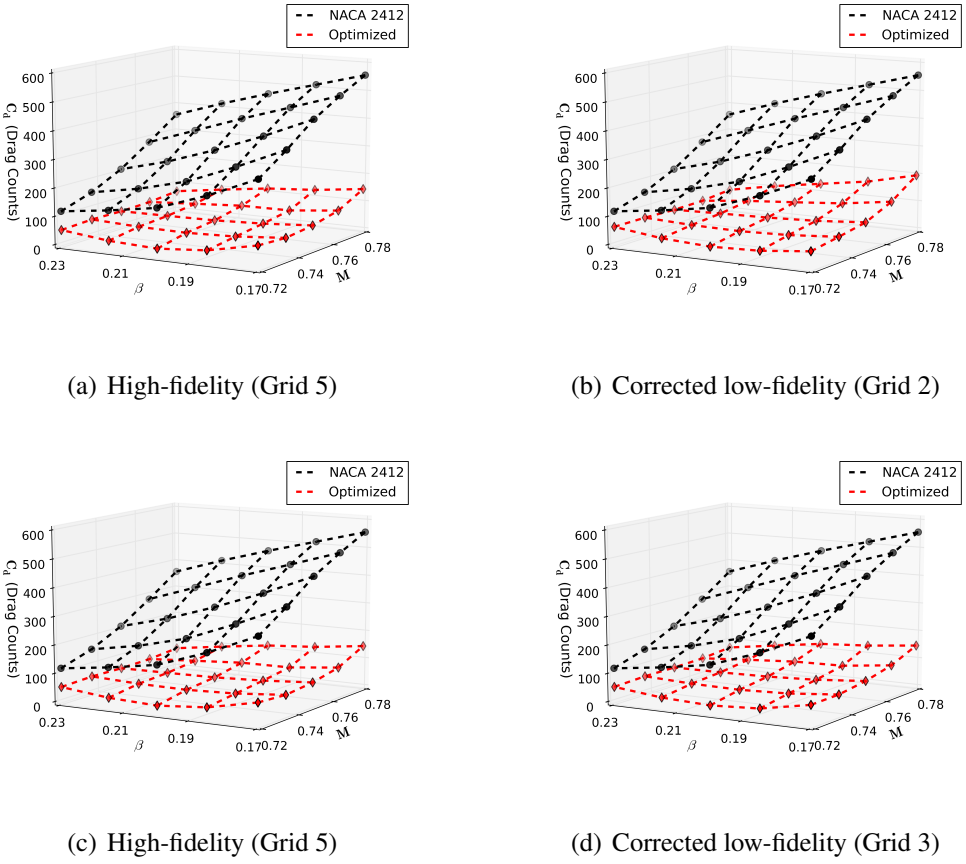

(a) High-fidelity (Grid 5)

(b) Corrected low-fidelity (Grid 2)

(c) High-fidelity (Grid 5)

(d) Corrected low-fidelity (Grid 3)

Figure 1.12. Drag coefficient values of the optimized airfoil and NACA 2412 for varying Mach number (M) and β parameter with grid levels 2 and 3 compared with grid level 5.

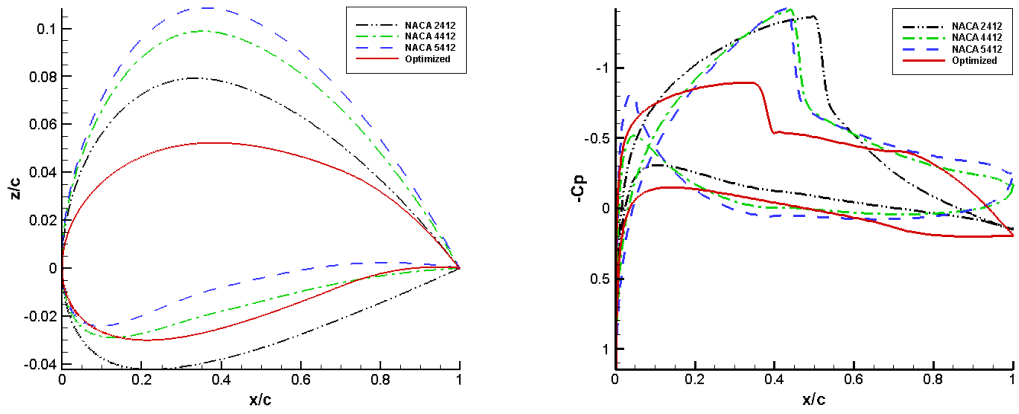

(a) (b)

Figure 1.13. Characteristics of the initial and optimized airfoils: (a) initial and optimized airfoil shapes, and (b) pressure coefficient plot at a lift coefficient of 0.55.

NACA 5412 have been tested as initial airfoils with the same formulation and setup for the robust optimization as mentioned in Section 5.1. The mean lift coefficient limit is set to $C_l^* = 0.55$. Figure 1.13(a) compares the initial airfoil designs with the optimum airfoil shape corresponding to CLF model using grid level 3. The pressure coefficient plot is also compared for all the initial airfoil designs with the optimum airfoil in Figure 1.13(b).

At a free-stream Mach number $M = 0.75$ and $\beta = 0.2$, all the initial airfoil designs have a strong shock on the top surface, whereas the strength of the shock is reduced considerably on the optimized airfoil. This is mainly due to the increase in minimum suction pressure and reduction in the maximum velocity on the top surface of the optimized airfoil. The aft camber compensates for the loss in lift in the suction region. Furthermore, the Mach and pressure contours for the optimized airfoil design are compared to NACA 2412 in Figure 1.14. The reduced shock strength and elimination of the shock induced flow separation over the optimized airfoil geometry can also be observed in this figure.

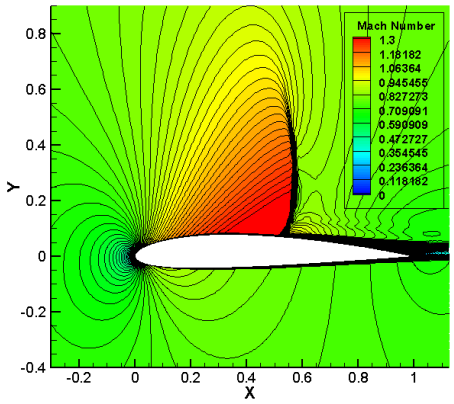

(a) NACA 2412: Mach contours

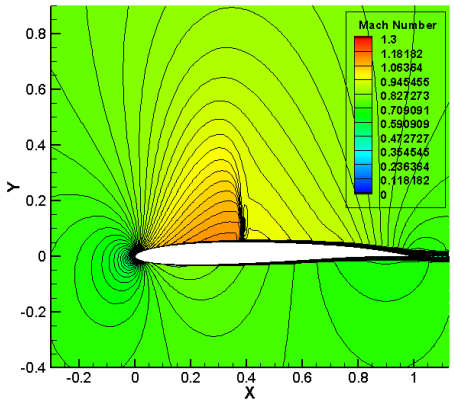

(b) Optimized design: Mach contours

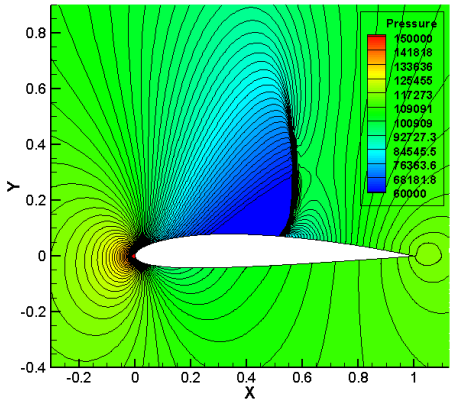

(c) NACA 2412: Pressure contours

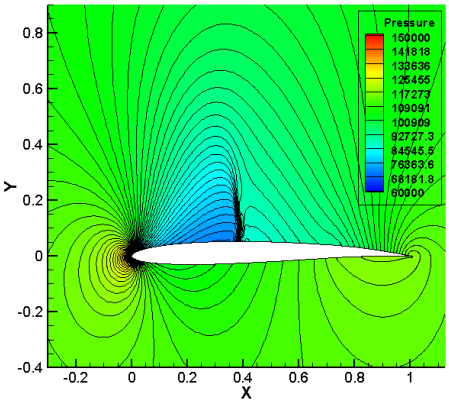

(d) Optimized design: Pressure contours

Figure 1.14. Comparison of Mach & pressure contours for NACA 2412 and the optimized airfoil design at a lift coefficient of 0.55.

6. CONCLUSIONS

The objective of this paper was to present a robust optimization algorithm for computationally efficient airfoil design under mixed (inherent and epistemic) uncertainty using a multi-fidelity approach. Stochastic expansions derived from the NIPC technique are used to create surrogate models utilized in the optimization process. In this work, a combined NIPC expansion approach is used, where both the design and the mixed uncertain parameters are the independent variables of the surrogate model. In order to reduce the computational cost, the high-fidelity CFD model is replaced by a suitably corrected low-fidelity one, the latter being evaluated using the same CFD solver but with a coarser mesh. The model correction is implemented to the low-fidelity CFD solutions utilized for the construction of stochastic surrogate by using a multi-point Output Space Mapping (OSM) technique.

The proposed methodology is demonstrated for the aerodynamic optimization of NACA 4-digit airfoils at transonic flow. The objective was to reduce the mean, standard deviation and the difference in standard deviation of the drag coefficient simultaneously to obtain an airfoil shape with minimum drag that is least sensitive to the change in uncertain parameters. The Mach number is treated as a normally distributed aleatory uncertain variable with a mean of $\mu = 0.75$ and standard deviation $\sigma = 0.015$. A geometric parameter β (from the thickness distribution formula) is treated as the epistemic uncertain parameter with a specified range of [0.17, 0.23]. The optimization is performed such that the mean lift coefficient is greater than or equal to 0.55. Two low-fidelity models (grid levels 2 and 3 from the grid convergence study) are chosen for the robust optimization study. After the correction is applied to both the low-fidelity models, the optimization results are compared to those obtained with the surrogates created with the high-fidelity model directly.

The results of both optimization cases confirmed the effectiveness of the multi-fidelity robust optimization approach with stochastic expansions. Although the optimized

design obtained by using the low-fidelity model (without correction) was comparable to that of the high-fidelity one, the statistics for the drag coefficient (for e.g., average mean C_d, average mean σ_{C_d} etc.) did not converge to the correct optimum. The accuracy in terms of convergence of statistics was achieved through the use of corrected low-fidelity model. As expected, corrected low-fidelity model based on grid level 3 performed better than the one based on grid level 2. In terms of computational cost, the proposed multi-fidelity technique outperforms the conventional approach that exclusively uses the high-fidelity model to create the surrogates. The design cost reduces to only 34 equivalent high-fidelity model evaluations (for CLF grid level 3) versus 168 for the conventional method. Overall this study demonstrates that the computational cost of robust design is reduced significantly by replacing the expensive high-fidelity model with a corrected low-fidelity model, without compromising on the accuracy.

ACKNOWLEDGMENT

Funding for this research for the first two authors was provided by the NASA Grant NNX14AN17A (Dr. Mujeeb Malik, program manager).

BIBLIOGRAPHY

[1] Oberkampf, W. L., and Helton, J. C., and Joslyn, C. A., and Wojtkiewicz, S. F., and Ferson, S., "Challenge problems: uncertainty in system response given uncertain parameters," *Reliability Engineering and System Safety*, Vol. 85, No. 1-3, 2004, pp. 11-19.

[2] Swiler, L. P., and Paez, T., and Mayes, R., "Epistemic Uncertainty Quantification Tutorial," *Proceedings of the IMAC XXVII Conference and Exposition on Structural Dynamics, Society for Structural Mechanics*, SAND 2008-6578C, 294, Orlando, FL, Feb 2009.

[3] Helton, J. C., and Johnson, J. D., and Oberkampf, W. L., "An exploration of alternative approaches to the representation of uncertainty in model predictions," *Reliability Engineering and System Safety*, Vol. 85, No. 1-3, 2004, pp. 39-71.

[4] Zhang, Y., Hosder, S., Leifsson, L., and Koziel, S., "Robust Airfoil Optimization Under Inherent and Model-Form Uncertainties Using Stochastic Expansions", AIAA-Paper 2012-0056, *50th AIAA Aerospace Sciences Meeting Including the New Horizon Forum and Aerospace Exposition*, Nashville, TN, January 9-12, 2012.

[5] Leifsson, L., Koziel, S., Zhang, Y., and Hosder, S., "Low-Cost Robust Airfoil Optimization by Variable-Fidelity Models and Stochastic Expansions", AIAA-Paper 2013-0631, *51th AIAA Aerospace Sciences Meeting Including the New Horizon Forum and Aerospace Exposition*, Grapevine, TX, January 7-10, 2013.

[6] Bandler, J.W., Cheng, Q.S., Dakroury, S.A., Mohamed, A.S., Bakr, M.H., Madsen, K., and Sondergaard, J., "Space mapping: the state of the art," *IEEE Trans. Microwave Theory Tech.*, Vol. 52, No. 1, 2004, pp. 337-361.

[7] Koziel, S., Bandler, J.W., and Madsen, K., "A space mapping framework for engineering optimization: theory and implementation," *IEEE Trans. Microwave Theory Tech.*, Vol. 54, No. 10, 2006, pp. 3721-3730.

[8] Koziel, S., Cheng, Q.S., and Bandler, J.W., "Space mapping," *IEEE Microwave Magazine*, Vol. 9, No. 6, 2008, pp. 105-122.

[9] Cheng, Q.S., Koziel, S., and Bandler, J.W., "Simplified space mapping approach to enhancement of microwave device models," *Int. J. RF and Microwave Computer-Aided Eng.*, Vol. 16, No. 5, 2006, pp. 518-535.

[10] Hosder, S., Walters, R.W., and Balch, M., "Point-Collocation Nonintrusive Polynomial Chaos Method for Stochastic Computational Fluid Dynamics" *AIAA Journal*, Vol. 48, No. 12, 2010, pp. 2721-2730.

[11] Bettis,B. R. and Hosder,S., "Quantification of uncertainty in aerodynamic heating of a reentry vehicle due to uncertain wall and freestream conditions", AIAA-Paper 2010-4642, *10th AIAA/ASME Joint Thermophysics and Heat Transfer Conference*, Chicago, IL, June, 2010.

[12] Wiener, N., "The Homogeneous Chaos", *American Journal of Mathematics*, Vol. 60, No. 4, 1994, pp. 897-936.

[13] Xiu, D., and Karniadakis, G.E., "Modeling Uncertainty in Flow Simulations via Generalized Polynomial Chaos," *Journal of Computational Physics*, Vol. 187, No. 1, May, 2003, pp. 137-167.

[14] Witteveen, J.A.S. and Bijl, H., "Modeling Arbitrary Uncertainties Using Gram-Schmidt Polynomial Chaos," AIAA-Paper-2006-896, 44^{th} *AIAA Aerospace Sciences Meeting and Exhibit*, Reno, NV, January 9-12, 2006.

[15] Eldred, M. S., Webster, C. G., and Constantine, P. G., "Evaluation of Non-Intrusive Approaches for Wiener-Askey Generalized Polynomial Chaos," AIAA-Paper 2008-1892, 10^{th} *AIAA Non-Deterministic Approaches Forum*, Schaumburg, IL, April, 2008.

[16] Walters, R. W., and Huyse, L., "Uncertainty Analysis for Fluid Mechanics with Applications," Tech rep., ICASE 2002-1, NASA/CR-2002-211449, NASA Langley Research Center, Hampton, VA, 2002.

[17] Najm, H. N., "Uncertainty Quantification and Polynomial Chaos Techniques in Computational Fluid Dynamics," *Annual Review of Fluid Mechanics*, Vol. 41, 2009, pp. 35-52.

[18] Hosder, S., and Walters, R. W., "Non-intrusive polynomial chaos methods for uncertainty quantification in fluid dynamics," *48th AIAA Aerospace Sciences Meeting*, Orlando, FL, January 4-7, 2010.

[19] Hosder, S., and Walters, R. W., and Balch, M., "Efficient Sampling for Non-Intrusive Polynomial Chaos Applications with Multiple Input Uncertain Variables," AIAA-Paper 2007-1939, 9^{th} *AIAA Non-Deterministic Approaches Conference*, Honolulu, HI, April, 2007.

[20] *ANSYS FLUENT Tutorial Guide, ver 14.5*, ANSYS Inc., Southpointe, 275 Technology Drive, Canonsburg, PA 15317, 2011.

[21] Anderson, J. D., "*Fundamentals of Aerodynamics,* 4^{th} *Edition*," McGraw-Hill, New York, 2010.

[22] Spalart, P. R., and Allmaras, S. R., "A One Equation Turbulence Model for Aerodynamic Flows," AIAA-Paper-92-0439, 38^{th} *AIAA Aerospace Sciences Meeting and Exhibit*, Reno, NV, January 6-9, 1992.

[23] Barth, T. J., Pulliam, T. H., and Buning, P. G., "Navier-Stokes Computation for Exotic Airfoils," AIAA-Paper-1985-0109, 23^{rd} *AIAA Aerospace Sciences Meeting*, Reno, NV, 1985.

[24] Hosder, S., Grossman, B., Haftka, R. T., Mason, W. H. and Watson, L. T., "Quantitative relative comparison of CFD simulation uncertainties for a transonic diffuser problem," *Combustion & Fluids*, Vol. 35, 2006, pp. 1444-1458.

[25] Abbott, I. H. and Von Doenhoff, A. E., *Theory of Wing Sections*, Dover Publications, 1959.

SECTION

2. CONCLUSIONS AND FUTURE WORK

2.1. CONCLUSIONS

In the presence of aleatory and multiple sources of epistemic uncertainties in the aerospace simulations, the DSTE approach can be implemented to carry out the statistical inference of output quantities of interest. In this work, an approach for mixed (aleatory and epistemic) UQ with evidence theory and stochastic expansions was presented. In specific, the aleatory variables were discretized into sets of intervals with appropriate BPA's according to their probability distributions. They were treated as well characterized epistemic variables in the DSTE analysis. Also, the Point-Collocation non-intrusive polynomial chaos (NIPC) was implemented for construction of a stochastic surrogate model with the overall objective of reducing the number of original function evaluations and achieving computational efficiency. The mixed UQ approach and verification of the minimum number of intervals for aleatory discretization were demonstrated on two examples: (1) three-variable variable Rosenbrock function and (2) transonic flow over a RAE 2822 airfoil. The results of these example studies showed that the NIPC based evidence theory is capable of capturing mixed uncertainty in case of multiple sources for epistemic variables. It was also shown that global bound approximation for the epistemic variables, which neglect the sources of uncertainty with beliefs can lead to overestimation of the output uncertainty.

The proposed DSTE approach was later extended to the system reliability and performance assessment of complex aerospace systems under mixed uncertainties through the

use of QMU methodology. A novel QMU framework was devised in terms of Dempster-Shafer structures (belief & plausibility) which can be used for performance assessment of a system under multiple types of uncertainty. In addition, the response quantities of interest for design performance and boundaries were represented with stochastic surrogates based on NIPC to reduce the computational cost of implementing DSTE for uncertainty quantification of high-fidelity complex system models. Two model problems were utilized to demonstrate the QMU methodology, which included various types of uncertainty representations for the performance metrics and limits. The results indicated the potential of the proposed QMU approach for the evaluation of safety and reliability of complex aerospace systems in terms of efficiency and effectiveness.

Finally, a robust optimization algorithm for computationally efficient airfoil design under mixed uncertainty using a multi-fidelity approach was presented. For this part of the research, a combined NIPC expansion method was used, where both the design and the mixed uncertain parameters were the independent variables of the surrogate model. In order to reduce the computational cost, the high-fidelity CFD model was replaced by a suitably corrected low-fidelity one, the latter being evaluated using the same CFD solver but with a coarser mesh. The model correction was implemented to the low-fidelity CFD solutions by using a multi-point Output Space Mapping (OSM) technique. The proposed methodology was demonstrated for the aerodynamic optimization of NACA 4-digit airfoils in transonic flow. The objective was to reduce the mean, standard deviation and the difference in standard deviation of the drag coefficient simultaneously to obtain an airfoil shape with minimum drag that is least sensitive to the change in uncertain parameters. The optimization results confirmed the effectiveness of the multi-fidelity robust optimization approach with stochastic expansions. In terms of computational cost, the proposed multi-fidelity technique outperformed the conventional approach that exclusively used the high-fidelity

model to create the surrogates. Overall this study demonstrated that the computational cost of robust design is reduced significantly by replacing the expensive high-fidelity model with a corrected low-fidelity model, without compromising the accuracy.

2.2. FUTURE WORK

Although significant improvement has been achieved for efficient implementation of DSTE for uncertainty quantification, there are certain areas which provide a leeway for future work. Some of these areas are listed below:

First, different combination rules to combine the evidences from different sources can be tested with the proposed approach. The current study explored the mixing and averaging rule of combination for different evidences. It will be interesting to compare the results of the example problems with different rules of combination of the evidences.

Second, the proposed approach can be applied to a large scale model problem with more number of uncertain variables using the dimension reduction technique based on sensitivity analysis. In the current study, no sensitivity analysis had been performed to reduce the dimension of the problem. The sensitivity results can be used to further reduce the computational cost of creating the surrogate response model.

Third, the proposed robust design optimization algorithm does not exploit the evidence theory concept for uncertainty quantification. An evidence based robust aerospace design optimization using the multi-fidelity approach can be applied to problems with mixed uncertainty (aleatory & multiple sources of uncertainty).

Lastly, the design approach can be applied to aerodynamic optimization problems under uncertainties with general shape parametrization techniques, such as B-splines, PARSEC, Hicks-Henne bump functions etc. This method would be able to analyze and design any airfoil geometry. However, since this approach involves more number of design

(control) points, it is not feasible to use the combined expansion approach (stochastic surrogate over both, design and uncertain parameters). One of the solutions is to create the stochastic surrogate at each iteration over uncertain variables only. Although the approach compromises on the computational cost, the accuracy of the surrogate used in the design process increases significantly, which in turn improves the accuracy and reliability in the optimal design.

BIBLIOGRAPHY

[1] Oberkamp, W. L., Diegert, K., V., Alvin, K., F., and Rutherford, B., M., "Variability, Uncertainty and Error in Computational Simulation," *ASME Proceedings of the* 7^{th} *AIAA/ASME Joint Thermophysics and Heat Transfer Conference*, Vol. HTD-vol. 357-2, 1998, pp. 259-72

[2] Smith, R., *Uncertainty Quantification: Theory, Implementation, and Applications*, SIAM books, Philadelphia, PA 19104-2688, USA.

[3] Rosic, B.V., and Diekmann, J.H., "Methods for the Uncertainty Quantification of Aircraft Simulation Models," *Journal of Aircraft*, doi: 10.2514/1.C032856.

[4] Kunstmann, H., Kinzelbach, W., and Siegfried, T., "Conditional first-order second-moment method and its application to the quantification of uncertainty in groundwater modeling," *Water Resources Research*, Vol. 38, No. 4, 2002, pp. 1-14.

[5] Zhao, Y.G., and Ono, T., "Moment Methods for Structural Reliability," *Structural Safety*, Vol. 23, 2001, pp. 47-75.

[6] Ogilvie, J.F., "A Monte-Carlo Approach to Error Propagation," *Computers & Chemistry*, Vol. 8, No. 3, 1984, pp. 205-207.

[7] Xiu, D., and Karniadakis, G.E., "Modeling Uncertainty in Flow Simulations via Generalized Polynomial Chaos," *Journal of Computational Physics*, Vol. 187, No. 1, 2003, pp. 137-167.

[8] Mathelin, L., Hussaini, M., and Zang, T., "Stochastic Approaches to Uncertainty Quantification in CFD Simulations," *Numerical Algorithms*, Vol. 38, No. 1-3, 2005, pp. 209-236.

[9] WestIV, T.K., and Hosder, S., "Uncertainty Quantification of Hypersonic Reentry Flows with Sparse Sampling and Stochastic Expansions", *Journal of Spacecraft and Rockets*, Vol. 52, Special Section on Numerical Simulation of Hypersonic Flows (2015), pp. 120-133.

[10] Prokhorov, Y.V., "Convergence of Random Processes and Limit Theorems in Probability Theory," *Theory of Probability & Its Applications*, Vol. 1, No. 2, 2006, pp. 157-214.

[11] Bae, H., Grandhi, R.V., and Canfield, R.A., "Epistemic Uncertainty Quantification Techniques Including Evidence Theory for Large-scale Structures," *Computers & Structures*, Vol. 82, No. 13-14, 2004, pp. 1101-1112.

[12] Koziel, S., and Leifsson, L., "Low-cost Parameter Extraction and Surrogate Optimization for Space Mapping Design Using EM-based Coarse Models," *Progress In Electromagnetics Research B*, Vol. 31, 2011, pp. 117-137.

[13] Koziel, S., and Leifsson, L., "Response correction techniques for surrogate-based design optimization of microwave structures," *International Journal of RF and Microwave Computer-Aided Engineering*, Vol. 22, No. 2, 2012, pp. 211-223.

VITA

Harsheel R. Shah was born in Mumbai city, India. After completing his schoolwork at St. Francis D' Assissi High School in Mumbai in 2001, Harsheel entered Sir M. V. College of Science & Commerce to further his interests in Science till 2003. He continued to pursue his undergraduate studies in Vidyavardhini's College of Engineering & Technology affiliated with Mumbai University. He graduated Cum Laude with a Bachelor of Science degree in Mechanical Engineering from Mumbai University in 2007. During the following two years, he was employed as a mechanical design engineer at Tecnimont ICB Pvt. Ltd in Mumbai, India. Over the course of his employment, he gained experience in designing static equipments like pressure vessels, storage tanks & heat exchangers. Along with his mechanical background, the urge to explore the aerospace domain brought him back to continue his graduate career at Missouri University of Science & Technology. He received a Master of Science with a major in Aerospace Engineering in 2011 and a Doctor of Philosophy in Aerospace Engineering in 2015.